REGULATION OF EPHRIN GENE PATHWAYS BY *MYCOBACTERIUM TUBERCULOSIS* IN MACROPHAGES

A Dissertation

by

AMMAR MOHAMMED ABDULLAH

Submitted to the Office of Graduate and Professional Studies of
Texas A&M University
in partial fulfillment of the requirements for the degree of

DOCTOR OF PHILOSOPHY

Chair of Committee,	Jeffrey D. Cirillo
Committee Members,	James E. Samuel
	Jon T. Skare
	Linda L. Logan
Head of Department,	James E. Samuel

May 2021

Major Subject: Medical Sciences

ABSTRACT

Mycobacterial species contain some of the most dangerous human pathogens described throughout history, responsible for millions of deaths each year. Interestingly, many mycobacteria can infect and replicate in one of our first lines of defense against pathogens, macrophages, whose primary role is finding and killing bacteria.

We infected human THP-1 monocytic cells, a common model for human macrophages, with *M. tuberculosis* (*Mtb*), the causative agent of tuberculosis, to better understand the mechanisms that allow pathogenic mycobacteria to survive and replicate within macrophages. We investigated the transcriptional expression profile of human macrophages after infection with *Mtb*. We found that the EphA (Erythropoietin-producing hepatoma) receptor subfamily member, EphA1, is induced by infection with *Mtb* and coordinates expression of a broad subset of metabolic, signal transduction and gene regulation pathways. The largest family of eukaryotic receptor tyrosine kinases, Eph receptors, mediate many vital cellular functions, including: tissue organization, cell adhesion, cell migration, immune responses, and granuloma formation in tuberculosis.

Expression of EphA1 and EphA2 receptors and their ligand, EphrinA1, were upregulated in a temporal manner from 15 min to 4 hours post-infection of THP-1-derived macrophages with *Mtb*. EphA2 expression was greater in *Mtb* infected EphA1$^{-/-}$ cells than in THP-1 cells, suggesting compensatory expression due to the absence of EphA1. *Mtb* induces higher levels of EphA1, EphA2, and EphrinA1 gene expression than heat-killed bacilli, suggesting that bacterial viability is involved in optimal expression. Similar to

EphA2 KO mice, EphA1$^{-/-}$ THP-1-derived macrophages display increased bacterial killing at later time points than wild type THP-1-derived macrophages.

RNA-Seq studies revealed that an EphA1 KO in THP-1-derived macrophages impacts a wide variety of cellular functions and pathways. EphA1 KO THP-1-derived macrophages differentially regulate metabolic, signal transduction and transcriptional regulation pathways during *Mtb* infection.

These data indicate that EphA receptors play a key role in modulation of tuberculosis immunity by macrophages and provide a foundation for detailed investigation of the role of Eph genes and their ligands in pathogenesis.

DEDICATION

This dissertation is dedicated to my family, who have helped me on this long path to my degree.

My father is the one who taught me the importance of hard work and self-control.

My mother, through her support and courage, gave me faith to make my dreams come true. To my five brothers and sister, thank you for your support and your affection.

My lovely wife and my four children, thank you from the depths of my heart for your tolerance, affection, inspiration and endless support during the good and hard times of our new life in the United States. Without you, I wouldn't have been able to do that. You are my inspiration and my encouragement.

God bless all of you.

ACKNOWLEDGEMENTS

My sincere appreciation goes to Dr. Jefferey D. Cirillo, chair of my committee, for his excellent support and encouragement through all my time in his laboratory. I deeply appreciate the wonderful opportunity he has presented me with. On this long journey, I am truly grateful for his patience, guidance, experience, and excellent assistance.

For their support and guidance during my research, my heartfelt gratitude goes to my committee members, Dr. James E. Samuel, Dr. Jon T. Skare, and Dr. Linda L. Logan. They did not delay, even though it took a portion of their precious time, to guide my study in the right direction.

I would like to express my gratitude to my sponsor, the Iraqi Ministry of Higher Education and Scientific Research (MOHESR), for selecting me to be a part of this prestigious scholarship program and for their support in regulating and financing my advanced studies.

My heartfelt appreciation goes to my friends, Madeleine G. Moule, Kent J. Koster, Maral Molaei, Preeti Sule, Thushara Galbadage, Sathish Kumar, Aaron Benjamin, Maksim Lebedev, and Mohammed M. Ibrahim, who have been of great support to my research project.

CONTRIBUTORS AND FUNDING SOURCES

Contributors

This research was supervised by a dissertation committee comprising of Chair Dr. Jefferey D. Cirillo of the Department of Microbial Pathogenesis and Immunology, Texas A&M University and committee members Dr. James E. Samuel Head of the Department of Microbial Pathogenesis and Immunology, Texas A&M University, Dr. Jon T. Skare of the Department of Microbial Pathogenesis and Immunology, Texas A&M University, and Dr. Linda L. Logan of the Veterinary Pathobiology Department, Texas A&M University. The experimental research was performed in the Microbial Pathogenesis and Immunology Department, Texas A&M University.

The Clinical TB-patient specimens were provided by Dr. Andrew DiNardo, Baylor College of Medicine, Houston.

All the dissertation work was completed independently by the author.

Funding Sources

A scholarship from the Ministry of Higher Education and Scientific Research (MOHESR) in Iraq supported the author and the work was supported in part by National Institutes of Health grants AI104960 and AI149383.

NOMENCLATURE

ADAM	A Disintegrin and Metalloproteinase
ADC	Albumin dextrose complex
ATP	Adenosine triphosphate
BCG	Bacillus Calmette–Guérin
Cas9	CRISPR associated protein 9
CFU	Colony-Forming Units
CRD	Cysteine-rich domain
CRISPR	Clustered regularly interspaced short palindromic repeats
DGE	Differential gene expression
DTH	Delayed-type hypersensitivity
Eph	Erythropoietin-producing hepatoma
FDR	False discovery rate
FN	Fibronectin
HDR	Homology-directed repair
HIV	Human immunodeficiency virus
IFNγ	Interferon Gamma
IGRA.	Interferon-Gamma Release Assay
IPA	Ingenuity Pathway Analysis
KO	Knockout
LBD	Ligand-binding domain
LTBI	Latent TB infection

LRT	Likelihood ratio test
LPS	Lipopolysaccharide
MAPK	Mitogen-activated protein kinase
MDR-TB	Multiple drug-resistant TB
MOI	Multiplicity of infection
MMP	Matrix metalloproteinase
Mtb	*Mycobacterium tuberculosis*
NHEj	Nonhomologous end joining
NGS	Next Generation Sequencing
NO	Nitrous oxide
OD	Optical density
PAM	Protospacer-adjacent motif
p75NTR	p75 neurotrophin receptor
PBMCs	Peripheral blood mononuclear cells
PBS	Phosphate-buffered saline
PMA	Phorbol 12-myristate 13-acetate
PRR	Pattern Recognition Receptor
PTB.	Phosphotyrosine binding
PTP	Protein tyrosine phosphatases
qRT-PCR	Quantitative real-time PCR
RBD	Receptor-binding domain
Ret	Rearranged during transfection

RPMI	Roswell Park Memorial Institute
SAM	Sterile α-motif
TB	Tuberculosis
TNF-α	Tumor necrosis factor-α
TLR	Toll-Like receptor
TrkB	Tropomyosin receptor kinase B
TST	Tuberculin skin test
WHO	World Health Organization
XDR-TB	Extensively drug-resistant -TB

TABLE OF CONTENTS

Page

LIST OF FIGURES

LIST OF TABLES

Page

CHAPTER I

INTRODUCTION

Tuberculosis

History of tuberculosis

Tuberculosis (TB) is a disease that has been known for thousands of years. It was discovered in the bone remnants of a TB patient in Liguria, Italy, from around 5,800 BC [1]. The disease was also recorded in the Pharaonic era in ancient Egypt [2]. The DNA of TB bacteria was identified in ancient Egyptian mummies dating back thousands of years [3]. The Greek historian, Hippocrates described tuberculosis as "phthisis" [2]. Estimates of TB deaths were high in London in the seventeenth century [4]. The industrial revolution resulted in an increased need for workers, and urbanization which in turn led to crowded workplaces and easier transmission and spread of the disease in Europe [2]. The European death rate from tuberculosis was as high as 25% in the nineteenth century [4].

Mycobacterium tuberculosis (*Mtb*), which was identified and described in Germany in 1882 by Robert Koch, is the bacteria that causes TB [2]. By the 20th century, in the developed world, individuals were enjoying improved nutrition, higher incomes, more adequate housing conditions, and less crowding. Thus, the rate of infection and death due to TB declined [4]. In 1946, a treatment was developed using an antibiotic called streptomycin. Other antibiotics were subsequently introduced, and eventually a multi-drug regimen was established that led to improved treatment outcomes and replaced the old clinic-based surgical system [2]. This improvement was short-lived, however, and in the early 1980s, the emergence of human immunodeficiency virus disease (HIV) led to a new

spread of TB, especially in sub-Saharan African. In addition to HIV, other *Mtb* strains have emerged that are resistant to many antibiotics. Moreover, many countries suffer from weak health systems and a lack of diagnostic tests, thus exacerbating the rate of infection and death [4].

Pathology of the disease in humans

TB is spread from infected to healthy persons through small droplets and aerosol that contain 1 to 200 bacilli. Pathological lesions' development begins upon inhalation of this aerosol and entry of these bacilli into the lungs [5, 6]. When the bacilli migrate to the alveoli of the lungs, they find macrophages that engulf them. These macrophages secrete proinflammatory cytokines after the bacteria stimulate Toll-Like Receptor (TLR) and Pattern Recognition Receptor (PRR) receptors. The macrophages in turn induce the recruitment of other immune cells to the bacteria's site. Neutrophils and monocytes are amongst the first cells to join them. If more bacteria are ingested and more cytokines and chemokines are secreted, early granulomas are produced. Dendritic cells, another player in phagocytosis of *Mtb*, contribute in granuloma formation. These immune cells then present the antigens of the *Mtb* to lymphocytes after migrating to nearby lymph nodes.

During these events, the granuloma continues to develop, starting from the center (which is filled with infected macrophages) and are surrounded by epithelioid macrophages, foam cells, and a few giant multinucleated cells, eventually ending with the lymphocytes. All of these cells are surrounded by a fibrous capsule [7]. The granuloma provides protection for the bacteria from IFNγ-producing lymphocytes, in addition to containing the infection. Changes in the granuloma center lead to necrosis, which

increases lipid and protein content due to the death of the macrophages. This causes a tissue change that gives a caseous appearance. The granuloma persists by a delayed-type hypersensitivity (DTH) response caused by continuous exposure to antigens. This provides an environment for the *Mtb* to survive and reproduce, both inside and outside the macrophages [7].

The environment of the granuloma is considered an aerobic environment in animals and humans [8, 9]. Therefore, it is crucial to take this aerobic environment into account when considering the metabolism of bacteria and antibiotic therapy [10]. In order to adapt to the granuloma environment, *Mtb* depends on the use of fatty acids in its metabolism process, low activity, slow replication, an increase in the thickness of the cell wall, and an inactive state [11]. Ghon's focus is the lesion located at the primary site of implantation. Before the granuloma can contain the bacilli, *Mtb* spreads to regional lymph nodes through lymphatics. Due to this spreading, granulomatous lymphangitis and lymphadenitis may result, leading to Ghon's focus on what is known as the primary Rank's complex. Dissemination via blood vessels can occur within the lungs or across organs. Because the upper lobe of the human lung is higher, oxygen pressure and the immune response is delayed, and *Mtb* growth in this region of the lung is favored [12]. Symptoms can range from people being asymptomatic to severe or life-threatening indicators, which are seen in approximately 10% of the infected people. This is due to the virulence of the bacteria, bacterial burden, suppression of the host's immunity, and genetic susceptibility of the infected person [13].

Mtb infection in healthy individuals can have two distinct presentations, either active disease or a latent TB infection (LTBI) [4]. This unique characteristic period of the disease (latent period) is for controls the disease. It is called latent tuberculosis infection when it is largely asymptomatic. In typical TB infection, people with immune deficiencies are victims of *Mtb*, causing symptoms to appear as a result of the proliferation of bacteria inside cells, resulting in active infections. The active disease usually occurs as a reactivation of latent infection [14]. The possibility of the bacteria reactivating from LTBI to an active form is more common in the years immediately after the initial infection; in people who are immunocompetent, this occurs about 10% of the time [4] People who are immunocompromised (e.g., HIV/AIDS patients) are more likely to be affected by the rapid onset of the active disease [15]. *Mtb* most commonly in the lungs, leads to pneumonia symptoms such as a cough that produces sputum. This may be accompanied by the appearance of bloody sputum. *Mtb* may also spread to other parts of the body. When this occurs, it is called extrapulmonary or miliary TB, which has been observed in many people with HIV [15]. Extrapulmonary TB affects tissue and organs outside the lungs in 15% of TB infected people. The central nervous system, genitourinary system, and skin are the most common organs showing extrapulmonary infections [16]. Infections may result from a reactivation of the latent bacteria, which can result in spread to new sites [17, 18].

Most cases of TB display characteristic lung lesions. These lesions are initially present as exudative bronchial pneumonia and develop into granuloma. As the disease progresses, the granuloma becomes necrotic, which is followed by the formation of a cavity [19]. Often, the fibrous capsule surrounding the granuloma will break, allowing the

TB bacilli to be released into the airway. If these bacilli multiply extracellularly, they will re-spread inside the lungs or travel outside the lungs through coughing in sputum [20]. At this stage, the number of macrophages and neutrophils in the sputum increases [21].

Diagnosis of tuberculosis

For many years, the tuberculin skin test (TST) was used to diagnose TB, especially latent TB. Injection mycobacterial proteins in the dermis lead to the development of an immune response to these proteins in infected person. This response is a delayed-type hypersensitivity (DTH) response, and it appears as an inflammatory reaction at the injection site [22]. This test has several problems, the most important of which is that after being injected with tuberculin, the patient is required to return after 48 to 72 hours so that the result can be read. This may not be possible for many patients, either because the clinic is far away or travel causes financial difficulties [23]. This test may also be affected by the BCG vaccine, which is given to many children around the world. This test can give a positive result for several types of non-mycobacterial bacteria, and thus is not very specific to TB exposure to infection [22].

As a result of these constraints, a second test was developed, the Interferon-Gamma Release Assay (IGRA). This is a serum test that evaluates the release of interferon-gamma by T-cells. This is accomplished by administering two types of mycobacterial antigens: ESAT-6 and CFP-10. The test is superior to TST, offering several advantages. It is more specific to TB, not affected by a previously-administered BCG vaccine, does not require a second visit to read the results, and is not affected by any other non-mycobacterial infection. However, this test requires a well-equipped laboratory and

the test is expensive, and therefore is not available to all people, especially in regions of the world with limited resources [23]. Despite IGRA being more specific, it does not distinguish between active and latent forms of the disease [4]. It cannot distinguish between those previously infected and treated and cases of reinfection.

However, the use of the IGRA grows more unreliable as the disease progresses from latent to active [24]. One form of the test actively in use is culturing the bacteria on solid culture media to diagnose active cases. Solid media are usually used because they are easy to handle; liquid media are faster but more expensive. One practical benefit of culture on media is the ability to run drug sensitivity tests for the cultured organism. One disadvantage is that it takes a long time to grow mycobacteria, even in automatic culture systems; the period exceeds two weeks, at best [25]. This is due to the slow growth of *Mycobacterium tuberculosis*, which takes 15-20 hours per division [4].

Microscopic examination of sputum smears and x-rays of the chest are two approved means of diagnosing TB in poor and middle-income countries [4]. After the discovery of TB bacteria, Ziehl-Neelson staining began to be used for microscopic examination of sputum smears in patients; it is still employed in many countries [2] as one of several initial rapid checks for TB. The sensitivity of the test depends mainly on the technician or examiner's performance and ranges in sensitively from 50% to 80% [25]. Also, HIV infection may affect the results of the examination and reduce the ability to recognize positive cases [26]. Fluorescent microscopy was developed with Auramine O staining to increase the sensitivity of microscopic tests of sputum smears [27].

After the invention of PCR, it became possible to perform DNA amplification to diagnose TB's active cases; this is known as the nucleic acid amplification test. A GeneXpert assay has also been developed that can determine the presence of TB bacteria and resistance to rifampicin. The assay can be carried out within two hours and does not require a high-performance laboratory. The assay has a sensitivity of 98% and specificity of 99.2% [28].

Symptoms of tuberculosis

Primary pulmonary TB is generally the primary infection, most often found in infants and children under five years of age who have not previously been exposed to TB bacteria. The symptoms are either subclinical or pneumonia in the lower and middle lobes and may be accompanied by pleural effusion X-rays do not definitely distinguish between it and other bacterial infections. The disease is typically confirmed by bacterial culture of the sputum [29]. Secondary (or reactivated) TB results from the reactivation of latent TB bacteria years or even decades after the initial infection. Common reasons for reactivation include immunosuppression resulting from HIV, malnutrition, smoking, organ transplantation, chronic corticosteroid use, chemotherapy, diabetes, and kidney failure [30]. Another reason for increased reactivation of the infection is a reduction in the count of CD4 cells [31]. Symptoms differ according to the immune status of the patient, but most are respiratory in nature, such as a long-term cough lasting more than two weeks. This stage is accompanied by general clinical symptoms such as fever, night sweats or chills, loss of appetite, fatigue, malaise, and weight loss [32, 33].

Most patients develop a cough that produces purulent sputum. The sputum also permeates the blood. Hemoptysis appears as a result of the shattering of dilated blood vessels in the walls of the chest cavity. Pleuritic chest pain is due to parenchymal inflammation. It affects areas during inspiration, especially while coughing. Some studies have indicated the presence of anemia, which leads to fatigue and general weakness. Leukocytosis has also been observed, increasing the number of white blood cells due to infection [34].

Treatment and Prevention of tuberculosis

Treatment for TB depends on a combination of several types of antibiotics, including rifampicin, isoniazid, pyrazinamide, and ethambutol. There are several recommendations for combining these antibiotics. According to the World Health Organization (WHO), the most acceptable is to give them together for two consecutive months and then take rifampicin and isoniazid for not less than four months. More recently, the WHO developed a directly observed therapy (DOT) involving giving medicines regularly to ensure that they are taken by the patient [35].

Mtb is known to develop drug resistance to the antibiotics used for treatment. Strains resistant to antibiotics are called drug-resistant TB strains. Multiple drug-resistant TB strains (MDR-TB) have been found, which are resistant to both rifampicin and isoniazid. Treating people with such strains of TB requires the use of four medicines at one time, a method that has been proven effective against the strain that causes this disease. These patients are usually given treatment for 18 months after the last test confirming the patient to be free from *Mtb*. Anti-TB treatments are organized as follows: first-line agents

given orally, injectable agents, fluoroquinolones, second-line agents given orally, and third-line agents [35]. The emergence of antibiotic-resistant strains reduces the chances of recovery from the disease. When a strain is resistant to isoniazid, rifampicin, one of the fluoroquinolones, and one of the injectable second-line agents, it is called extensively drug-resistant (XDR-TB). People with such a strain are difficult to treat, and the method of treatment is more complicated [36].

After two weeks of treatment with rifampicin and isoniazid, TB patients with a positive smear are not contagious to others [37]. If treatment continues regularly after that point, they are not able to transmit infection, even if the sputum smear remains positive. The separation remains necessary for patients during the first two weeks of treatment to ensure that infection is not transmitted. Wearing protective clothing and masks is necessary for doctors and nurses during the treatment phase, but after two weeks of treatment, it is not essential [38, 39].

Because TB is no longer widespread, the quest to develop TB antibiotics has diminished. The last innovation in this area was in the mid-twentieth century. Currently, the development of anti-TB therapy is ongoing, but efforts have not been particularly useful [40]. One strategy for reducing the spread of TB is vaccination. However, only the BCG vaccine is currently available, which is considered to have relatively little efficacy against pulmonary TB, especially in adults [41]. Consequently, there is an urgent need for the development of new vaccines with greater effectiveness to eradicate the disease all over the world. Besides, new treatment methods for bacteria must be developed to ensure

the elimination of the disease. Currently, many vaccines are in the development or clinical stages of trials [42].

There is also an ongoing need to develop an improved vaccine that has the ability to enhance the efficacy of the BCG vaccine in newborns, one that it is safe for use in most populations, such as those that are endemic or have high rates of HIV. Many experiments have been conducted for this purpose, including those using attenuated mycobacteria that have a genetic mutation, and those that employ pathogenic and non-pathogenic bacteria. There are also ongoing attempts to find alternatives to the BCG vaccine by using parts of the TB bacteria's DNA or *Mtb* antigens, either in combination with BCG or alone [43].

Epidemiology

TB infection occurs upon entry of a microbe. It is usually either latent (that is, without clinical symptoms) or subclinical. Symptoms rapidly appear in some of those infected, but only a small percentage. It is possible for the latent infection to turn active, and thus such persons can then infect healthy people [44]. Vaccinating uninfected people, early diagnosis and treatment of those with active TB, and treatment of latent TB all reduce the incidence of spread to the uninfected [44-46]. One of the factors most influencing TB infection is exposure to individuals with untreated active TB. The incidence rate is higher for same-household individuals in close contact with the infected [46]. Infection outside the household also significantly contributes to the number of infected people. However, the possibility of infection remains challenging to determine. It depends largely on the rate of contact with people with TB, severity of the disease among those infected, and sharing air in closed places with limited ventilation, which is the most dangerous [46]. After

becoming infected with TB bacteria, an individual may not immediately develop the active form of the disease, but the likelihood of progression increases with acquired immunodeficiency disease or factors that lead to immunosuppression, such as steroids, cancer chemotherapy, and diabetes [47].

The WHO estimated about 10 million cases (between 9.0 to 11.1 million) in 2018. The estimated TB deaths were 1.2 million among HIV-negative people and 251,000 among those who were HIV positive. TB affects all age groups and both sexes, but in 2018 it was found that men 15 years of age and over were 57% of those with the disease. Women accounted for 32%, while children under the age of 15 did not exceed 11%. As for TB cases in those infected with HIV, the rate was 8.6% [48].

Mycobacterium tuberculosis

Organism

Mtb is of the family of Mycobacteriaceae and the order Actinomycetales. They are non-motile, non-spore forming, rod-shaped, and aerobic. The bacterial division is slow (generation time 15-20 hours) and resistant to detergents and many antibiotics. Due to the hydrophilic cell wall properties, the bacteria can withstand both the environment and acid/alcohol nature, so the bacterium is classified as “acid-fast”. The cell wall structure is different than other prokaryotic cells. It has high lipid content of around 60%. In addition to peptidoglycan, the other major components are mycolic acids, cord factor, and wax-D. The mycolic acid and arabinogalactan form a hydrophobic barrier for the bacterium. Due to the transfer of proteins to the plasma membrane and porins into the mycotic acid layer,

hydrophilic substances will be imported into the cell. Beyond this is the pseudo-capsule layer, made up of polysaccharides, protein, and lipids [49, 50].

Due to the thick layers of lipids in the bacterial wall, dyes are challenging to take up easily. But the bacillus resists decoloring when an acid-alcohol solution is applied to remove the dye. *Mycobacterium* bacteria can stained with traditional dyes, such as Ziehl-Neelsen or Kinyoun with carbol fuchsine [51, 52]. Also, fluorescent dyes such as auramine dye are used for staining *Mtb* [53].

Genome of Mtb

The entire *Mycobacterium tuberculosis* genetic map was published in 1998 [54]. About 4,000 genes have been identified in the 4.4 base-paired bacterial genome. The genome was detected to contain approximately 65.6% of GC, a trait present in most aerobic prokaryotes [55].

Mycobacterium tuberculosis can synthesize all the essential amino acids, vitamins, and enzymes, employing all the genes that synthesize these components. Most of these genes produce enzymes that carry out lipogenesis and lipolysis. The bacterial genome also contains genes that encode glycolytic enzymes and enzymes that participate in the anabolic pentose phosphate pathway. These enzymes produce NADPH and pentose sugar, which are involved in the kerb's and glyoxylate cycle, leading to carbohydrates and lipids production. At the same time, *Mycobacterium* can survive in different oxygen content environments such as lung, macrophage, and granuloma due to the possession of enzymes that it uses in aerobic, microaerophilic, and anoxic in electron transport [54]. *Mycobacterium* genome contains repetitive DNA sequences that include insertion

sequences, direct repeats, major polymorphic tandem repeats, and polymorphic GC-rich repetitive sequences [56].

The Ephrin system

Eph (erythropoietin-producing hepatocellular carcinoma) is a well-known tyrosine kinases family. It was first found in the erythropoietin-producing human hepatocellular carcinoma cell line, due to this line's high expression of the EphA1 receptor [57]. Eph families are divided into two classes, based on ligand affinity and sequence similarity: EphA and EphB [58]. Ligands are divided into two classes, EphrinA and EphrinB, based on the binding of their receptors. There are nine EphA receptors (EphA1 to EphA8, and EphA10), which match the ligands (EphrinA1 to EphronA5). EphB consists of five receptors (EphB1 to EphB4, and EphB6) that correspond to the ligands (EphrinB1 to EphrinB3) in mammalian cells [59]. Two receptors can interact with interclass ligands: EphA4 can interact with EphrinB ligands, and EphB2 can interact with EphrinA5 [60] (see Figure 1). Since Eph receptors and ligands are linked to a membrane, the interaction between cells is essential for activation, leading to repulsion or attraction between cells through cell migration, motion, and axon guidance [61, 62]. Ephrin receptors have an essential role in axon guidance, cell migration, tissue boundary construction, angiogenesis, and segmentation through embryonic growth [63, 64].

In adulthood, Eph receptors have a role in the metabolism of bones, differentiation of stem cells, and long-term potentiation [65, 66]. The Eph-Ephrin system has an important function in the pathogenesis of many diseases [67]. These receptors have

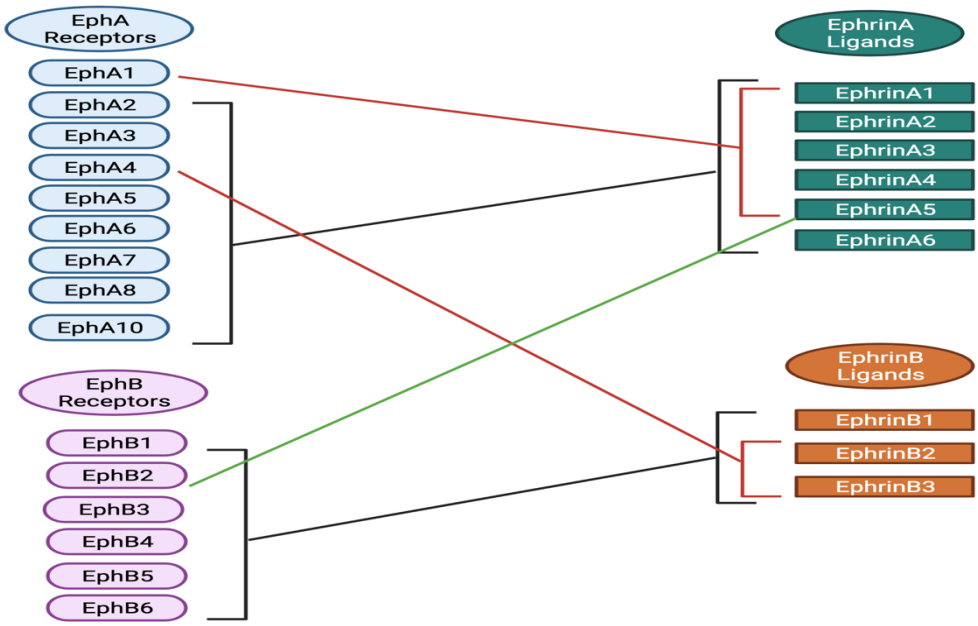

Figure 1. Classification of Eph receptors and their ligands in human.

reportedly been expressed in many cancer cells and tumors. Eph receptors influence the development, angiogenesis, migration, invasiveness, and metastasis of various kinds of tumors. Moreover, this system is implicated in healing nervous system injuries, degeneration of neurons, diabetes, viral infections, and bone disorder diseases [68].

Structure of Eph receptor

The extracellular domain of the Eph receptor contains an N-terminal ligand-binding domain (LBD), cysteine-rich domain (CRD), sushi domain, epidermal growth factor-like domain, and two fibronectin (FN) type III repeats. The intracellular domain contains a juxta-membrane domain, two conserved tyrosine residues, a kinase domain, sterile α-motif (SAM), and a PDZ-binding motif [69].

Affinity for the Ephrin ligands is determined by the LBD since it consists of a hydrophobic channel and polar part on the bottom of the LBD, which is vital for

interaction Ephrin-B ligands [59, 70]. The juxta-membrane section links with the kinase domain in the inactive state [71]. When the ligand of the Eph receptor, Ephrin, binds the Eph receptor, it is activated by phosphorylation of two tyrosine residues in the kinase domain, with one located in the juxta-membrane section and one in the kinase domain [72, 73].

Releasing the kinase active site through phosphorylation of the tyrosine residue in the kinase domain prompts the repositioning of this piece. It is unknown how the Eph receptor-Ephrin association enhances the autophosphorylation of Eph receptors. The likelihood of autophosphorylation depends on the concentration of Eph receptors through the binding of Ephrin ligands, leading to transphosphorylation. Also, the clustering of the Eph receptors likely disrupts the juxta-membrane segment, initiating activation of the receptors [74]. Some domains, such as CRD, FNIII repeats, and SAM, are included in Eph/Ephrin cluster construction [75]. The main domains involved in cis-interaction with Ephrin are FNIII repeats [76, 77]. The SAM domain stabilizes gathering; however, it is not necessary for Eph receptor clustering [69, 78]. Many tyrosine residues are phosphorylated after clustering, developing associated spots for intracellular adaptors [79]. Src Homology 2 or Phosphotyrosine binding (PTB) domains link with the binding sites of cytoplasmic targets after phosphorylation of the tyrosine in the juxta-membrane segment. Protein tyrosine phosphatases (PTP) are downstream signaling molecules that interact with the SAM domain after phosphorylation and oligomerization [80, 81].

Structure of the Ephrin ligand

Ephrin ligands are characterized by the conserved receptor-binding domain (RBD). When the Eph receptor binds with its ligand, the hydrophobic loop of the RBD inserts into the hydrophobic core of the LBD. There are two subclasses of ligands, based on the attachment of the ligands to the cell membrane: EphrinA and EphrinB. Glycosylphosphatidyl inositol anchors the EphrinA to the cell membrane. Since EphrinA has no cytoplasmic domain, it relies on a link with coreceptors for more signaling such as Tropomyosin receptor kinase B (TrkB), rearranged during transfection (Ret), and the p75 neurotrophin receptor (p75NTR) [82, 83]. Conversely, EphrinB has a transmembrane domain and conserved cytoplasmic segment, followed by a C-terminal PDZ-binding motif [84] The cytoplasmic segment is enriched with tyrosine residues that phosphorylate during the binding of their receptor [85, 86].

Clustering of Eph and Ephrin

Eph receptors cluster by a seeding mechanism to achieve the optimal activity. There are two interfaces for this mechanism. The first is heterodimerization between the Eph receptor and ligand. The second is gathering between two neighboring Eph receptors. Recognition and binding of the Eph receptor and ligand are the first steps in clustering [87]. Heterodimerization of the Eph receptors and ligands is followed by hetero-tetramerization, creating hetero-tetramers that can form a ring organization whereby each receptor binds two ligands, and each ligand binds two receptors [88].

The hetero-tetramers of Eph ligands and Eph receptors interact, accumulating into hetero-oligomeric clusters. These clusters of receptors may bind with other hetero-

tetramers, leading the Eph receptors to organize into an arrangement and non-bound Eph receptors being recruited [89]. Receptor assembly comes from LBD-LBD binding by salt bridges and hydrogen bonds. Meanwhile, the CRD-CRD binding occurs by van der Waals bonds [90]. Ligands that interact with Eph receptors and then the cluster can initiate signaling. Non-clustered or soluble ligands cannot initiate signaling and work as antagonists. Ligand clustering increases the concentration of Eph receptors to prompt downstream signaling [91]. Eph receptors and Ephrin are distributed across the cell surface in cholesterol-rich lipid rafts. These rafts allow trans-signaling between the Eph receptors and ligands in opposite cells and prevent cis-signaling in the same cell [92]. Cis-signaling eliminates trans-interaction between the Eph and ligand and stops the initiation of tyrosine phosphorylation [93].

Signaling

Bidirectional signaling, or forward signaling, occurs when Eph receptors and Ephrin ligands bind [68]. The Eph-Ephrin signal is complex because of the many potential Eph-Ephrin interactions, variations in co-expression of Eph receptors, cis-signaling affecting the signal, and overlap with diverse signaling pathways [79] The signaling implement may vary according to the cell type and organ situation, so the Eph-Ephrin pair may cause opposing reactions such as adhesion and retraction. Phosphorylation of the Eph receptor can induce cell-cell isolation or trigger cell-cell adhesion through kinase-independent signaling pathways [93, 94]. Eph receptor bidirectional signaling involves many functions, such as the formation of the cytoskeleton dynamics and architecture. Actin stress fiber depolymerization is the

most frequent cellular response to Eph receptor activation, leading to a collapse of the cytoskeleton and cell-cell segregation [94].

Organization of Eph/Ephrin signaling

Control of signaling via the Eph/Ephrin interaction can be achieved in various ways and at different levels. Transcriptional and post-transcriptional regulation can be performed at the RNA degree [95]. Some proteins affect the signaling of Eph/Ephrin, such as PTP ligand interaction in cis, γ-secretases, and matrix metalloproteinases (MMP) like A Disintegrin and Metalloproteinase (ADAM). Other molecules, such as PTP, prevent the phosphorylation of Eph receptors and counteract Eph receptor endocytosis [96]. Ephrin-induced clustering stimulates the interaction between the Eph receptor and ADAM. ADAM disrupts the Eph/Ephrin interaction through EphrinA cleaving, causing cell de-adhesion. MMP and γ-secretases cleave EphrinB ligands, generating an intracellular domain that induces downstream signaling [97]. Trans-endocytosis, including ingestion of whole transmembrane EphB-EphrinB molecules, leads to de-adhesion of the cell, which is another way to end Eph/Ephrin interaction [93].

RNA-Seq

RNA-Seq is a recent development. It is now a common tool used in molecular biology to understand aspects of genetic function [98, 99]. One of the techniques used in RNA-Seq to detect the presence and quantity of RNA molecules is Next Generation Sequencing (NGS) technologies. The high throughput RNA-Seq method allows for the

performance of genome-wide characterizations without prior knowledge of the RNA sequences [100, 101]. The RNA-Seq method can detect all types of RNA, including mRNA and long non-coding RNA. It can also determine the structure of a gene, patterns of gene expression under different biological conditions, and quantity of copies of genes [100].

RNA-Seq is mainly used in differential gene expression (DGE) analysis. Since its inception, DGE analysis assays have not changed substantially. This process is nearly standard across all laboratories, beginning with RNA extraction and followed by mRNA enrichment or depletion of rRNA, cDNA synthesis, and establishment of an adaptor-ligation sequencing library with millions of reads for each sample on a high throughput platform. The process ends with computerized mathematical operations. Sequencing alignment and assembly of sequences deliver the transcriptome, counting the number of reads that overlap between the transcript, filtering, and normalizing samples, and calculating statistics to identify significant changes in gene expression and whether there are single or groups of genes. Currently, RNA-Seq can be done on many different tissues and a wide variety of organisms, including humans [102, 103].

CRISPR Cas9

To accurately edit DNA and modify genomic information, molecular machines are required that contain two main parts or domains: one that can bind to specific sites in DNA and one that can accurately distinguish among target binding sites. The second domain can break two strands of DNA or organize a specific sequence [104, 105].

Recently, a new technique has emerged that allows for precise manipulation of a specific genetic sequence. This technique was taken from the bacterial defense mechanism against the phage, called the clustered regularly interspaced short palindromic repeats (CRISPR) and CRISPR associated protein 9 (Cas9) system. This mechanism is modified for genome editing and engineering using the guide-RNA platform for DNA targeting [106]. This technique is used to clarify gene function and the relationship of certain genes to the occurrence and development of the disease. It is also used to modify disease-causing mutations, inhibits activated oncogenes, or activate cancer-suppressing genes, among other modifications [107-109]. This technique can be utilized to target multiple genomic loci in a single experiment, that is, multiple genes simultaneously, by the means to the use of programmable internal nuclease technology. [110]

This significantly speeds up researchers' understanding of pathological processes, which share a set of multiple genes such as tumor development genes. Also, use a single-guide RNA libraries and CRISPR-based genome screens to recognize drug target genes or disease resistance genes, cancer inhibitors, and to evaluate drug targets. [111, 112] Genome engineering with CRISPR Cas9 is a promising method for treating genetic diseases and disorders, such as cancers, neurodegeneration, hereditary blood diseases, cystic fibrosis, muscle atrophy, congenital immune disorders, and hereditary cardiovascular disease [113-115].

While there are many promising advantages to using CRISPR technology, some obstacles still exist that prevent its employment in treatment [116]. To be fully able to use the technology in clinical applications, work must first be done to remove these barriers,

including eliminating any unwanted off-target mutations in sites with sequences of target sites. [117, 118]. The major question is how Cas9 can target 20 bases in a genome of millions to billions of bases, breaking the double DNA only in the designated sequences. There are several biochemical and structural studies of Cas9 that have attempted to determine how it targets specific DNA fragments, as well as the short protospacer-adjacent motif (PAM), with the ultimate goal of better understanding the mechanisms by which CRISPR Cas9 functions. By altering the RNA guide sequence, Cas9 can be programmed to target new sites on DNA [119].

Cas9, from Streptococcus pyogenes, is a large endonuclease (1,368 amino acids) that is multi-domain and multifunctional. This endonuclease works by cutting the DNA after a PAM (3 pb). The two active domains are the HNH-like nuclease domain, which cleaves the complementary DNA strand of the guide RNA that is the target strand, and the RuvC-like nuclease domain, which cleaves the DNA strand corresponding to the complementary strand that is not the target strand [120, 121]. These endonucleases cause a double-strand break in DNA at the target gene locus. Breaking the DNA leads to activation of the repair process of nonhomologous end joining (NHEj) or homology-directed repair (HDR). NHEj is initiated in the absence of a template leading to insertions and/or deletions (indels), so it disrupts the target loci. HDR activates in the presence of a template matching the target locus to make a precise mutation [120].

Because of the ease and accuracy of using the CRISPR Cas9 system, it becomes a successful method for genome editing and modification. However, there are points that must be taken into consideration when adopting this method. First, it is the process of

introducing a Cas9 and gRNA into a cell. It is essential to insert two to allow for successful identification of the binding site and DNA strand break. Inserting them at the same time is more complicated than if they are entered separately. Currently, several methods can be used to deliver them into a cell, such as electroporation, nucleofection, and lipofectamine. The plasmids expressing Cas9 and gRNA are used in mammalian cells to create the lentivirus and then insert it into target cells [121, 122]. Second, genotyping must be conducted after making modifications with CRISPR Cas9. A pair of primers flanking the target site can be used with the T7 endonuclease I assay to determine the modifications [123, 124] PCR products can also be employed to find mutations using the restriction fragment length polymorphism assay. To support the assay, sequence analysis is conducted to detect modifications [125, 126]. Finally, Cas9 produces mutations in its target and maybe in off-target mutations, so off-target influence should be considered. The off-target mutations can cause undesirable modifications.

Finally, EphA receptors are not well known in infectious diseases. Microarray study found that EphA2 and EphA3 expression are induced in epithelial cells infected with *Neisseria gonorrheae* [127]. Another studies displayed that the EphA1 and EphA3 genes are triggered in THP-1 and U937 after infection with the *Mtb* [128, 129]. Eph receptors, mediate many vital cellular functions, including tissue organization, cell adhesion, cell migration, immune response, and granuloma formation in tuberculosis disease [130]. The aim of this research is to use in vitro experimental methods to gain insight into the role of the EphAl and EphA2 receptors and their ligands, EphrinA1 in *Mtb* infected macrophages.

CHAPTER II

ROLE OF EPHRIN GENES IN *MYCOBACTERIUM TUBERCULOSIS* INFECTED MACROPHAGES

Introduction

One of the largest tyrosine kinase families is the group of hepatocellular carcinoma receptors producing erythropoietin (Eph), which has many vital functions in organisms because of its mediating role [131]. Eph families are divided into two classes based on ligand affinity and sequence similarity: EphA and EphB [58]. Ligands are divided into two categories, EphrinA and EphrinB, based on the binding of their receptors. These receptors bind with ligands on corresponding cell surfaces. This allows for the activation of both attached cells, as the signals are bidirectional in terms of generating change [132].

These receptors express on the surfaces of many cell types, including neurons, epithelial cells, and vascular endothelial cells. Some studies have shown the presence of many EphA receptors on different immune cells [133]. These signals influence cellular processes and interactions such as cell adhesion, cell migration, and tissue border formation [86]. Expression of the EphA2 receptor has been shown in hematopoietic tissue, as well as in adherent tonsil cells with a dendritic appearance [134]. Lymphocytes are one of such examples of cells that express these receptors. Their importance is still unclear, but some evidence suggests their involvement in differentiating and modulating the response of T-lymphocytes [135]. T-cells show EphA1 receptor expression in the blood, thymus gland, and lymph organs [136]. Whether central or memory cells, T-cells in the blood show expression of EphA1 receptors at both the RNA and protein levels [137].

Mycobacterium tuberculosis (*Mtb*) resides within host phagocytes and granuloma tissue, even though it is not mandatory for an intracellular pathogen to do so. After exposure to and infection by aerosol droplets containing these bacteria, *Mtb* is phagocytosed by macrophages [138]. Macrophages are the first line of defense against *Mtb* in the lungs. They engulf the *Mtb* after encountering the pathogen [139]. Ingestion of bacteria by the macrophages activates the inflammatory response by stimulating the TLR ligands on the bacterial wall's surface., these macrophages are invaded by mycobacteria, amplifying the immune response by releasing chemokines to recruit other macrophages in the lung tissue and monocytes in the blood circulation, redirecting them to the lung's infected area [140]. Simultaneously, *Mtb* triggers an intracellular signaling cascade in macrophages, which works as a defense mechanism against the bacteria through oxidative stress and cytokines secretion. The phagocytic and lysosome particles in the macrophages are attached to acidic phagolysosomes for disposal, but protective mechanisms for disrupting the completion of phagocytosis have evolved in mycobacteria [141]. Mycobacteria can escape from phagosomes and reach the cytosols of invaded cells [6]. This escape accelerates macrophage death by necrosis and leads to an increase in bacterial growth [142].

A previous study indicated the induction of EphA1, EphA2, and EphrinA1 gene expressions after mouse macrophages were infected with *Mtb* [130]. Since these receptors have an essential role in many cells (including immune cells), they may also have a crucial role in human macrophages. To study the role of these receptors in human macrophages, we examined the expression of EphA1, EphA2, and EphrinA1 genes in human monocytes

(i.e., THP-1 cells) after differentiation and infection with *Mtb*. Transcript levels were evaluated using a quantitative real-time PCR (qRT-PCR). To address the role of EphA1 in THP-1 cells, we constructed a mutation in this gene using the CRISPR Cas9 technique and an EphA1 knockout THP-1 cell line (EphA1-KO THP-1). We compared the wild-type THP-1 cells with the EphA1-KO THP-1 cells using post-infection RNA-Seq analysis with *Mtb* to detect the upregulated and downregulated genes and estimate the pathways related to the stimulation of this receptor. These data show the importance of Eph receptor and its link to the rest of the genes and other gene pathways after infection induction with *Mtb*. This topic was previously analyzed in mouse macrophages [130]. Herein it is clarified in human macrophages.

Materials and Methods

Human cells and culture conditions

THP-1 cells (human monocytes) (ATCC TIB-202) were cultured in six-well plates at a density of 2 x 10^6 cells/well with Roswell Park Memorial Institute (RPMI) medium (Quality Biological) supplemented with 10% heat-inactivated fetal bovine serum, 100 mM phorbol 12-myristate 13-acetate (PMA) for 48 h to differentiate the cells to macrophages. After resting the cells for 24 hr they were treated with 50 units/ml of human INFγ (Roche Diagnostics GmbH) plus 0.2 μg/ml of lipopolysaccharide (E.coli LPS; SIGMA) for 6 h to activate them [143].

Bacterial strains and culture conditions

M. tuberculosis strain mc^27000 was grown from the frozen stocks of bacteria that were stored at -80°C was grown in 7H9 broth (Difco) enriched with 0.5% glycerol, 0.25% Tween-80, 24 μg/ml pantothenate, 0.2% of casamino acid, and 10% albumin dextrose complex (ADC). The *M. tuberculosis* mc^27000 was cultured at 37°C for three to four weeks. Bacterial cultures were grown until an optical density (OD) 600 nm of ~1.0. The quantity of viable bacteria was determined by plating serial dilutions for determination of Colony-Forming Unit (CFU) using 7H9 agar enriched with 0.5% glycerol, 24 μg/ml pantothenate, 0.2% of casamino acid, and 10% ADC [144, 145].

Macrophage infections

The differentiated and activated THP-1 cells were seeded in six-well plates at a density of 2 x 10^6 cells/well in RPMI medium supplemented with 10% heat-inactivated fetal bovine serum. These cells were infected with M. tuberculosis mc^27000 at a multiplicity of infection (MOI) of 100 (bacteria:cells) for 15 m, 30 m, 1 h, 2 h, and 4 h. The incubation temperature was 37°C in a 5% CO2 atmosphere. Extracellular bacteria were removed by washing twice with warm sterile phosphate-buffered saline (PBS) after 30 minutes of infection. For 1hr, 2hrs, and 4hrs of infection, fresh RPMI medium supplemented with 10% heat-inactivated fetal bovine serum was added to the infected cells in triplicate, which were then incubated for the remaining period of time at 37°C in 5% CO2. The infected THP-1 cells were treated with TRIzol (15596026; ambion) for mRNA isolation, or lysed with 0.1% Triton-X-100 for 10 minutes to enumerate the intercellular bacteria [146].

Total RNA extraction and qRT-PCR

Total mRNA extraction and qRT-PCR were performed as described previously [144]. Briefly, TRIzol reagent (15596026; ambion) was used to extract mRNA from the macrophages according to the manufacturer's instructions. The cDNA was synthesized from the isolated mRNA using the SuperScript III First-Strand kit (oligo-dt primers) (18080-051; Invitrogen). Then, qPCR was performed by using the primers for EphA1, EphA2, and EphrinA1. The quantity of mRNA for each gene was measured using SYBR Green and a PowerUp Master Mix (A25742; Applied Biosystems). The specific primers used in this qRT-PCR are listed in Table 1. Negative controls for the reaction were total RNA and without template (NTC). The relative expressions of EphA1, EphA2, and EphrinA1 were normalized to the endogenous control GAPDH gene using the $2^{-\Delta\Delta Ct}$ cycle threshold method. Calculation of fold induction was based on the Ct values to quantify transcript levels.

Construction of EphA1 knockout in THP-1 cells using CRISPR Cas9

We constructed a knockout mutant in THP-1 cells. EphA1 mutant THP-1 cells were constructed and designed THP-1-EphA1-KO using a modified protocol, as described previously [121, 144]. We used the CRISPR Cas9 to generate the mutation employing the Lipofectamine 3000 (L3000-008; Invitrogen) to produce the lentivirus; the procedure was completed per the manufacturer's instructions. Day 1, 2 x 10^6 cells/well were plated in each well of the six-well plate (four wells Eph and one well control - no plasmid) for 24 h with a DMEM medium. The DMEM medium was replaced with a lentiviral packaging medium (1 ml) before transfecting by an hour. The components of the lentiviral packaging

medium were 1) 237 ml of Opti-MEM I reduced serum medium, 2) GlutaMAX supplement (2.5 ml), 3) FBS 12.5 ml, and 4) 500 µl of sodium pyruvate (100 mM). LentiCas9-EGFP (Addgene 63592), EphA1 sgRNA (Addgene 75589; the sequence CGA CTC ACC TCG ATC CAC AT (Exon 10)), and EphA1 sgRNA (addgene-75591; the sequence AAG CCC AAA ATG GAG TGT CA (Exon 6)) plasmids were used for lentivirus production.

After 24 h, 90% of the confluent lenti-x cells were transfected in the Opti-MEM medium, using two tubes for each well. Tube 1 had Opti-MEM 250 µl and 7 µl Lipofectamine 3000 (put in at the last minute before the mix and valid for 15 minutes in the Opti-MEM). Tube 2 had 250 µl Opti-MEM, 2 µg of plasmid for the Cas9 or gRNA for each gene, 1 µg PMD2-G plasmid, 1.5 µg pPAX-2 plasmid, and 6 µl P 3000 reagent. After transferring Tube 1 to Tube 2, the contents were mixed and incubated for 15 minutes at room temperature. The transfection mixture was then added to the lenti-x packaging cell. Then, 0.5 ml of the transfection mixture was added to each well in a dropwise fashion, with care being taken not to dislodge the cells.

After 16 h, the media were changed to the DMEM medium, 2 ml in each well. After 48 hours, the viral supernatant was removed and centrifuged for 10 min at 300 x g at room temperature. 1 ml of the viral supernatant of each plasmid was used to transduce 3 x 10^5 THP-1 cells. Polybrene (TR-1003-G; Sigma-Aldrich) was added in a quantity of 8 µg/ml and centrifuged at 1,170 x g for 1 h at 37°C. Then, the THP-1 cells were incubated at 37°C. After 48 h, the second viral supernatant was removed and centrifuged for 10 min at 300 x g at room temperature. Next, 1 ml of the second viral supernatant of each plasmid

was used to transduce the THP-1 cells and 8 μg/ml of polybrene was added and centrifuged at 1,170 x g for 1 h at 37°C. The THP-1 cells were then incubated at 37°C. After 24 h, the media of the THP-1 cells were changed to RPMI media (with a penicillin and streptomycin antibiotics) and incubated at 37°C. After another 24 h, the media of the THP-1 cells were changed to RPMI media (with a penicillin and streptomycin antibiotics plus 5 ng/ml of Blastcidin or 0.5 ng/ml of Puromycin) and incubated at 37°C. After an additional two days, the media of the THP-1 cells were again changed with RPMI media (with a penicillin and streptomycin antibiotics antibiotics) and incubated at 37°C. After seven days of resting, the media of the THP-1 cells were changed with the RPMI media (with a pen strep antibiotic plus 5 ng/ml of Blastcidin or 0.5 ng/ml of Puromycin) and incubated at 37°C. At the final 48 h, the media of the THP-1 cells were changed with the RPMI media (with a penicillin and streptomycin antibiotics) and incubated at 37°C.

Viability of Mycobacterium tuberculosis

The differentiated and activated wild-type and EphA1-KO-THP-1 cells (12 wells for each type of cells) were seeded in 24-well plates at a density of 5 x 10^5 cells/well in RPMI medium supplemented with 10% heat-inactivated fetal bovine serum. Twelves autoclaved coverslips were put in the well-plate for staining the cells after 12 days of infection. These cells were infected with *Mtb* $mc^2$7000 at a multiplicity of infection (MOI) of 1 (bacteria:cells) for 30 m, 6 days, and 12 days. The incubation temperature was 37°C in a 5% CO2 atmosphere. Extracellular bacteria were removed by washing twice with warm sterile phosphate-buffered saline (PBS) after 30 minutes of infection. For 6 and 12 days, fresh RPMI medium supplemented with 10% heat-inactivated fetal bovine serum

was added to the infected cells in triplicate, which were then incubated for the remaining period of time at 37°C in 5% CO2, and were replaced every 4 days. The *M. tuberculosis* $mc^2$7000 that was used for THP-1 cells infection was cultured at 37°C for three to four weeks. Bacterial cultures were grown until an optical density (OD) 600 nm of ~0.01. The quantity of viable bacteria was determined by plating serial dilutions for determination of Colony-Forming Units (CFU) using 7H9 agar enriched with 0.5% glycerol, 24 µg/ml pantothenate, 0.2% of casamino acid, and 10% ADC.

RNA-Seq

Transcriptome analysis was assessed by mRNA-Seq using 3'-TagSeq sequencing for single-end reads of 100 nucleotides (nt) in length. Bioinformatics analyses were performed using Texas A&M High Performance Research Computing. Trimmomatic program was used for trimming the raw reads from the adaptor contamination and Illumina adaptors used while sequencing [144]. The end reads were evaluated with a per base sequence quality score; reads with scores less than 30 and shorter than 20 bp were not taken. The selected end reads were mapped to the human genome and aligned and spliced using the STAR mapper program [145, 146]. An HTSeq tool was applied to count the transcripts mapped to the gene exon features [147]. The EdgeR package in the R statistical platform was employed to compare the reads count data [148]. Genes that expressed less than 1 million reads (< 1 CPM) were not counted in the data analysis. Variations in library sizes were estimated, relying on the normalization factors. Dispersion estimation for the reads was performed to correct the batch effects. These effects were reduced using an EdgeR package [149]. The likelihood ratio test (LRT) function was applied to evaluate the

expression values among the treatment libraries. The top tag of the tables was applied for the interruption and pathway analyses. Thresholds of an adjusted p-value < 0.05 and log2FC value were used to obtain differential expression of genes (DEGs). We determined the differential gene expression between the uninfected and infected cells at different time points utilizing Limma, an open source R-based software package. The GO category enrichment analysis for the DEGs was completing using WebGestalt. The Ingenuity Pathway Analysis platform (IPA, QIAGEN Inc.) was performed to complete the top tag differential expression pathway analyses. The genes that were selected in the pathway analyses had false discovery rate (FDR) values < 0.05 and logFC > 2 and also to identify significant canonical pathways and network activation and their respective roles in molecular and cellular functions in the upregulated and downregulated directions. The IPA platform was used to execute the comparative analyses of the results of the pathway core analyses.

Confirmation of RNA-Seq analysis via qRT-PCR

RNA-Seq data were confirmed for 12 selected genes using quantitative real-time PCR, with GAPDH as a housekeeping gene. The same samples that used for transcriptomic analysis were used in this qRT-PCR. The primers used in this study are listed in Table 1. The quantity of mRNA for each gene was measured using SYBR Green utilizing a PowerUp Master Mix (A25742; Applied Biosystems). The reactions were performed in 10 ul reaction volume containing 0.25 ul of each primer (10 μM), 5 ul of 2x SYBR Green PowerUp Master Mix, and 4.5 ul cDNA (80 ng). The qRT-PCR reactions were completed using Applied Biosystem plus instrument (StepOnePlus Real-Time PCR

System). Negative controls for the reaction were the total RNA and without template (NTC). The comparative Ct ($2^{-\Delta\Delta Ct}$) method was applied to calculate the relative expression, normalized to the reference GAPDH gene.

Table 1. Primers that were used in RT-qPCR.

Gene name	Forward primer	Reverse primer
EphA1	ATCTTTGGGCTGCTGCTTGG	GCTTGTCCTCTCGATCCACATC
EphA2	GGCAGGAGTTGGCTTCTTTAT	GGGCTTCAGTTGTTCTGACTT
EphrinA1	TCAAAGAAGGACACAGCTACTAC	CCTGAGGACTGTGAGTGATTT
GAPDH	CCAGGTGGTCTCCTCTGACTT	GTTGCTGTAGCCAAATTCGTTGT
DUSP1	ACCACCACCGTGTTCAACTTC	TGGGAGAGGTCGTAATGGGG
EGR1	GGTCAGTGGCCTAGTGAGC	GTGCCGCTGAGTAAATGGGA
PSAT1	TGCCGCACTCAGTGTTGTTAG	GCAATTCCCGCACAAGATTCT
DUSP10	TGAAGCACACTCGGATGACC	CCTCGAACTCTAGCAACTGCC
SGK1	CATATTATGTCGGAGCGGAATGT	TGTCAGCAGTCTGGAAAGAGA
CLK1	AGAGACCATGAAAGCCGGTAT	CATGTGAACGACGATGTGAAGT
NFKBIA	ACCTGGTGTCACTCCTGTTGA	CTGCTGCTGTATCCGGGTG
RHCG	CCTCGGTGGCAATATCCAGTG	GAAGCCGATGATGAGGGCA
ANKRD44-IT1	TCGAGGGGTGTTTAATGAGC	CTGTCCTTCCCTTTTGTGGA
ANKS1A	CGTGGCTGACTCAAAAGGCT	GGCTGTCTCGTTGTCATTGTTC
AMPK	TTTGCGTGTACGAAGGAAGAAT	CTCTGTGGAGTAGCAGTCCCT
mTOR	TCCGAGAGATGAGTCAAGAGG	CACCTTCCACTCCTATGAGGC

Statistical analysis

The experimental data are presented as mean ± SE. The GraphPad Prism9 (GraphPad Software, Inc.) was used to do all statistical analysis. Statistical significance was determined using an ANOVA test. Differences were considered for p-values less than 0.05.

Results

RT- PCR, and qPCR to determine the mRNA levels of EphA1, EphA2 and EphrinA1 on wild-type THP-1 cells post-infection by Mtb mc27000

The EphA1, EphA2, and EphrinA1 expressions were determined at the mRNA level after macrophage infection with *Mtb*. Wild-type THP-1 cells (human monocytes) were differentiated and activated before infection with *Mtb* $mc^2$7000. The expressions of EphA1, EphA2, and EphrinA1 were determined in the THP-1 cells using qRT-PCR. The fold change of these genes was calculated by the difference in the average ratio of the genes to the GAPDH gene, and then normalized to uninfected controls The EphA1 transcript level increased 1-fold at 30 m and 3-fold increases at 4 h timepoint over the uninfected control in the wild-type THP-1 infected with active *Mtb* $mc^2$7000 (see Figure 2).

The expression of EphA2 was elevated 1-fold at 15 min and reached 2.5-fold after 4 h of infection (see Figure 3). The EphrinA1 expression was upregulated 1-fold over the uninfected control at 15 min and peaked at over 14-fold at 4 h of infection (see Figure 4). These data show that EphA genes and their ligand EphrinA1 expression were induced during the early stage of wild-type THP-1 cell infection with *Mtb* $mc^2$7000.

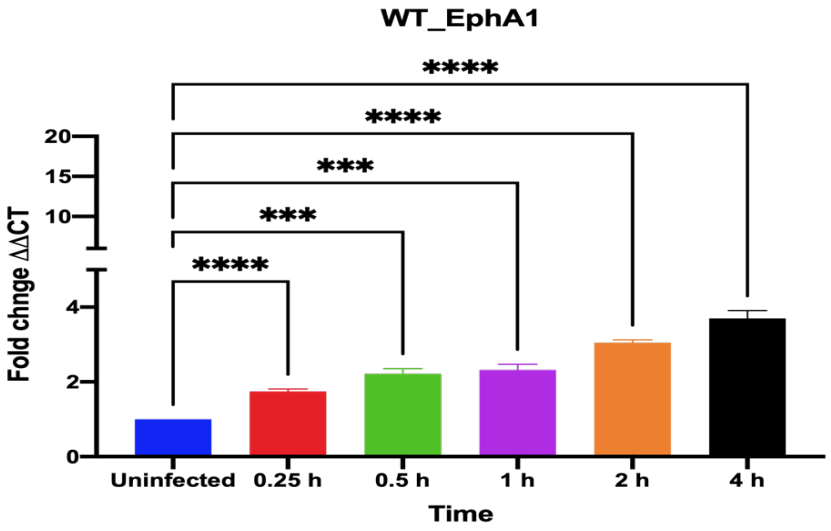

Figure 2. Transcript levels of EphA1 in wild-type THP-1 cells after *Mtb* infection. The EphA1 transcript levels were assessed in different time points (0.25, 0.5, 1, 2, and 4 hrs) after infection by quantitative real-time PCR using total RNA. The transcript levels were calculated relative to GAPDH control housekeeping gene values are expressed to fold change in gene expression for infected cells compared to uninfected controls. Errors bars represent the slandered errors from the means of three independent experiments. *, $P < 0.05$; **, $P < 0.01$; ***, $P < 0.001$; ****, $P < 0.0001$.

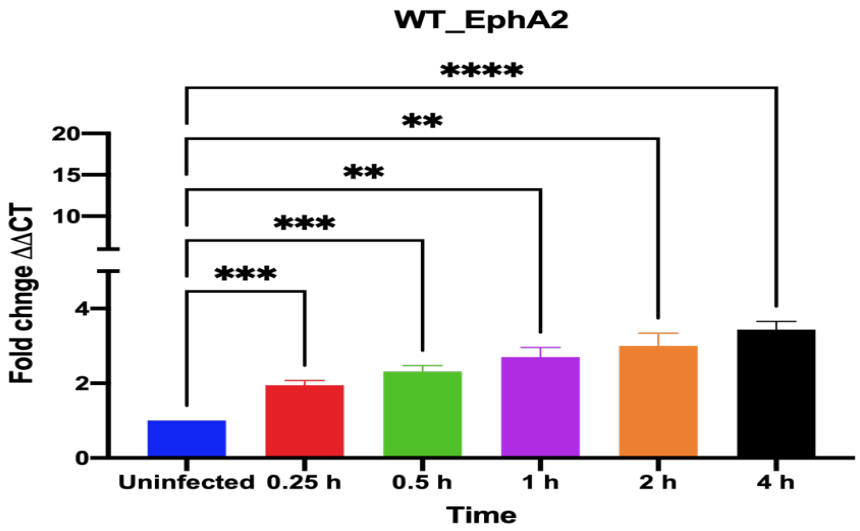

Figure 3. Transcript levels of EphA2 in wild-type THP-1 cells after Mtb infection. The EphA2 transcript levels were assessed in different time points (0.25, 0.5, 1, 2, and 4 hrs) after infection by quantitative real-time PCR using total RNA. The transcript levels were calculated relative to GAPDH control housekeeping gene values are expressed to fold change in gene expression for infected cells compared to uninfected controls. Errors bars represent the slandered errors from the means of three independent experiments. *, P < 0.05; **, P < 0.01; ***, P < 0.001; ****, P < 0.0001.

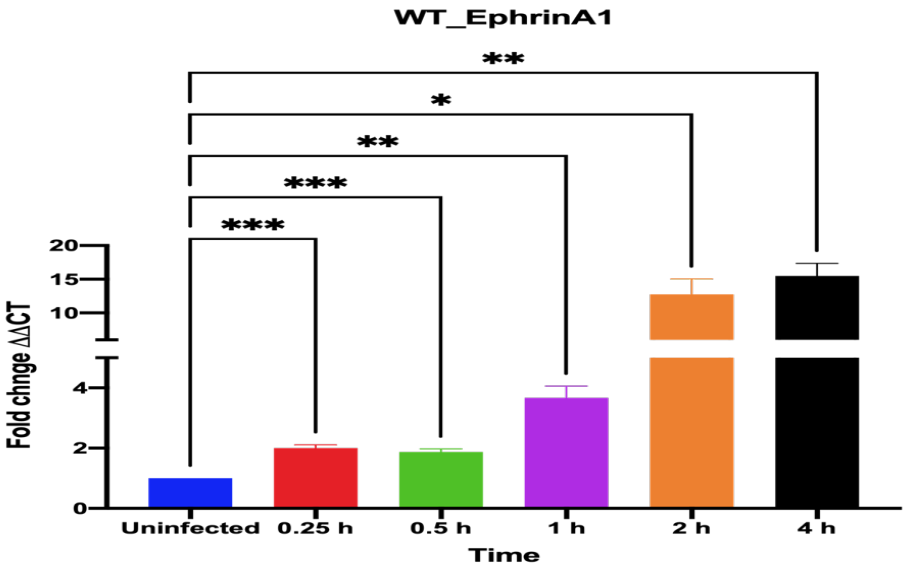

Figure 4. Transcript levels of EphrinA1 in wild-type THP-1 cells after *Mtb* infection. The EphrinA1 transcript levels were assessed in different time points (0.25, 0.5, 1, 2, and 4 hrs) after infection by quantitative real-time PCR using total RNA. The transcript levels were calculated relative to GAPDH control housekeeping gene values are expressed to fold change in gene expression for infected cells compared to uninfected controls. Errors bars represent the slandered errors from the means of three independent experiments. *, P < 0.05; **, P < 0.01; ***, P < 0.001; ****, P < 0.0001.

Construction and confirmation of an EphA1 mutant by CRISPR/Cas9 mutagenesis

The CRISPR/Cas9 applied lentiCas9-EGFP (addgene 63592) vector, sgRNA (addgene 75589) vector, and (addgene-75591) vector to the THP-1 cells. The sgRNA for the EphA1 gene were CGA CTC ACC TCG ATC CAC AT (Exon 10) and AAG CCC AAA ATG GAG TGT CA (Exon 6) (sgRNA sequences). The off-target of these sgRNA were checked on the Chop-Chop website: first, sgRNA target bases 6182 to 6201, and second, sgRNA target bases 1565 to 1584. The loci of both the wild and mutant cell lines were PCR-cloned and sequenced. The alignment showed fragment of exon 6 has deletion of nucleotides 1574 to 1581 in the cells that treated with CRISPR-Cas9. The sequences of the WT-THP-1 and EphA1-KO-THP-1 are shown in Figure 5.

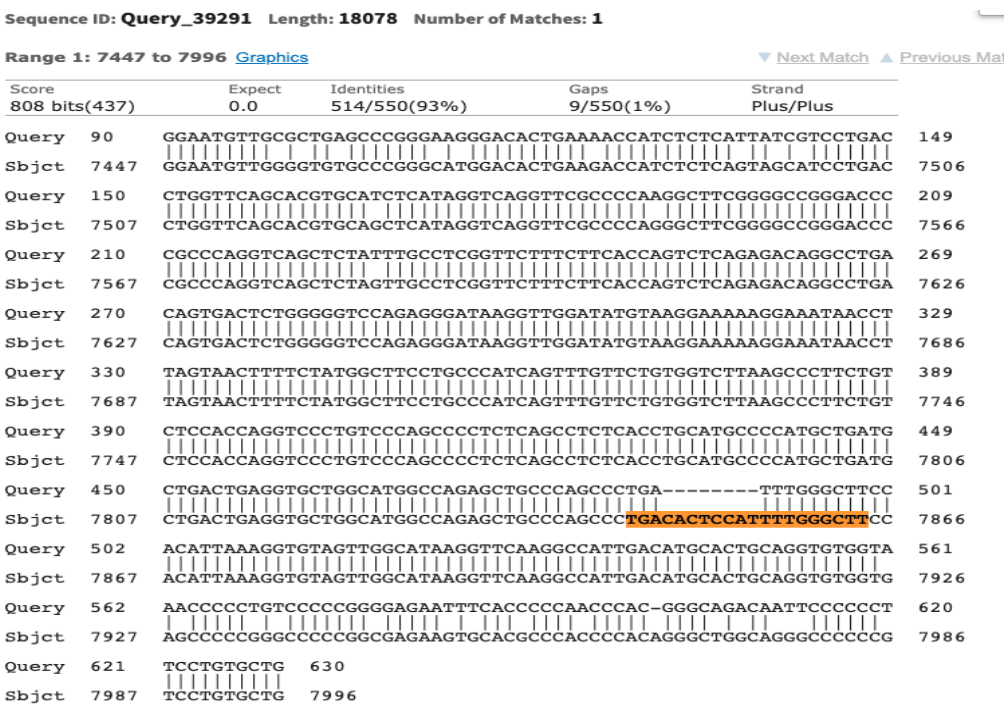

Figure 5. CRISPR guide RNA (gRNA) targets (Orange) targets bases 1565 to 1584. The alignment showed fragment of exon 6 has a deletion of nucleotides 1574 to 1581 in the cells that treated with CRISPR-Cas9.

RT- PCR, and qPCR to determine the mRNA levels of EphA1, EphA2 and EphrinA1 on EphA1-KO THP-1 cells post-infection by Mtb $mc^2$7000

To determine the EphA1, EphA2, and EphrinA1 expressions at the mRNA level post-infection, EphA1 knockout THP-1 cells (EphA1-Ko-THP-1 cells) were differentiated and then activated prior to infection. Expression of the EphA1 gene in the EphA1-Ko-THP-1 cells decreased after infection with *Mtb* $mc^2$7000 (see Figure 6). The expression of EphA2 increased 1-fold at 15 min and reached over 3.5-fold after 4 h of infection of the EphA1-Ko-THP-1 cells (see Figure 7). The EphrinA1 expression was upregulated 1-fold compared to the uninfected control at 15 min, and peaked at over 12-fold at 4 h of infection of the EphA1-Ko-THP-1 cells (see Figure 8). These data indicate that the EphA2 gene and its ligand EphrinA1 expression were induced during the early stage of the EphA1-Ko-THP-1 cell infection. The EphA1 gene induction failed due to the knockout gene from the EphA1-Ko-THP-1 cells. The EphA2 expression increased in the EphA1-KO-THP-1 cells more than in the wild-type THP-1 cells at 4 h, indicating compensatory expression due to reduction of EphA1 expression (see Figure 10).

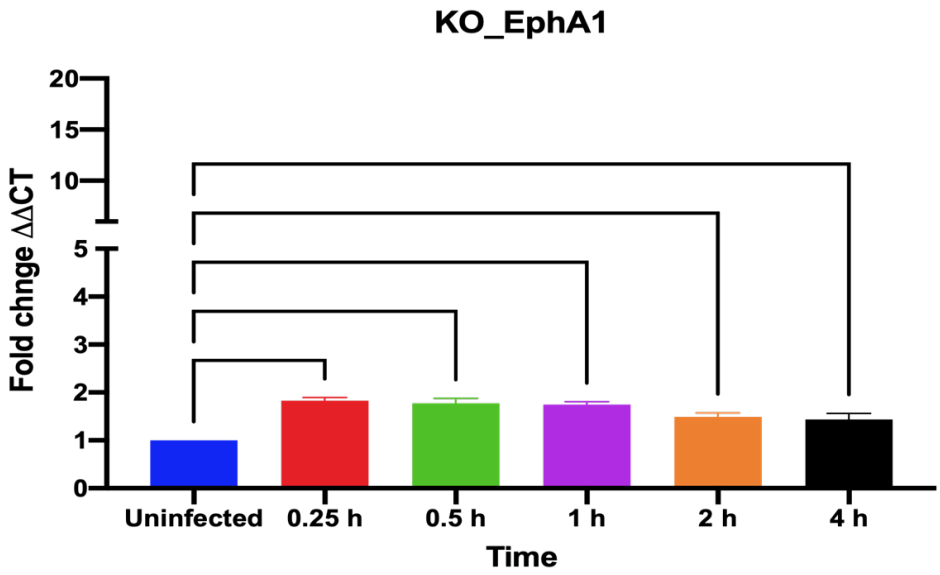

Figure 6. Transcript levels of EphA1 in EphA1-KO THP-1 cells after *Mtb* infection. The EphA1 transcript levels were assessed in different time points (0.25, 0.5, 1, 2, and 4 hrs) after infection by quantitative real-time PCR using total RNA. The transcript levels were calculated relative to GAPDH control housekeeping gene values are expressed to fold change in gene expression for infected cells compared to uninfected controls. Errors bars represent the slandered errors from the means of three independent experiments. *, P < 0.05; **, P < 0.01; ***, P < 0.001; ****, P < 0.0001.

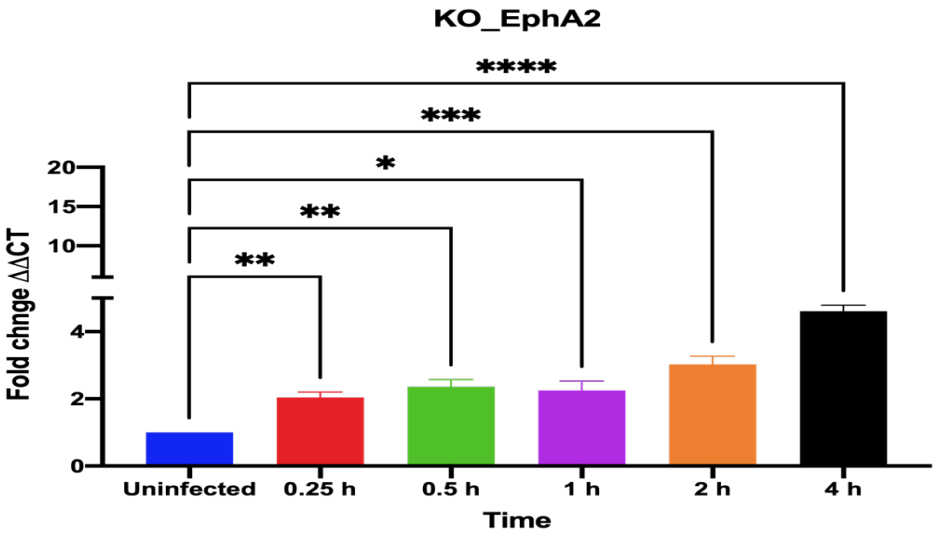

Figure 7. Transcript levels of EphA2 in EphA1-KO THP-1 cells after *Mtb* infection. The EphA2 transcript levels were assessed in different time points (0.25, 0.5, 1, 2, and 4 hrs) after infection by quantitative real-time PCR using total RNA. The transcript levels were calculated relative to GAPDH control housekeeping gene values are expressed to fold change in gene expression for infected cells compared to uninfected controls. Errors bars represent the slandered errors from the means of three independent experiments. *, P < 0.05; **, P < 0.01; ***, P < 0.001; ****, P < 0.0001.

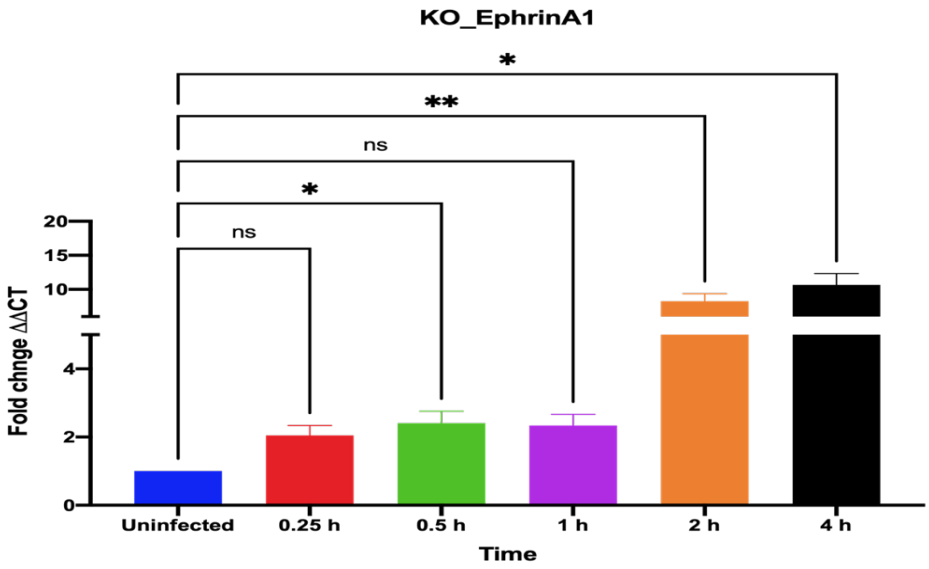

Figure 8. Transcript levels of EphrinA1 in EphA1-KO THP-1 cells after Mtb infection. The EphrinA1 transcript levels were assessed in different time points (0.25, 0.5, 1, 2, and 4 hrs) after infection by quantitative real-time PCR using total RNA. The transcript levels were calculated relative to GAPDH control housekeeping gene values are expressed to fold change in gene expression for infected cells compared to uninfected controls. Errors bars represent the slandered errors from the means of three independent experiments. *, P < 0.05; **, P < 0.01; ***, P < 0.001; ****, P < 0.0001.

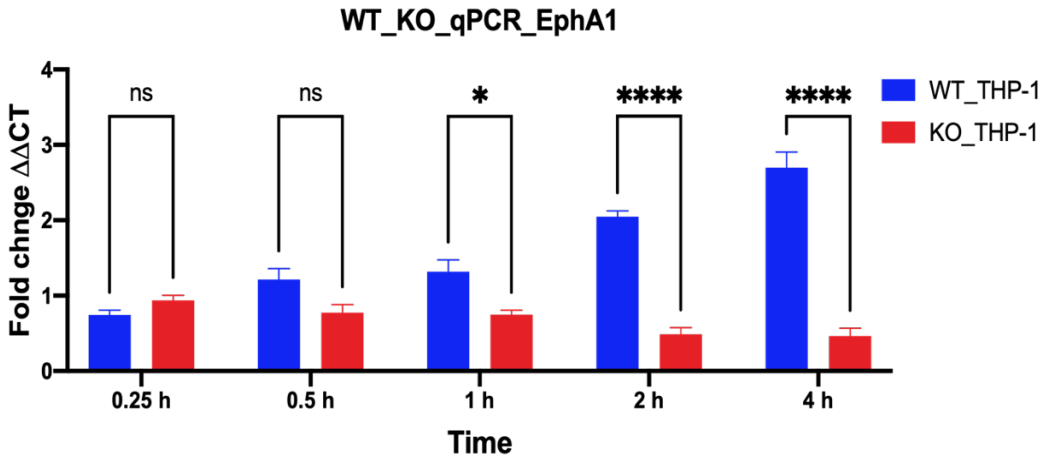

Figure 9. Comparison the transcript levels of EphA1 in wild-type and EphA1-KO THP-1 cells after *Mtb* infection. The EphA1 transcript levels were assessed in different time points (0.25, 0.5, 1, 2, and 4 hrs) after infection by quantitative real-time PCR using total RNA. The transcript levels were calculated relative to GAPDH control housekeeping gene values are expressed to fold change in gene expression for infected cells compared to uninfected controls. Errors bars represent the slandered errors from the means of three independent experiments. *, P < 0.05; **, P < 0.01; ***, P < 0.001; ****, P < 0.0001.

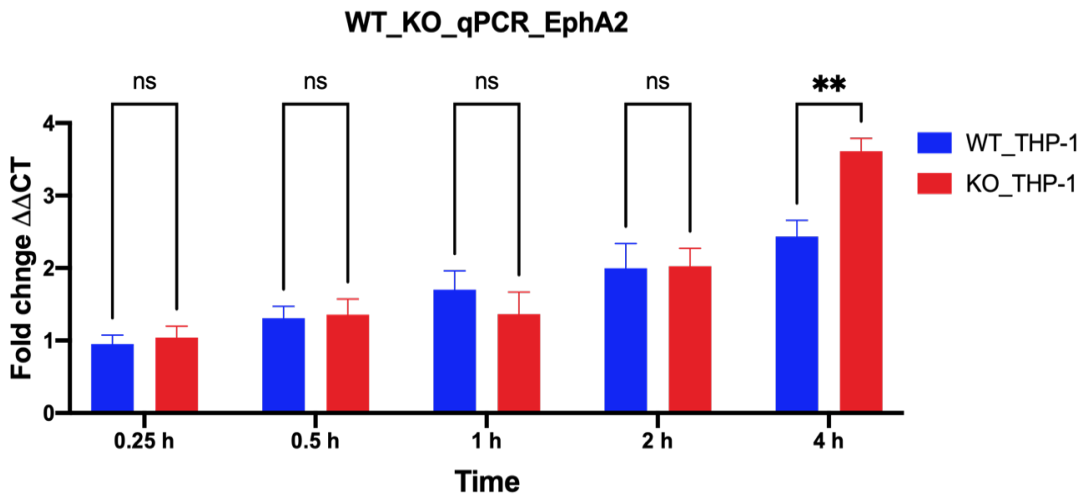

Figure 10. Comparison the transcript levels of EphA2 in wild-type and EphA1-KO THP-1 cells after *Mtb* infection. The EphA2 transcript levels were assessed in different time points (0.25, 0.5, 1, 2, and 4 hrs) after infection by quantitative real-time PCR using total RNA. The transcript levels were calculated relative to GAPDH control housekeeping gene values are expressed to fold change in gene expression for infected cells compared to uninfected controls. Errors bars represent the slandered errors from the means of three independent experiments. *, P < 0.05; **, P < 0.01; ***, P < 0.001; ****, P < 0.0001.

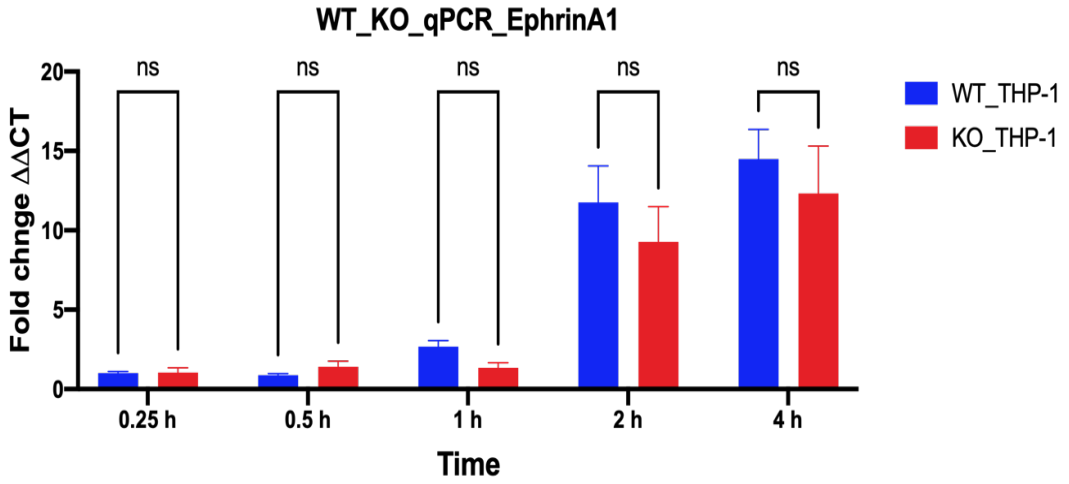

Figure 11. Comparison the transcript levels of EphrinA1 in wild-type and EphA1-KO THP-1 cells after *Mtb* infection. The EphrinA1 transcript levels were assessed in different time points (0.25, 0.5, 1, 2, and 4 hrs) after infection by quantitative real-time PCR using total RNA. The transcript levels were calculated relative to GAPDH control housekeeping gene values are expressed to fold change in gene expression for infected cells compared to uninfected controls. Errors bars represent the slandered errors from the means of three independent experiments. *, P < 0.05; **, P < 0.01; ***, P < 0.001; ****, P < 0.0001.

Viability of Mtb in EphA1-KO-THP-1 cells

To identify the viability of *Mtb* in EphA1-Ko-THP-1 cells, *M. tuberculosis* $mc^{2}7000$ was used to infect WT-THP-1 and EphA1-KO-THP-1 cells. The cells were infected at 30 minutes, 6 and 12 days. The quantity of intracellular *Mtb* in these cells showed no significant differences at 30 m and 6 days after infection, whereas the number of bacteria showed elevation in the WT-THP-1 cells after 12 days of infection (see Figure 12).

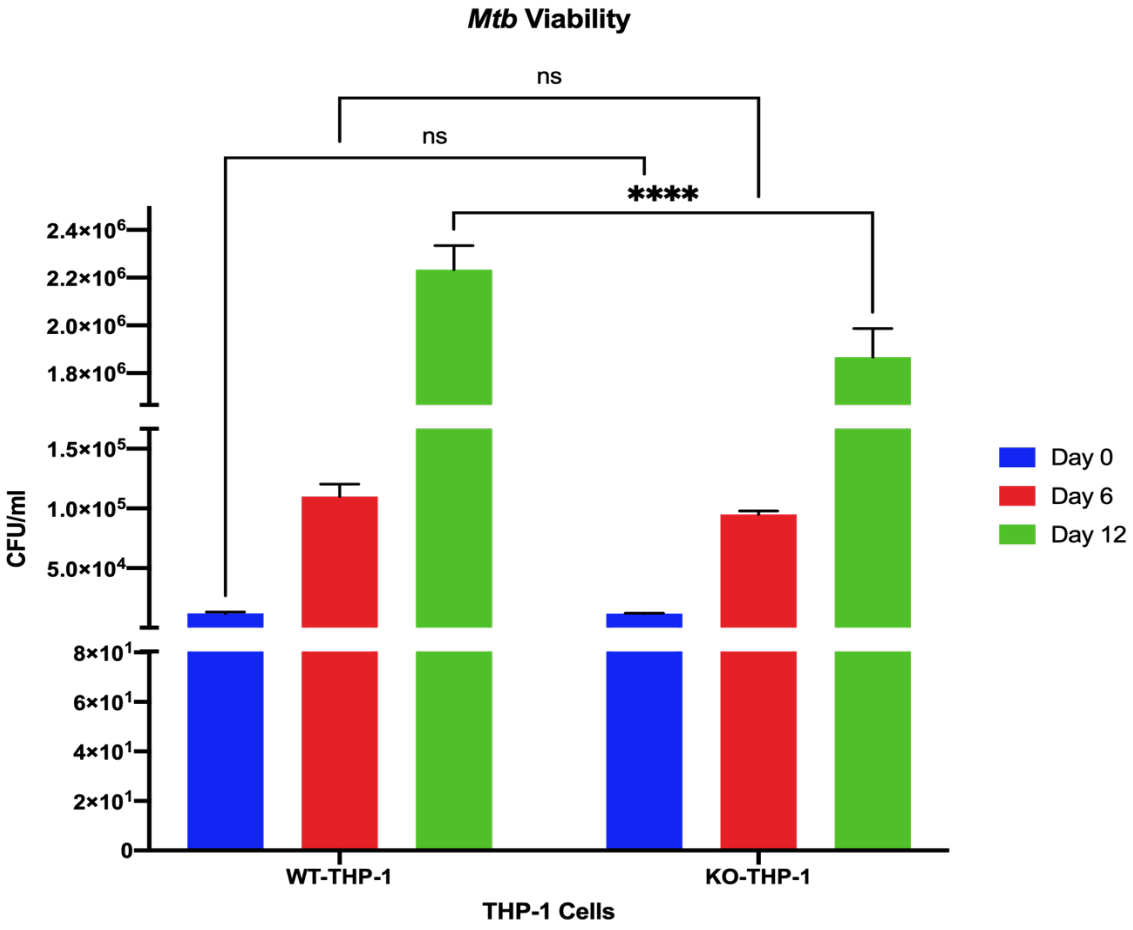

Figure 12. Infection of WT-THP-1 and EphA1-KO-THP-1 cells by *Mycobacterium tuberculosis* at different incubation times

RNA-Seq analysis of the EphA1-KO THP-1 cells compared to the wild-type macrophages with Mtb

To identify the molecular changes and measure gene expression in the wild-type THP-1 (WT-THP-1) and mutant EphA1-KO-THP-1 cells after infection with *Mtb*, an RNA-Seq analysis was performed. Six samples from each time point (15 m, 30 m, 1 hr, 2 hrs, and 4 hrs) were compared to uninfected cells in WT-THP-1 and mutant THP-1 cells after infection with *Mtb* (see Figure 13). After calculation of the gene expression levels and filtering out unexpressed genes, 18,182 genes remained.

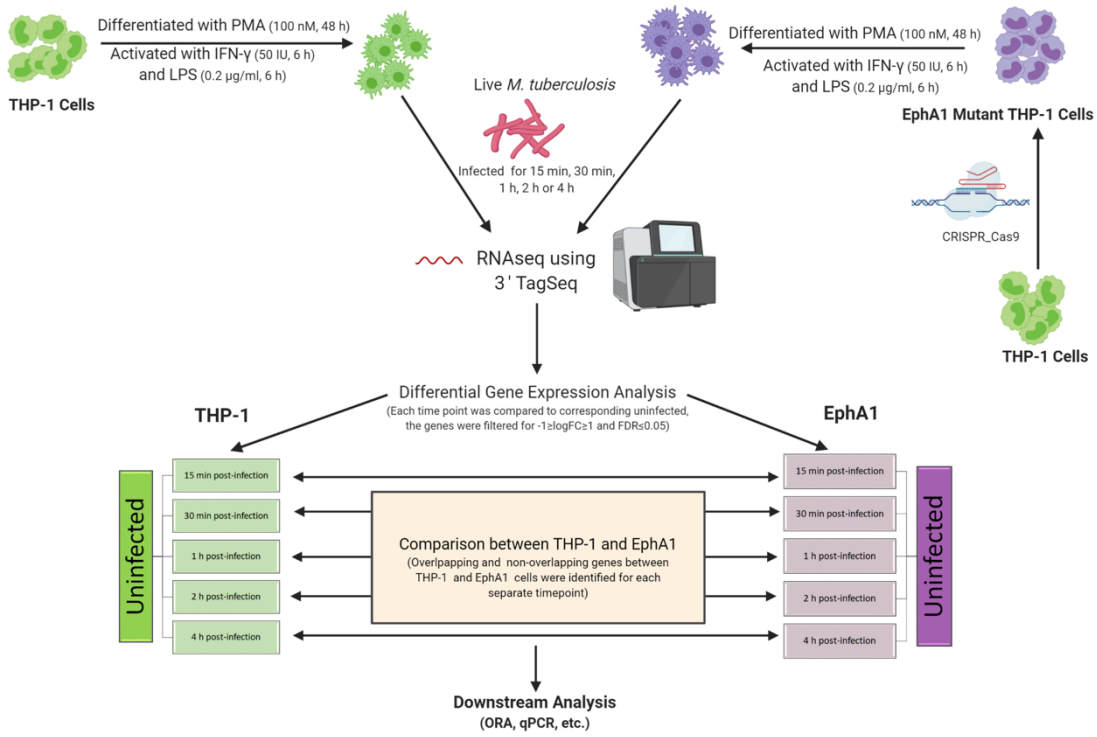

Figure 13. Schematic of RNASeq for the wild type and EphA1-KO THP-1 cells after *Mtb* infection.

a- Infection of Wild-type THP-1 cells with M. tuberculosis induced genes expression

The analysis of RNA-Seq indicated the number of upregulated and downregulated genes in different time point of infection in WT-THP-1 cells are showing in Table 2. The number of differentially expressed genes increased from 227 during first 30 minutes to 904 genes at 4 hrs after *Mtb* infection compared with uninfected THP-1 cells.

Table 2. Number of upregulated and downregulated genes in different time point of infection with *Mtb* in WT-THP-1 cells

Time point	Upregulated genes	Downregulated genes	Total
15 minutes	0	0	0
30 minutes	15	212	227
1 hour	51	12	63
2 hours	184	61	245
4 hours	569	335	904

The Ingenuity Pathway Analysis (IPA) classified the DEGs to many annotated molecules in different time point as shows in Table 3.

Table 3. Classification of DEGs to canonical pathways at various time points of infection with *Mtb* in WT-THP-1 cells

Time point	Top five Canonical Pathways
15 minutes	0
30 minutes	Oxidative Phosphorylation Mitochondrial Dysfunction EIF2 Signaling Clathrin-mediated Endocytosis Signaling Systemic Lupus Erythematosus Signaling
1 hour	HMGB1 Signaling Erythropoietin Signaling Regulation of IL-2 Expression in Activated and Anergic T Lymphocytes Corticotropin Releasing Hormone Signaling Thrombopoietin Signaling
2 hours	Unfolded protein response Inhibition of Angiogenesis by TSP1 NRF2-mediated Oxidative Stress Response Coronavirus Pathogenesis Pathway Endoplasmic Reticulum Stress Pathway
4 hours	Assembly of RNA Polymerase II Complex NRF2-mediated Oxidative Stress Response Senescence Pathway Induction of Apoptosis by HIV1 Pancreatic Adenocarcinoma Signaling

Molecules participated in canonical pathways were identified in each time point compared to uninfected cells that were significant based on P-value and Z-score (Table 1). Post 30 minutes of infection, Coronavirus Pathogenesis Pathway was the most activated pathway. FOS was upregulated while RPS10, RPS15A, and RPS28 genes were downregulated. The top inhibited pathway was Oxidative Phosphorylation, involving six genes, COX6A1, NDUFA11, NDUFA13, NDUFB8, SDHC, and UQCR11, all of which were upregulated.

At one hour after infection, HMGB1 Signaling pathway was the top activated pathway with five upregulated genes included in this pathway, FOS, JUN, OSM, RHOB, and TGFB1. In contrast, the inhibited pathway at that time point was ERK/MAPK Signaling, relying on DUSP1, DUSP2, DUSP4 genes that were downregulated, and FOS gene which was upregulated.

After two hours of infection, the NRF2-mediated Oxidative Stress Response pathway was the activated pathway with highest Z-score and involved DNAJB2, DNAJB9, HERPUD1, JUN, JUND, MAFF, MAFG, and SQSTM1 genes that showed upregulation pattern, whereas inhibited pathway was p38 MAPK Signaling with two downregulated genes, DUSP1, DUSP10, and three upregulated genes, DDIT3, TGFB1, and TIFA.

At the end of infection, four hours, the top activated pathway was NRF2-mediated Oxidative Stress Response, containing DNAJB1, DNAJB2, DNAJB4, DNAJB9, EIF2AK3, HERPUD1, HMOX1, JUN, JUND, MAFG, MAP2K3, MGST2, PIK3CG, RAP1A, SQSTM1, and TXNRD1 genes that showed upregulation, and KEAP1 gene that showed downregulation. On the other side, Myc Mediated Apoptosis Signaling was the inhibited pathway encompassing upregulated genes ADRB2, CASP8, CASP9, and TNFRSF1A, and downregulated genes MDM2, NFKB2, and TRAF2.

b- Infection of EphA1-KO-THP-1 cells with M. tuberculosis induced genes expression

The results of RNA-Seq analysis identified the number of upregulated and downregulated genes in EphA1-KO-THP-1 cells in different time point of *Mtb* infection compared with uninfected as mentioned in (Table 4). The number of differentially

expressed genes increased from 1 at 15 minutes to 329 genes at 4 hrs after *Mtb* infection compared with uninfected EphA1-KO-THP-1 cells.

Table 4. Number of upregulated and downregulated genes in different time point of infection with *Mtb* in EphA1-KO-THP-1 cells

Time point	Upregulated genes	Downregulated genes	Total
15 minutes	1	0	1
30 minutes	113	155	268
1 hour	0	0	0
2 hours	73	26	99
4 hours	200	129	329

The Ingenuity Pathway Analysis (IPA) classified the DEGs to many annotated molecules in different time point as shows in (Table 5).

Table 5. Classification of DEGs to canonical pathways at various time points of infection with *Mtb* in EphA1-KO-THP-1 cells

Time point	#Top five of Canonical Pathways
15 minutes	0
30 minutes	EIF2 Signaling Oxidative Phosphorylation Mitochondrial Dysfunction Regulation of eIF4 and p70S6K Signaling Sirtuin Signaling Pathway
1 hour	0
2 hours	Induction of Apoptosis by HIV1 Protein Kinase A Signaling Hypoxia Signaling in the Cardiovascular System 4-1BB Signaling in T Lymphocytes IL-17A Signaling in Fibroblasts
4 hours	NRF2-mediated Oxidative Stress Response Death Receptor Signaling Induction of Apoptosis by HIV1 Apoptosis Signaling Necroptosis Signaling Pathway

Molecules participated in canonical pathways were identified in each time point compared to uninfected cells that were significant based on P-value and Z-score (Table 5. At 30 minutes of infection, the top activated pathway was EIF2 Signaling, effected by ten upregulated genes, EIF3F, RPL18A, RPL26, RPL3, RPL32, RPL6, RPS25, RPS27, RPS28, and RPS3A. Conversely, the top inhibited pathway was Coronavirus Pathogenesis Pathway, involving four genes, RPS25, RPS27, RPS28, and RPS3A that showed downregulation during this time point.

On the second hour of infection, Hypoxia Signaling in the Cardiovascular System was the activated pathway with highest Z-score and involved CREB5, NFKBIA, NFKBID, and VEGFA genes with upregulation pattern, while inhibited pathway was

Erythropoietin Signaling, the main genes influenced in this pathway were NFKBIA, NFKBID, OSM, and TNFSF9 that exposed down regulation in all genes.

After 4 hours of infection, NRF2-mediated Oxidative Stress Response pathway activated with downregulated MAF gene, but EIF2AK3, MAFG, PRKCH, and SQSTM1 were upregulated genes, excluding DNAJB2, DNAJB9, NQO2, PIK3CG genes were unclear if they were upregulated or down regulated in this pathway.

Downregulated BIRC3 gene and upregulated ACIN1, CASP10, CASP8, TNFRSF1A, and TNFSF10 are the genes that were inhibited in the Death Receptor Signaling pathway.

Gene enrichment analysis to compare between WT-THP-1 cells and EphA1-KO-THP-1 cells transcriptomes

Gene ontology (GO) and gene set enrichment analysis (GSEA) were performed for WT-THP-1 cells and EphA1-KO-THP-1 cells in most highly differentially expressed genes based on adjusted $P<0.05$ and $\log2FC>1$. We investigated the most pathways that induced prior to infection. We observed that genes differentially expressed in different time points. Those genes are involved in two major cellular components GO terms nucleus region and cell transporting compartment region figure 16 A. DEGs are clustered in two groups, figure 16 B, indicating an upregulated activity in cell cycle and division along with transporting activity at the cell membrane and extracellular region. It worth noting that chromosome compaction was detected giving the rise to potentially epigenetic changes.

Further analysis of data was performed using KEGG analysis, where genes enriched for KEGG pathways arranged according to significance as follow; Cytokine-

cytokine receptor interaction, cell cycle, Hematopoietic cell lineage, Viral protein interaction with cytokine and cytokine receptor, p53 signaling pathway, and Rheumatoid arthritis figure 17 A. The top five detected KEGG pathways according gene ratio involvement analysis revealed enriched genes in Herpes simplex virus 1 infection, Rheumatoid arthritis, Cell cycle, IL-17 signaling pathway, and Neutrophil extracellular trap formation figure 17 B. Clustering analysis demonstrates that genes were clustered in five groups and enriched for five pathways include Neutrophil extracellular trap formation, Cell cycle, IL-17 signaling pathway, Rheumatoid arthritis, and progesterone-mediated oocyst maturation figure 17 C. Interestingly, Cell cycle, progesterone-mediated oocyst maturation and Neutrophil extracellular trap formation pathways are mostly related with innate immune response. On the other hand, IL-17 signaling pathway, Rheumatoid arthritis and cytokine interactions are pathways are related with adaptive immune response (see Figure 17). Together, all these pathways are important in tuberculosis disease in general.

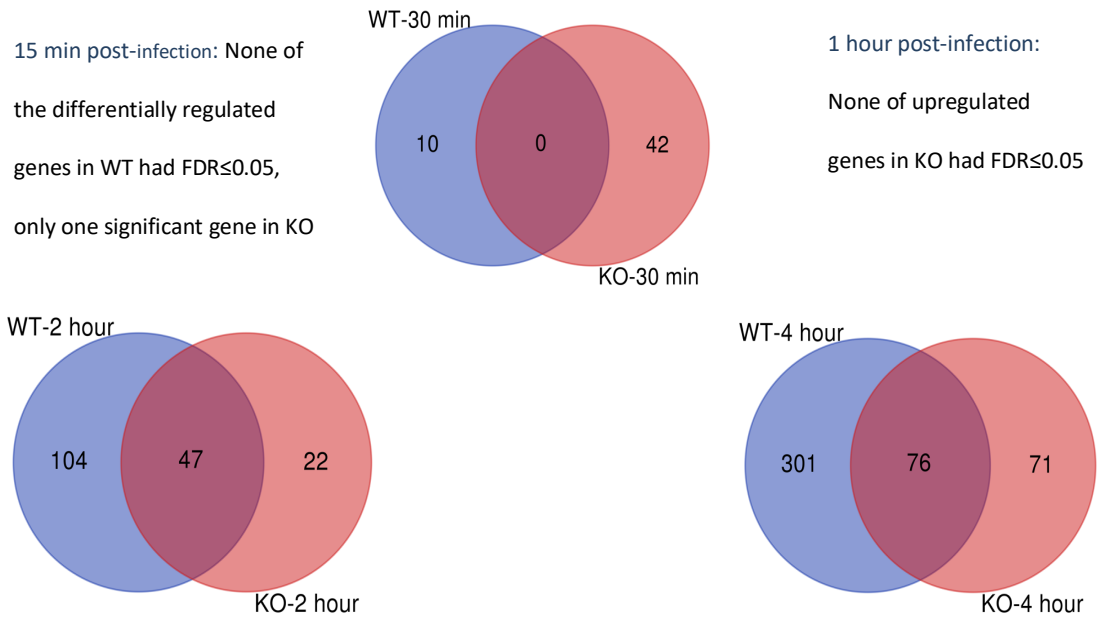

Figure 14. Overlap of differentially expressed upregulated genes between WT-THP-1 and EphA1-KO-THP-1 cells infected by *Mtb*.

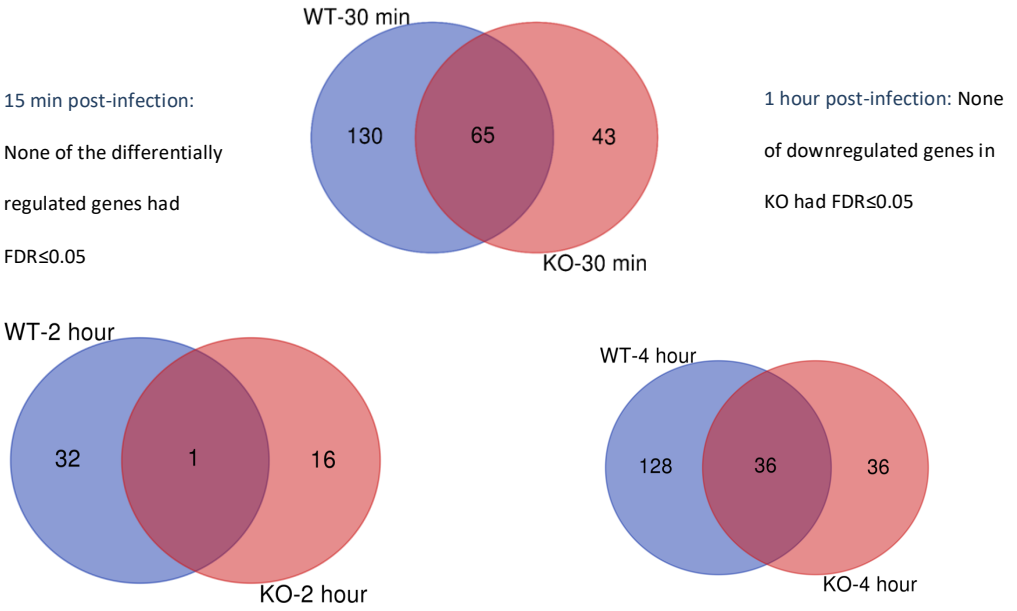

Figure 15. Overlap of differentially expressed downregulated genes between WT-THP-1 and EphA1-KO-THP-1 cells infected by *Mtb*.

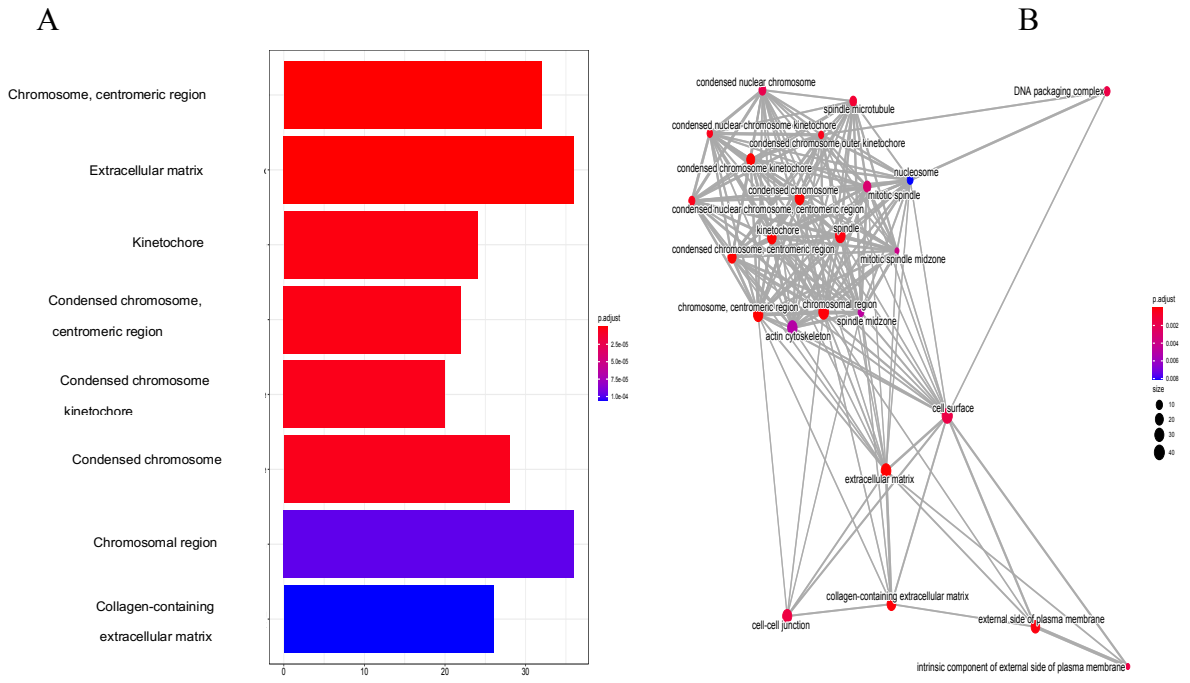

Figure 16. Gene ontology (GO) and gene set enrichment analysis (GSEA) for WT-THP-1 cells and EphA1-KO-THP-1 cells based on the most differentially expressed genes (P<0.05). (A) enriched cellular components. (B) DEGs clusters. Red and blue colors refer to the significance measure, most significant and significant respectively.

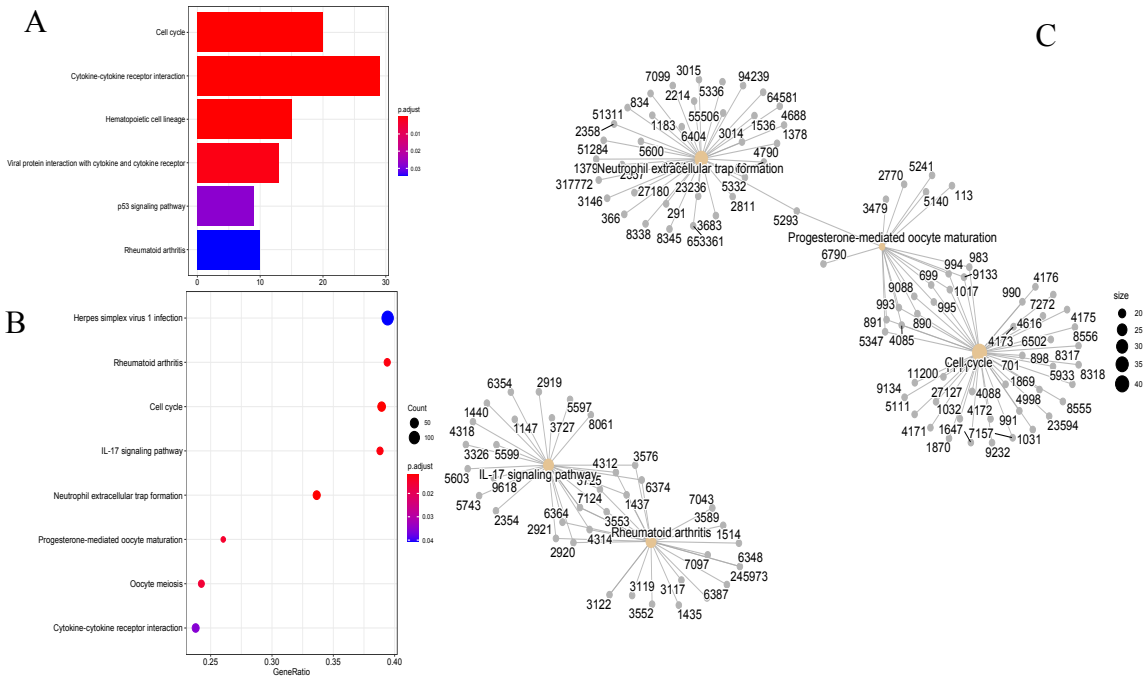

Figure 17. KEGG enrichment analysis on comparison between WT-THP-1 cells and EphA1-KO-THP-1 cells. (A) KEGG pathways arranged according to significance. (B) KEGG pathways according gene ratio involvement analysis. (C) DEGs clusters enriched in KEGG pathways. Red and blue colors refer to the significance measure, most significant and significant respectively.

qRT-PCR analysis of the 12 genes.

We selected 12 genes from DEGs (DUSP1, EGR1, PSAT1, DUSP10, SGK1, CLK1, NFKBIA, RHCG, ANKRD44-IT1, ANKS1A, AMPK, and mTOR) to validate the accuracy of RNASeq data. The results showed that these DEGs in wild-type THP-1 cells were similar to what was found in the RNASeq analysis. The expression levels of the DUSP1 gene were significantly increased 5-folds and 3-folds at the 1 and 2 hrs of infection respectfully, while decreased at 15 m, 30 m, and 4hrs of infection (see Figure 18). The EGR1 gene expression levels showed a significant increasing pattern at 30 m and 1 hr than 15 m, 2, and 4 hrs infected cells (see Figure 19). PSAT1 gene showed a little drop of expression at 2 and 4 hrs than at 30 m (1.5-fold change) (see Figure 20). Fold change of gene expression of the SGK1 gene was increased during 1 hr of infection; however, it decreased during other time points of infection (see Figure 21). DUSP10 gene expression was less than 2-fold at 15 and 30 m of infection but increased significantly at 1, 2, 4 hrs of infection (see Figure 22). CLK1 gene expression increased 4-folds through the 1 and 4hr, and it was significant compared to 30 m of infection (see Figure 23). NFKBIA gene expression increased significantly at 1 and 2 hrs more than at 15, 30 m, and 4 hrs (see Figure 25). A significant rise of RHCG gene expression was noticed at 2 and 4 hrs (15-folds and 12-folds, respectively), but not at 15m -1hr of infection (see Figure 29). ANKRD44-IT1, ANSKS1A, and mTOR gene expressions were decreased persistently from 15 m to 4 hrs of infection (see Figure 24, Figure 26, Figure 28). No significant changes were recorded in the expression of the AMPK gene at all time points of infection (see Figure 27).

Interestingly, we have observed that these differential expression genes, corresponding to this EphA1-KO THP-1 cells' RNASeq findings. The expression levels of the DUSP1 gene were significantly increased 3-folds and 5-folds at the 1 and 2 hrs of infection respectfully, while decreased at 15, 30 m, and 4hrs of infection (see Figure 18). The EGR1 gene expression levels showed a significant decreasing pattern starting at 2 and 4 hrs of infected cells (see Figure 19). PSAT1 gene showed higher expression at 1, 2, and 4 hrs (15-, 9-, and 10-folds respectively) than at 15 and 30 m of infection (see Figure 20). Fold change of gene expression of the SGK1 gene was increased during 1 hr of infection; however, it decreased during other time points of infection (see Figure 21). CLK1 gene expression increased 1.5-folds through 4 hrs of infection (see Figure 23). NFKBIA gene expression increased significantly at 2 and 4 hrs more than at 15, 30m, and 1 hr (see Figure 25). A significant rise of RHCG gene expression was noticed at 2 and 4 hrs (2-folds and 4-folds respectively), but not at 15m to 1hr of infection (see Figure 29). ANKRD44-IT1 and ANSKS1A gene expressions were decreased persistently from 15 m to 4 hrs of infection (see Figure 24, Figure 26). Expression of mTOR gene showed a significant decrease at 1 hr time less than all other timepoints (see Figure 28). No significant changes were noted in DUSP10 and AMPK genes' expression at all time points of infection (see Figure 22 and Figure 27).

Comparison between wild-type THP-1 cells and EphA1-KO THP-1 cells in gene expressions of the 12 genes after infection by *Mtb* showed differences and similarities at different time points. We noted higher expression of DUSP1 gene at 1 hr, while lower at 2 hrs in WT-THP-1 cells than EphA1-KO THP-1 cells (see Figure 18). EGR1 gene

expression was higher in EphA1-KO THP-1 cells than WT-THP-1 cells at 15 min, but no differences at the rest of the time points (see Figure 19). PSAT1 gene expression was significantly higher at 15 m, 1 h, 2 hrs, and 4 hrs in EphA1-KO THP-1 cells than WT-THP-1 cells (see Figure 20). Significantly, SGK1 gene expression was developed to be higher at 1 hr and 2 hrs in WT-THP-1 cells than EphA1-KO THP-1 cells (see Figure 21). DUSP10 and CLK1 gene expressions persistently were higher in WT-THP-1 cells than EphA1-KO THP-1 cells at 1 hr, 2 hrs, and 4 hrs of infection (Figure 22 and Figure 23). ANKS1A gene showed increased expression at 15 m and 1hr of infection in the WT-THP1 cells more than EphA1-KO THP-1 cells (see Figure 24). NFKBIA gene expression was observed higher in WT-THP-1 cells than EphA1-KO THP-1 cells at 1 hr, but lower at 4 hrs time point of infection (see Figure 25). ANKRD44-ITI gene expression has fluctuated; it was higher at 30 m and 2 hrs in the WT-THP-1 cells more than EphA1-KO THP-1 cells but was lower in WT-THP-1 cells less than EphA1-KO THP-1 cells (see Figure 26). The expression in the mTOR gene was more deficient in WT-THP-1 cells less than EphA1-KO THP-1 cells (see Figure 28). At 15 m of infection, AMPK gene expression was lower in WT-THP-1 less than EphA1-KO THP-1 cells (see Figure 27). RHCG gene expression was noticed at 2 hrs and 4 hrs higher in WT-THP-1 cells than EphA1-KO THP-1 cells (see Figure 29).

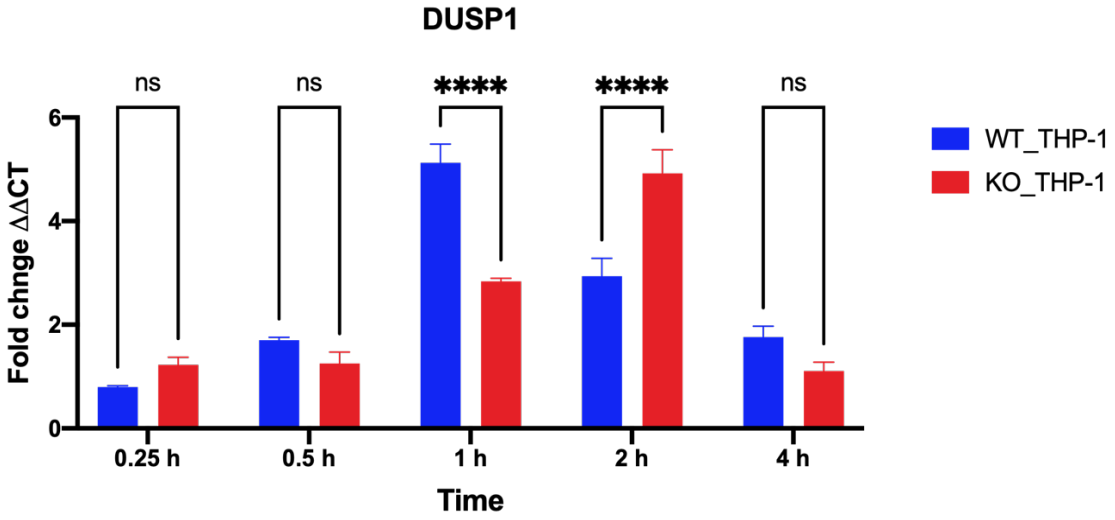

Figure 18. Comparison the transcript levels of DUSP1 in wild-type and EphA1-KO THP-1 cells after *Mtb* infection. The DUSP1 transcript levels were assessed in different time points (0.25, 0.5, 1, 2, and 4 hrs) after infection by quantitative real-time PCR using total RNA. The transcript levels were calculated relative to GAPDH control housekeeping gene values are expressed to fold change in gene expression for infected cells compared to uninfected controls. Errors bars represent the slandered errors from the means of three independent experiments. *, P < 0.05; **, P < 0.01; ***, P < 0.001; ****, P < 0.0001

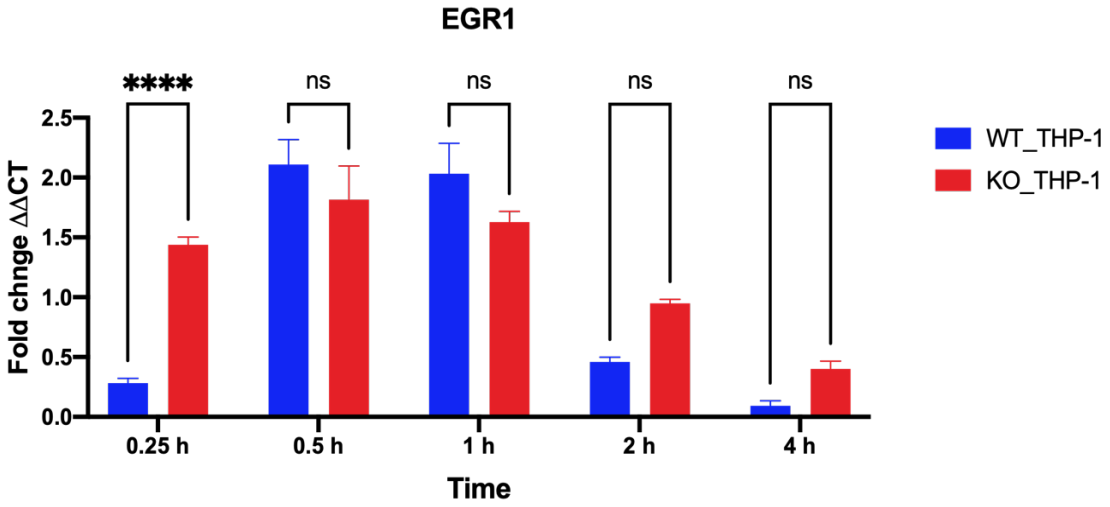

Figure 19. Comparison the transcript levels of EGR1 in wild-type and EphA1-KO THP-1 cells after *Mtb* infection. The EGR1 transcript levels were assessed in different time points (0.25, 0.5, 1, 2, and 4 hrs) after infection by quantitative real-time PCR using total RNA. The transcript levels were calculated relative to GAPDH control housekeeping gene values are expressed to fold change in gene expression for infected cells compared to uninfected controls. Errors bars represent the slandered errors from the means of three independent experiments. *, P < 0.05; **, P < 0.01; ***, P < 0.001; ****, P < 0.0001.

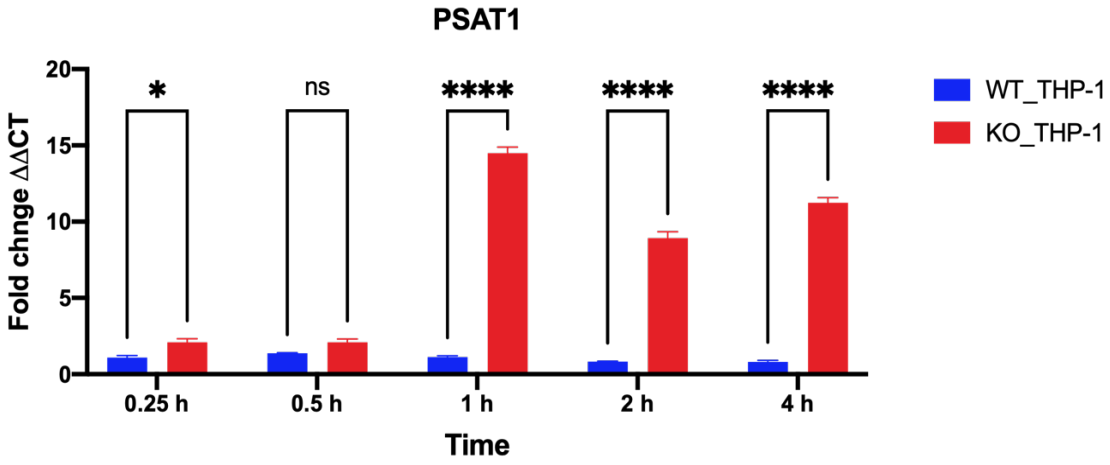

Figure 20. Comparison the transcript levels of PSAT1 in wild-type and EphA1-KO THP-1 cells after *Mtb* infection. The PSAT1 transcript levels were assessed in different time points (0.25, 0.5, 1, 2, and 4 hrs) after infection by quantitative real-time PCR using total RNA. The transcript levels were calculated relative to GAPDH control housekeeping gene values are expressed to fold change in gene expression for infected cells compared to uninfected controls. Errors bars represent the slandered errors from the means of three independent experiments. *, P < 0.05; **, P < 0.01; ***, P < 0.001; ****, P < 0.0001.

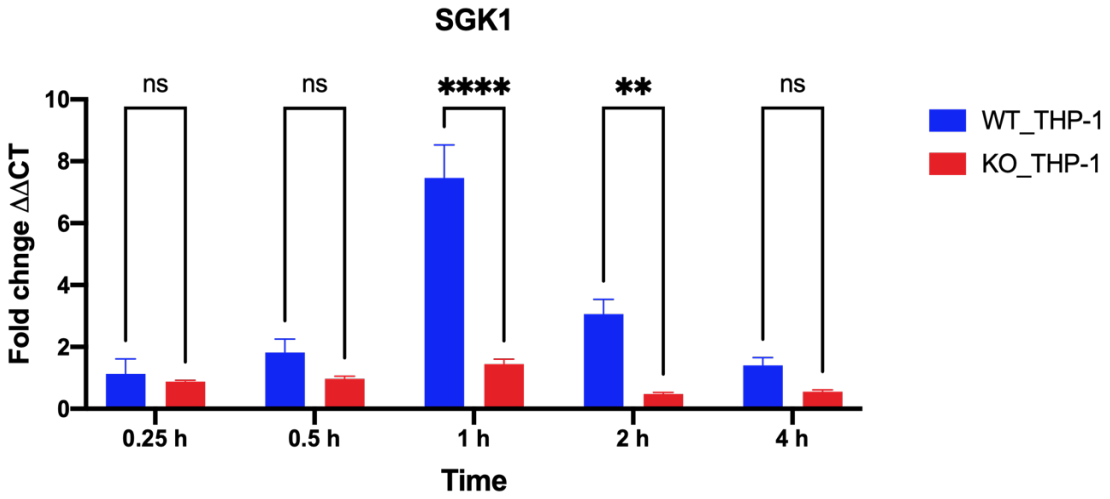

Figure 21. Comparison the transcript levels of SGK1 in wild-type and EphA1-KO THP-1 cells after *Mtb* infection. The SGK1 transcript levels were assessed in different time points (0.25, 0.5, 1, 2, and 4 hrs) after infection by quantitative real-time PCR using total RNA. The transcript levels were calculated relative to GAPDH control housekeeping gene values are expressed to fold change in gene expression for infected cells compared to uninfected controls. Errors bars represent the slandered errors from the means of three independent experiments. *, P < 0.05; **, P < 0.01; ***, P < 0.001; ****, P < 0.0001.

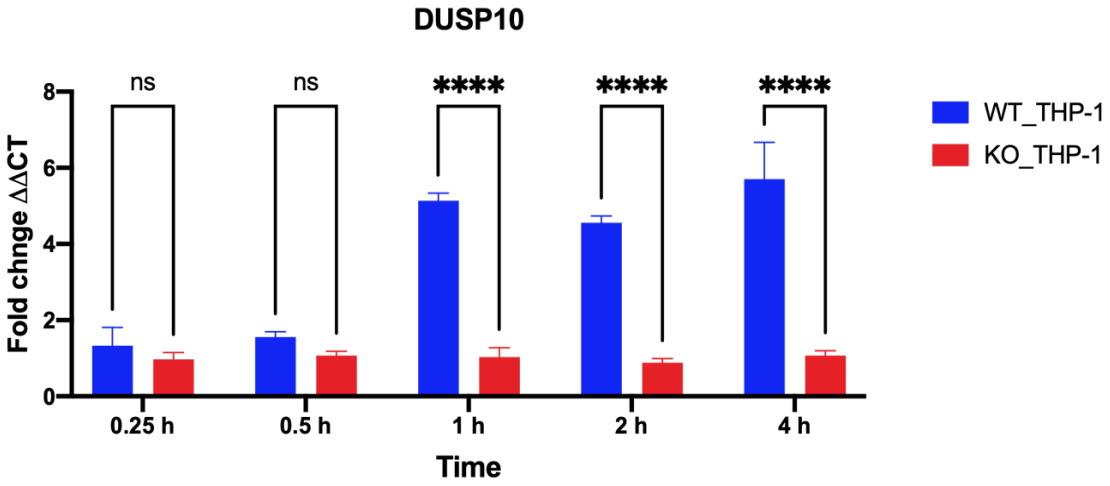

Figure 22. Comparison the transcript levels of DUSP10 in wild-type and EphA1-KO THP-1 cells after *Mtb* infection. The DUSP10 transcript levels were assessed in different time points (0.25, 0.5, 1, 2, and 4 hrs) after infection by quantitative real-time PCR using total RNA. The transcript levels were calculated relative to GAPDH control housekeeping gene values are expressed to fold change in gene expression for infected cells compared to uninfected controls. Errors bars represent the slandered errors from the means of three independent experiments. *, P < 0.05; **, P < 0.01; ***, P < 0.001; ****, P < 0.0001.

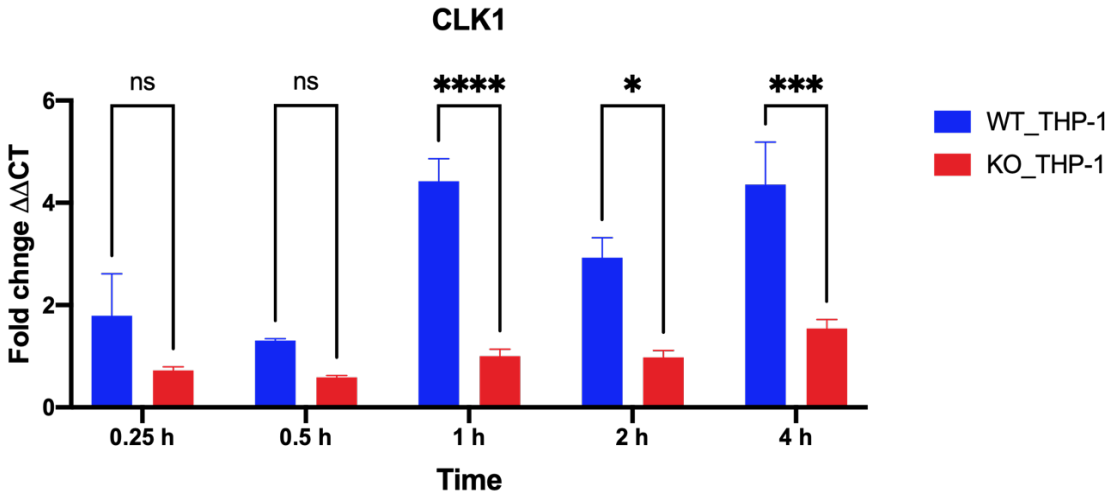

Figure 23. Comparison the transcript levels of CLK1 in wild-type and EphA1-KO THP-1 cells after *Mtb* infection. The CLK1 transcript levels were assessed in different time points (0.25, 0.5, 1, 2, and 4 hrs) after infection by quantitative real-time PCR using total RNA. The transcript levels were calculated relative to GAPDH control housekeeping gene values are expressed to fold change in gene expression for infected cells compared to uninfected controls. Errors bars represent the slandered errors from the means of three independent experiments. *, P < 0.05; **, P < 0.01; ***, P < 0.001; ****, P < 0.0001.

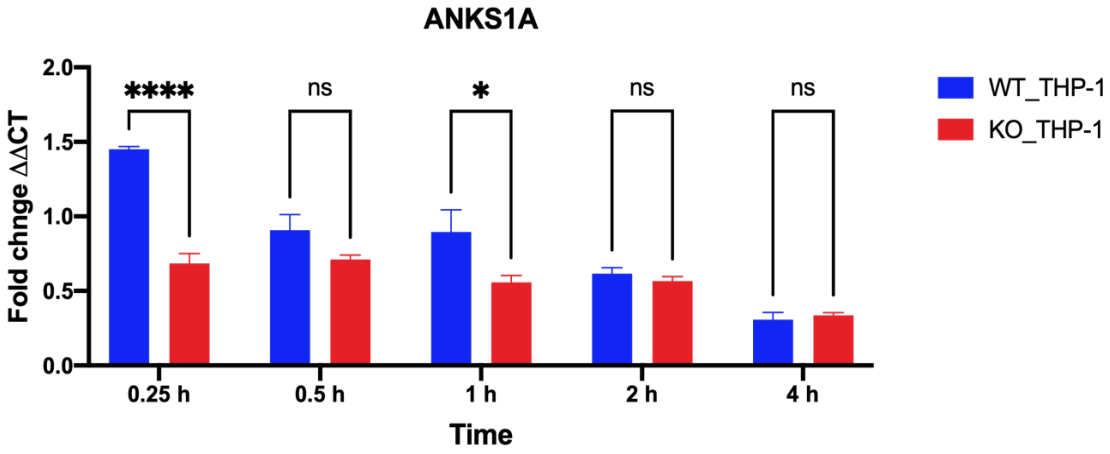

Figure 24. Comparison the transcript levels of ANKS1A in wild-type and EphA1-KO THP-1 cells after *Mtb* infection. The ANKS1A transcript levels were assessed in different time points (0.25, 0.5, 1, 2, and 4 hrs) after infection by quantitative real-time PCR using total RNA. The transcript levels were calculated relative to GAPDH control housekeeping gene values are expressed to fold change in gene expression for infected cells compared to uninfected controls. Errors bars represent the slandered errors from the means of three independent experiments. *, P < 0.05; **, P < 0.01; ***, P < 0.001; ****, P < 0.0001.

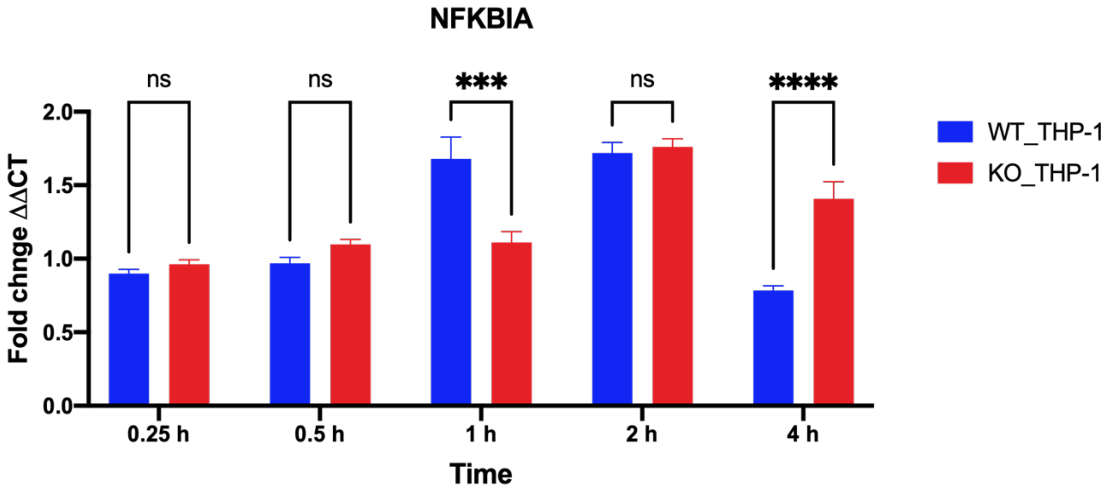

Figure 25. Comparison the transcript levels of NFKBIA in wild-type and EphA1-KO THP-1 cells after *Mtb* infection. The NFKBIA transcript levels were assessed in different time points (0.25, 0.5, 1, 2, and 4 hrs) after infection by quantitative real-time PCR using total RNA. The transcript levels were calculated relative to GAPDH control housekeeping gene values are expressed to fold change in gene expression for infected cells compared to uninfected controls. Errors bars represent the slandered errors from the means of three independent experiments. *, P < 0.05; **, P < 0.01; ***, P < 0.001; ****, P < 0.0001.

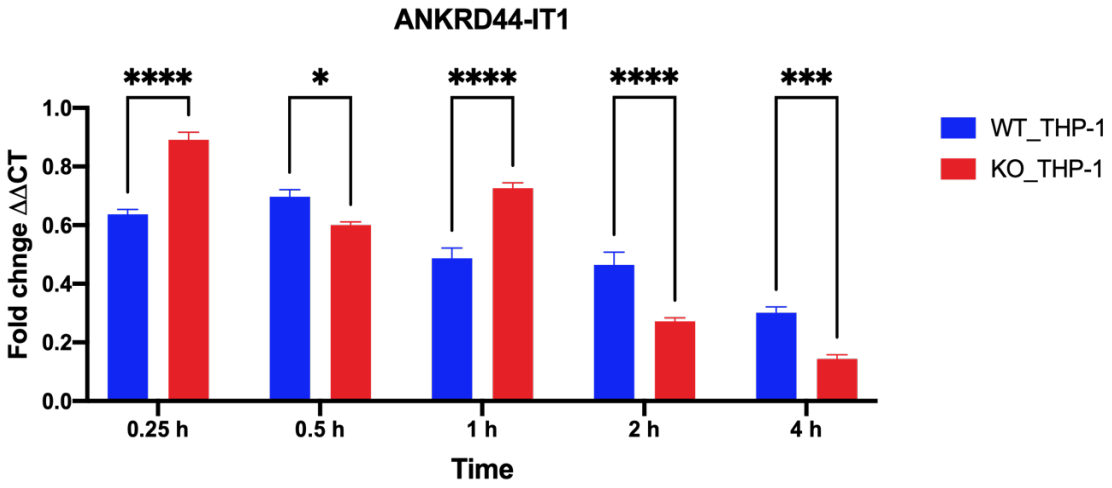

Figure 26. Comparison the transcript levels of ANKRD44-IT1 in wild-type and EphA1-KO THP-1 cells after *Mtb* infection. The ANKRD44-IT1 transcript levels were assessed in different time points (0.25, 0.5, 1, 2, and 4 hrs) after infection by quantitative real-time PCR using total RNA. The transcript levels were calculated relative to GAPDH control housekeeping gene values are expressed to fold change in gene expression for infected cells compared to uninfected controls. Errors bars represent the slandered errors from the means of three independent experiments. *, P < 0.05; **, P < 0.01; ***, P < 0.001; ****, P < 0.0001.

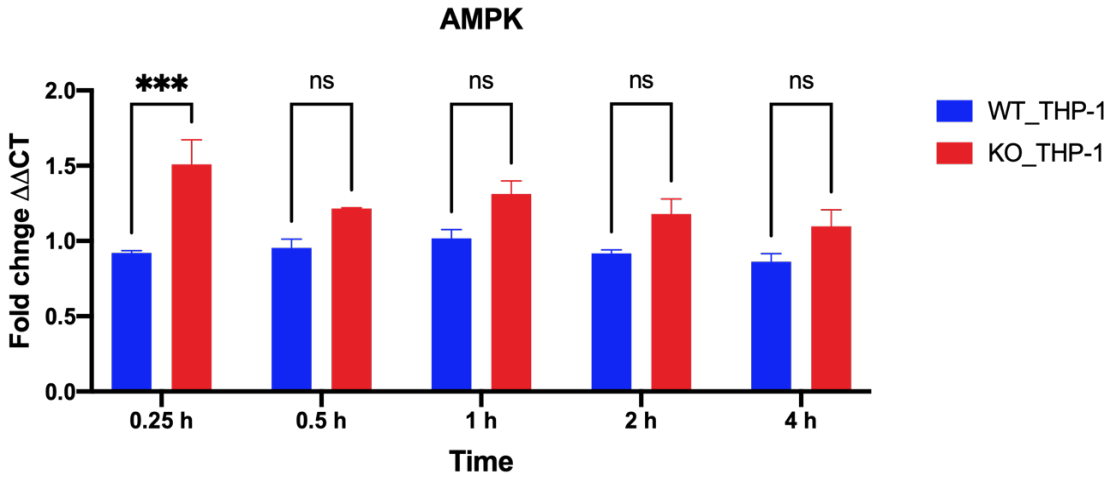

Figure 27. Comparison the transcript levels of AMPK in wild-type and EphA1-KO THP-1 cells after *Mtb* infection. The AMPK transcript levels were assessed in different time points (0.25, 0.5, 1, 2, and 4 hrs) after infection by quantitative real-time PCR using total RNA. The transcript levels were calculated relative to GAPDH control housekeeping gene values are expressed to fold change in gene expression for infected cells compared to uninfected controls. Errors bars represent the slandered errors from the means of three independent experiments. *, P < 0.05; **, P < 0.01; ***, P < 0.001; ****, P < 0.0001.

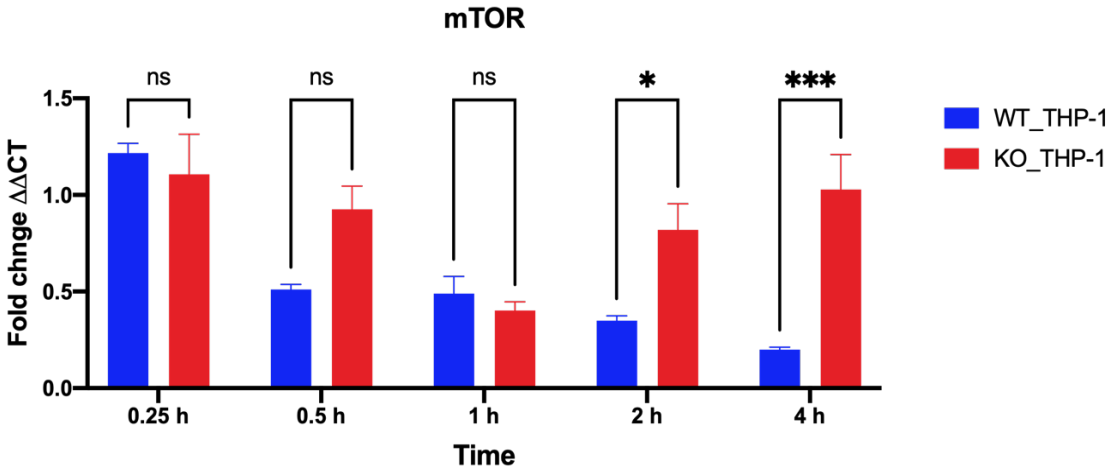

Figure 28. Comparison the transcript levels of mTOR in wild-type and EphA1-KO THP-1 cells after *Mtb* infection. The mTOR transcript levels were assessed in different time points (0.25, 0.5, 1, 2, and 4 hrs) after infection by quantitative real-time PCR using total RNA. The transcript levels were calculated relative to GAPDH control housekeeping gene values are expressed to fold change in gene expression for infected cells compared to uninfected controls. Errors bars represent the slandered errors from the means of three independent experiments. *, P < 0.05; **, P < 0.01; ***, P < 0.001; ****, P < 0.0001.

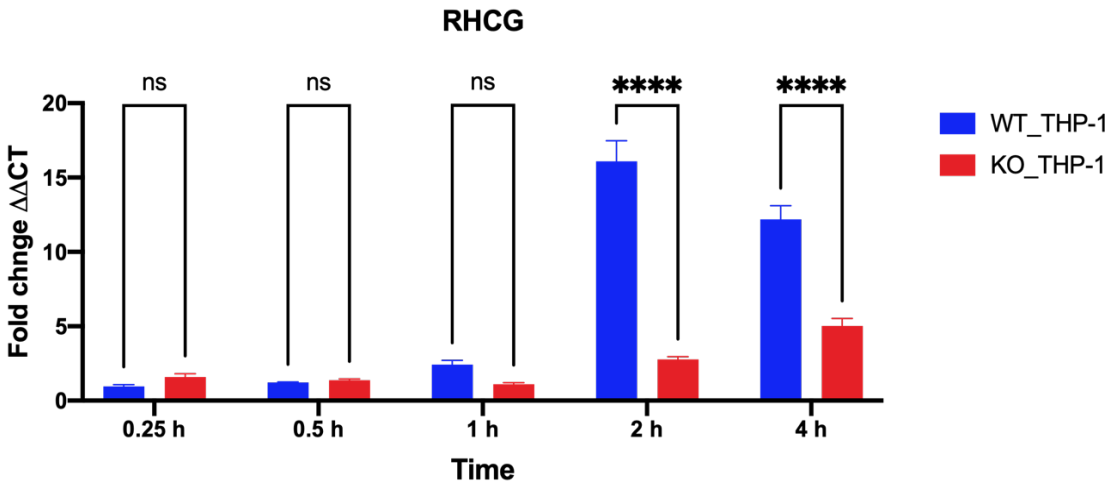

Figure 29. Comparison the transcript levels of RHCG in wild-type and EphA1-KO THP-1 cells after *Mtb* infection. The RHCG transcript levels were assessed in different time points (0.25, 0.5, 1, 2, and 4 hrs) after infection by quantitative real-time PCR using total RNA. The transcript levels were calculated relative to GAPDH control housekeeping gene values are expressed to fold change in gene expression for infected cells compared to uninfected controls. Errors bars represent the slandered errors from the means of three independent experiments. *, P < 0.05; **, P < 0.01; ***, P < 0.001; ****, P < 0.0001.

Discussion

In order to expose the role of Eph receptors during *Mtb* infection, macrophages (THP-1 cells) were utilized. EphA1 expression was induced during infection of the wild-type THP-1 cells with active *Mtb* by 1-fold at 30 m, reaching 3-fold at 4 h of infection (compared to the uninfected control). These results show the ability of *Mtb* to induce EphA1 gene expression in macrophages. EphA2 was induced through *Mtb* infection of THP-1 cells at 15 m and peaking at 4 h post-infection to 2.5-fold (compared to the uninfected control). Similarly, induction of EphA2 gene expression was showed through *Mtb* infection in macrophages. EphrinA1, a ligand of the EphA1 and EphA2 receptors, was also induced due to the infection of THP-1 cells with active *Mtb*. This began with a 1-fold induction at 15 m and extended to over 14-fold at 4 h. According to this elevation, *Mtb* was found to strongly induce the EphrinA1 ligands in the THP-1 cells.

These results confirm that EphA1 and Epha2 receptors and their ligand, EphrinA1, were induced due to *Mtb* infection. Accordingly, *Mtb* must initiated intracellular molecules and events to cause this induction. After macrophages devour *Mtb* and present it as antigen-presenting cells, they trigger several signaling pathways, including mitogen-activated protein kinase (MAPK) pathways, which in turn lead to the release of inflammatory cytokines such as interleukins-12 (IL-12) and tumor necrosis factor-α (TNF-α) [147-149]. EphA receptors have been found to have an inhibition role in the regulation of MAPK [150]. Since mycobacteria can proliferate within macrophages and stimulate EphA receptors' production, infection and proliferation directly contributes to the weakening of macrophages and the prevention of *Mtb* elimination. These mechanisms

rely on blocking the MAPK signals, thereby reducing microbicidal activity in the macrophages. One of the consequences of this blockage is the impairment of the production of inflammatory cytokines that are important for *Mtb* elimination. Many immune cells express EphA receptors (e.g., T-cells, DCs, granulocytes), so additional studies are needed to determine the downstream signaling pathways [151]. One study showed an induction of EphA1 and EphA2 during *Mtb* infection and an increase in cytokines' expression. The research also confirmed a rise in nitrous oxide (NO) inside the EphA2$^{-/-}$ macrophages after *Mtb* infection. This explains the survival of *Mtb* in EphA2$^{-/-}$ macrophages over that of wild-type macrophages [130].

Our data showed the viability of *Mtb* inside WT-THP-1 was higher than in EphA1$^{-/-}$ THP-1 cells. This showed the role of EphA1 molecule to enhance the proliferation and survival of *Mtb* in macrophages.

The EphA1-KO-THP-1 cells showed decreased EphA1 gene expression, while EphA2 and Ephrina1 increased 3.5-fold and 12-fold, respectively, at 4 h of infection. The EphA2 expression increased in the wild-type THP-1 cells more than in the EphA1-KO-THP-1 cells at 4 h, indicating that there was compensatory expression due to the reduction of the EphA1 expression (Figure 10). This was noticed in a previous study [130].

The transcriptional level analysis uncovers that the DEGs were involved in many pathways related to immunity and metabolism such as Coronavirus pathogenesis, Oxidative phosphorylation, HMGB1 Signaling pathway, ERK/MAPK Signaling, NRF2-mediated Oxidative Stress Response pathway, p38 MAPK Signaling, Assembly of RNA Polymerase II Complex, and Myc Mediated Apoptosis Signaling in the WT-THP-1 cells,

while EIF2 Signaling, Coronavirus Pathogenesis, Hypoxia Signaling in the Cardiovascular System, Erythropoietin Signaling, NRF2-mediated Oxidative Stress Response pathway, and Death Receptor Signaling pathway in the EphA1-KO-THP-1 cells.

Of these pathways, the Coronavirus pathogenesis pathway in interestingly, as it is activated in wild type THP-1 cells, while inhibited in EphA1-KO-THP-1 cells after 30 minutes of infection. Coronavirus pathogenesis pathway genes (RPS10, RPS15A, RPS25, RPS27, RPS28, and RPS3A) are related with encoding ribosomal proteins and involved in protein synthesis [152]. The interactions of these ribosomal proteins with viral RNA for biosynthesis of virus proteins have been shown to be necessary for viral replication in the hosts [153].

RPs genes are also involved in a host of extra-ribosomal functions. Ribosome assembly by individual RNAs and RPs is a closely controlled process in normal situations, with unassembled RPs being rapidly degraded. These free RPs can, in some cases, participate in a broad range of extra-ribosomal functions, including cell cycle progression control, immune signals, and cellular growth [154].

At 30 minutes of WT-THP-1-*Mtb* infection, Oxidative phosphorylation was inhibited. Oxidative phosphorylation is the pathway that cells use to produce adenosine triphosphate (ATP). In this metabolic pathway, cells use enzymes to oxidize nutrients to release chemical energy. This pathway occurs in mitochondria in most eukaryotes, especially aerobic organisms [155]. The transcriptional changes of host metabolism observed inhibition in oxidative phosphorylation, which means more dependent on

glycolysis pathway. Most host immune cells utilize this bioenergetic strategy for the rapid generation of ATP due to the infection by *Mtb* [156, 157].

At one hour after infection, High mobility group box protein1 (HMGB1) Signaling pathway was the top activated pathway. HMGB1 is an endogenous protein released during stress into the extracellular environment [158-160]. HMGB1 can bind TLR4 in a concentration-dependent way [161, 162]. The existence of CD14 as a co-receptor on macrophages is an essential factor of activation for the HMGB1-dependent TLR4 receptor in vitro [163]. HMGB1 was found to make immune-stimulatory complexes with cytokines, endogenous, and exogenous ligands (e.g., bacterial lipopolysaccharide (LPS)), stimulating the immune cells directly with the innate immune receptors [164, 165]. HMGB1 is related to the activity of many molecules and their ligands, such as LPS (TLR4 ligand), CpG-ODN (TLR9 ligand), or Pam3CSK4 (TLR1: TLR2 ligand) in a synergistic way when added to human peripheral blood mononuclear cell (PBMC) [165].

ERK/MAPK Signaling, was the one of pathways that inhibited after one hour of *Mtb* infection in the WT-THP-1 cells. ERK/MAPK kinases possess several targets in the nucleus, which include transcription factors and other kinases such as ERK1, ETS1, ATF2, MITF, MAPKAPK2, amongst others. Production of IFN-γ as a result of *Mtb* infection is related to the ERK/MAPK phosphorylation. Mitogen-activated protein kinases (MAPKs) are responsible for various features of immune responses, involving the start of innate immunity, stimulation of adaptive immunity, and ending of immune responses via cell death and controlling T cells [166, 167]. MAPKs are essential for macrophage activation as they phosphorylate and activate molecules downstream. *Mycobacterium*-

induced proinflammatory cytokines, such as TNF-α and interleukin 1, depend on MAPK activation [168]. There is evidence that the extracellular signal-regulated kinase (ERK) has a role in the antimycobacterial activity of antigen-presenting cells. ERK and MAPKs regulate IFN-γ releasing against *Mtb* by a mechanism that involves cyclic adenosine monophosphate response element-binding protein CREB [169].

After two to four hours of WT-THP-1 and at four of EphA1-KO THP-1 cells infection, the NRF2-mediated Oxidative Stress Response pathway was the activated pathway. Nuclear respiratory factor 2 (NRF2) is a transcriptional factor that responds to many harmful conditions such as reactive oxygen species [170, 171], and plays an essential function in cellular detoxification and stress responses[172]. Additionally, it is responsible for antioxidation and metabolism [173]. NRF2 was reported to be a prominent player in the inhibition of proinflammatory gene expression [174]. In normal circumstances, NRF2 binds Kelch-like ECH-associated protein 1 (KEAP1) and continues to do so in the cytoplasm [170, 175]. When NRF2 activity occurs due to stress signals, the linkage between KEAP1 protein is detached, releasing NRF2, and then it is present in the nucleus as a transcriptional factor [176]. This explains why it should be suppressed during *Mtb* infection.

After two hours of infection, p38 MAPK Signaling was the top inhibited pathway. The p38 MAP kinases works as a portal for signal transduction and is active in a number of biological processes. Inflammation, cell cycle, cell death, growth, and cell differentiation all support from p38 as a signal transduction mediator [177]. The p38 MAPK plays a major role in organizing the host's immune response by controlling the

production of proinflammatory cytokines such as IL-1β or TNF during infection [178]. TNF- stimulates the p38 MAPK pathway [179]. However, stimulation of p38 MAPK in two hours of *Mtb* infection was not enough.

Myc Mediated Apoptosis Signaling was the inhibited pathway after WT-THP-1 infection by *Mtb*. Myc Mediated Apoptosis Signaling, a transcriptional factor associated with apoptosis intracellular environment, showed a reduction of survival factors [180]. Myc is a regulator of cell growth, proliferation, differentiation, metabolism, and apoptosis [181]. Myc expression increases cells' sensitivity to proapoptotic disruption, such as DNA damage, genotoxic stress, and death receptor signaling [182]. Mitogens is responsible for inducing Myc expression, doing so via downregulation during the differentiation of cells [183]. Myc is associate with many cancer-related mutations that lead to the development of the disease. It is also implicated in many activities of certain enzymes involved in DNA metabolism and many other metabolic pathways. Meanwhile, it suggested that Myc is the regulator of cell cycle machinery [184].

EphA1-KO-THP-1 cells

At 30 minutes of EphA1-KO-THP-1 *Mtb*-infection, the top activated pathway was Eukaryotic initiation factor 2 (EIF2) Signaling. EIF2 is a eukaryotic initiation factor contributing to many eukaryotic translation initiations. EIF2 mediates binding of met-tRNA to the ribosome. Phosphorylation of EIF2 by eif2-α kinase regulates the protein synthesis responses to different environmental stresses [185]. The increased activity of EIF2 allows for an increase in proliferation of *Mtb* inside macrophages. A significant increase in the eif2-α kinase was found in TB-associated caseous granulomas in humans.

On the second hour of infection, Hypoxia Signaling in the Cardiovascular System was the activated pathway. The hypoxia signaling pathway is managed by the hypoxia-inducible factor (HIF). Many studies suggested that hypoxia and inflammation have a related relationship [186, 187]. Stabilization of HIF reduces tissue inflammation and stimulates repair [188-190]. The hypoxia signaling pathway prolongs leukocytes' functions, reduces the bacterial burden, and increases reactive nitrogen species (RNS) by stabilizing HIF during TB infection [191].

At two hours of infection, inhibited pathway was Erythropoietin Signaling. Erythropoietin is a glycoprotein hormone; it plays a central role in the proliferation, development, and survival of erythroid progenitor cells [192]. Erythropoietin binds the erythropoietin receptor, leading to the autophosphorylation of Jak2 kinase, a kinase associated with the receptor [192, 193]. Jack2 can activate many intracellular pathways such as Ras/MAP, STAT transcriptional factors, and phosphatidylinositol 3-kinase [194]. In cases of untreated systemic bacterial infections in lactobacillus, erythropoietin reduces the protective immune response. These are usually associated with chronic diseases such as tuberculosis due to the release of TNF-α and interleukin-6, which enhance pathogen growth and disease progression [195].

After four hours of infection, Death Receptor Signaling pathway was inhibited. Death receptors are a part of the tumor necrosis factor family. Signaling activation through the death receptor plays a vital role in regulating the adaptive immune response [196]. Cellular necrosis is regulated by many pathways (e.g., Death receptor signaling). Death receptors and Toll-like receptors can generate an intracellular signaling complex with the

participation of several proteins such as Fas-associated death domain (FADD), caspase 8, and rest in peace 3 (RIPK3) and other regulatory proteins [197, 198]. Necrotic cell death is described as inflammation that leads to spilling cell contents into the extracellular environment. *Mtb* has been implicated in the induction of necrosis pathways. In the host cells with *Mtb*, necrotic cell death occurs, leading to the escape of the bacteria outside of the cells. However, the immune response recruits the phagocytic cells to uptake the extracellular bacteria leading to replication and dissemination of the bacteria.

CHAPTER III

DIFFERENCES IN EPHRIN GENE PATHWAYS IN MACROPHAGES INFECTED WITH LIVE AND DEAD *MYCOBACTERIUM TUBERCULOSIS*

Introduction

The Eph family is one of the largest families of tyrosine kinase receptors in the genome of mammalian cells. These receptors' interactions with their ligands lead to many activities in the cells, including cell motility, cytoskeletal remodeling, and cell adhesion/repulsion. All of these activities depend on the type of cells [199]. Eph families are divided into two classes, based on ligand affinity and sequence similarity: EphA and EphB [58]. Ligands are divided into two categories, EphrinA and EphrinB, based on the binding of their receptors. These receptors bind with ligands (EphrinA) on corresponding cell surfaces. This allows for the activation of both attached cells, as the signals are bidirectional in terms of generating change [132]. There is evidence that EPH receptors and their ligands have an influence on inflammatory responses [151].

Ephrin1 gene expression was reported in endothelial cells when treated with lipopolysaccharide (LPS) and pro-inflammatory cytokines, interleukin-1 (IL-1) and tumor necrosis factor (TNF-α). LPS influenced many Eph receptors such as EphA1, EphA2, EphA3, EphB3, and EphB4 and their ligands (EphrinA1, EphrinA3, and EphrinB2) in the liver and lung of rats. TNF-α is the cytokine that releases from macrophages and affects the innate immune response. Since the macrophage is the first defense line against *Mtb*, the interaction between macrophage and *Mtb* induces many pro-inflammatory cytokines

such as IL-1, IL-6, IL-12, TNF-α, and IL-10 [200]. EphA2 and EphrinA1 expression were induced in the mouse lungs after infected with live *Mycobacterium tuberculosis* [201]. We studied the possible differences in the Eph receptors by treated THP-1 cells (macrophage) with live and heat-killed *Mtb* (HK-*Mtb*). We sought to characterize the HK-*Mtb* role on the induction of EphA1, EphA2, or EphrinA1 gene expression in THP-1 cells (macrophage).

Materials and Methods

Human cells and culture conditions

THP-1 cells (human monocytes) (ATCC TIB-202) were cultured in six-well plates at a density of 2 x 10^6 cells/well with Roswell Park Memorial Institute (RPMI) medium (Quality Biological) supplemented with 10% heat-inactivated fetal bovine serum, 100 mM phorbol 12-myristate 13-acetate (PMA) for 48 h to differentiate the cells to macrophages. After resting the cells for 24 hr, they were treated with 50 units/ml of human INFγ (Roche Diagnostics GmbH) plus 0.2 μg/ml of lipopolysaccharide (*E.coli* LPS; SIGMA) for 6 hrs to activate them [143].

Bacterial culture and heat inactivation conditions

M. tuberculosis strain $mc^2$7000 was grown from the frozen stocks of bacteria that were stored at -80°C was grown in 7H9 broth (Difco) enriched with 0.5% glycerol, 0.25% Tween-80, 24 μg/ml pantothenate, 0.2% of casamino acid, and 10% albumin dextrose complex (ADC). The *M. tuberculosis* $mc^2$7000 was cultured at 37°C for three to four weeks. Bacterial cultures were grown until an optical density (OD) 600 nm of ~1.0. The

quantity of viable bacteria was determined by plating serial dilutions to determine Colony-Forming Unit (CFU) using 7H9 agar enriched with 0.5% glycerol, 24 µg/ml pantothenate, 0.2% of casamino acid, and 10% ADC [144, 145].

For inactivation of *M. tuberculosis* $mc^2$7000, bacterial culture medium heated at 80° C for 30 minutes. To assessed the viability of the bacteria, heat-killed *M. tuberculosis* (HK-*Mtb*) bacteria was cultured in 7H9 agar enriched with 0.5% glycerol, 24 µg/ml pantothenate, 0.2% of casamino acid, and 10% (ADC) for six weeks at 37° C in 5% CO2 [13].

Macrophage infections

The differentiated and activated THP-1 cells were seeded in six-well plates at a density of 2 x 10^6 cells/well in RPMI medium supplemented with 10% heat-inactivated fetal bovine serum. These cells were infected with heat-killed *M. tuberculosis* $mc^2$7000 (HK-*Mtb*) at optical density for 15 m, 30 m, 1 h, 2 h, and 4 h. The incubation temperature was 37°C in a 5% CO_2 atmosphere. Extracellular HK-*Mtb* were removed by washing twice with warm sterile phosphate-buffered saline (PBS) after 30 minutes of infection. After 1hr, 2hrs, and 4hrs, fresh RPMI medium supplemented with 10% heat-inactivated fetal bovine serum was added to the infected cells in triplicate, which were then incubated for the remaining period of time at 37°C in 5% CO_2. The infected THP-1 cells were treated with TRIzol (15596026; ambion) for mRNA isolation or lysed with 0.1% Triton-X-100 for 10 minutes to enumerate the intercellular bacteria [146].

Total RNA extraction and qRT-PCR

Total mRNA extraction and qRT-PCR were performed as described previously [201]. Briefly, TRIzol reagent (15596026; ambion) was used to extract mRNA from the macrophages according to the manufacturer's instructions (15596026; ambion). The cDNA was synthesized from the isolated mRNA using the SuperScript III First-Strand kit (oligo-dt primers) (18080-051; Invitrogen). Then, qPCR was performed by using the primers for EphA1, EphA2, and EphrinA1. The quantity of mRNA for each gene was measured using SYBR Green and a PowerUp Master Mix (A25742; Applied Biosystems). The specific primers used in this qRT-PCR are listed in Table 6. Negative controls for the reaction were total RNA and without template (NTC). The relative expressions of EphA1, EphA2, and EphrinA1 were normalized to the endogenous control GAPDH gene using the $2^{-\Delta\Delta Ct}$ cycle threshold method. Calculation of fold induction was based on the Ct values to quantify transcript levels.

RNA-Seq

Transcriptome analysis was assessed by mRNA-Seq using 3'-TagSeq sequencing for single-end reads of 100 nucleotides (nt) in length. Bioinformatics analyses were performed using Texas A&M High Performance Research Computing. Trimmomatic program was used for trimming the raw reads from the adaptor contamination and Illumina adaptors used while sequencing [202]. The end reads were evaluated with a per base sequence quality score; reads with scores less than 30 and shorter than 20 bp were not taken. The selected end reads were mapped to the human genome and aligned and spliced using the STAR mapper program [203, 204]. An HTSeq tool was applied to count the

transcripts mapped to the gene exon features [205]. The EdgeR package in the R statistical platform was employed to compare the reads count data [206]. Genes that expressed less than 1 million reads (< 1 CPM) were not counted in the data analysis. Variations in library sizes were estimated, relying on the normalization factors. Dispersion estimation for the reads was performed to correct the batch effects. These effects were reduced using an EdgeR package [207]. The likelihood ratio test (LRT) function was applied to evaluate the expression values among the treatment libraries. The top tag of the tables was applied for the interruption and pathway analyses. Thresholds of an adjusted p-value < 0.05 and log2FC value were used to obtain differential expressions (DEGs). We determined the differential gene expression between the uninfected and infected cells at different time points utilizing Limma, an open source R-based software package. The GO category enrichment analysis for the DEGs was completing using WebGestalt. The Ingenuity Pathway Analysis platform (IPA, QIAGEN Inc.) was performed to complete the top tag differential expression pathway analyses. The genes that were selected in the pathway analyses had false discovery rate (FDR) values < 0.05 and logFC > 2 and also to identify significant canonical pathways and network activation and their respective roles in molecular and cellular functions in the upregulated and downregulated directions. The IPA platform was used to execute the comparative analyses of the results of the pathway core analyses.

Confirmation of RNA-Seq analysis via qRT-PCR

RNA-Seq data were confirmed for 12 selected genes using quantitative real-time PCR, with GAPDH as a housekeeping gene. The same samples used for transcriptomic

analysis were used in this qRT-PCR. The primers used in this study are listed in Table 6. The quantity of mRNA for each gene was measured using SYBR Green utilizing a PowerUp Master Mix (A25742; Applied Biosystems). The reactions were performed in 10 ul reaction volume containing 0.25 ul of each primer (10 uM), 5 ul of 2x SYBR Green PowerUp Master Mix, and 4.5 ul cDNA (80 ng). The qRT-PCR reactions were completed using Applied Biosystem plus instrument (StepOnePlus Real-Time PCR System). Negative controls for the reaction were the total RNA and without template (NTC). The comparative Ct ($2^{-\Delta\Delta Ct}$) method was applied to calculate the relative expression and normalized to the reference GAPDH gene.

Table 6. Primers that were used in RT-qPCR.

Gene name	Forward primer	Reverse primer
EphA1	ATCTTTGGGCTGCTGCTTGG	GCTTGTCCTCTCGATCCACATC
EphA2	GGCAGGAGTTGGCTTCTTTAT	GGGCTTCAGTTGTTCTGACTT
EphrinA1	TCAAAGAAGGACACAGCTACTAC	CCTGAGGACTGTGAGTGATTT
GAPDH	CCAGGTGGTCTCCTCTGACTT	GTTGCTGTAGCCAAATTCGTTGT
DUSP1	ACCACCACCGTGTTCAACTTC	TGGGAGAGGTCGTAATGGGG
EGR1	GGTCAGTGGCCTAGTGAGC	GTGCCGCTGAGTAAATGGGA
PSAT1	TGCCGCACTCAGTGTTGTTAG	GCAATTCCCGCACAAGATTCT
DUSP10	TGAAGCACACTCGGATGACC	CCTCGAACTCTAGCAACTGCC
SGK1	CATATTATGTCGGAGCGGAATGT	TGTCAGCAGTCTGGAAAGAGA
CLK1	AGAGACCATGAAAGCCGGTAT	CATGTGAACGACGATGTGAAGT
NFKBIA	ACCTGGTGTCACTCCTGTTGA	CTGCTGCTGTATCCGGGTG
RHCG	CCTCGGTGGCAATATCCAGTG	GAAGCCGATGATGAGGGCA
ANKRD44-IT1	TCGAGGGGTGTTTAATGAGC	CTGTCCTTCCCTTTTGTGGA
ANKS1A	CGTGGCTGACTCAAAAGGCT	GGCTGTCTCGTTGTCATTGTTC
AMPK	TTTGCGTGTACGAAGGAAGAAT	CTCTGTGGAGTAGCAGTCCCT
mTOR	TCCGAGAGATGAGTCAAGAGG	CACCTTCCACTCCTATGAGGC

Statistical analysis

The experimental data are presented as mean ± SE. The GraphPad Prism9 (GraphPad Software, Inc.) was used to do all statistical analysis. Statistical significance

was determined using an ANOVA test. Differences were considered for p-values less than 0.05.

Results

RT- PCR, and qPCR to determine the mRNA levels of EphA1, EphA2, and EphrinA1 on wild-type THP-1 cells post-infection by live Mtb mc^{2}7000

EphA1, EphA2, and EphrinA1 expressions were determined at mRNA level following macrophage infection with live *Mtb* (live-*Mtb*). THP-1 cells (human monocytes) were differentiated and activated prior to *Mtb* mc^{2}7000 infection. Expressions of EphA1, EphA2, and EphrinA1 were determined in THP-1 cells using qRT-PCR. The results were evaluated against the variation between specific genes and the GAPDH average ratio and then normalized to uninfected controls in order to calculate the fold change for each gene. The EphA1 transcript level increased 1-fold in the THP-1 cells infected with *Mtb* mc^{2}7000 at 30 minutes, and it grew 3-fold further at 4 hours post-infection. (see Figure 30).

EphA2 expression was raised 1-fold at 15 min and reached 2.5-fold after four h of infection (see Figure 31). EphrinA1 was up-regulated 1-fold over the uninfected control at 15 min and more than 14-fold at four hrs post infection (see Figure 32). These results indicate that EphA genes and their ligand, EphrinA1, expression was induced during the early stages of live-*Mtb* mc^{2}7000 wild-type THP-1 cell infection.

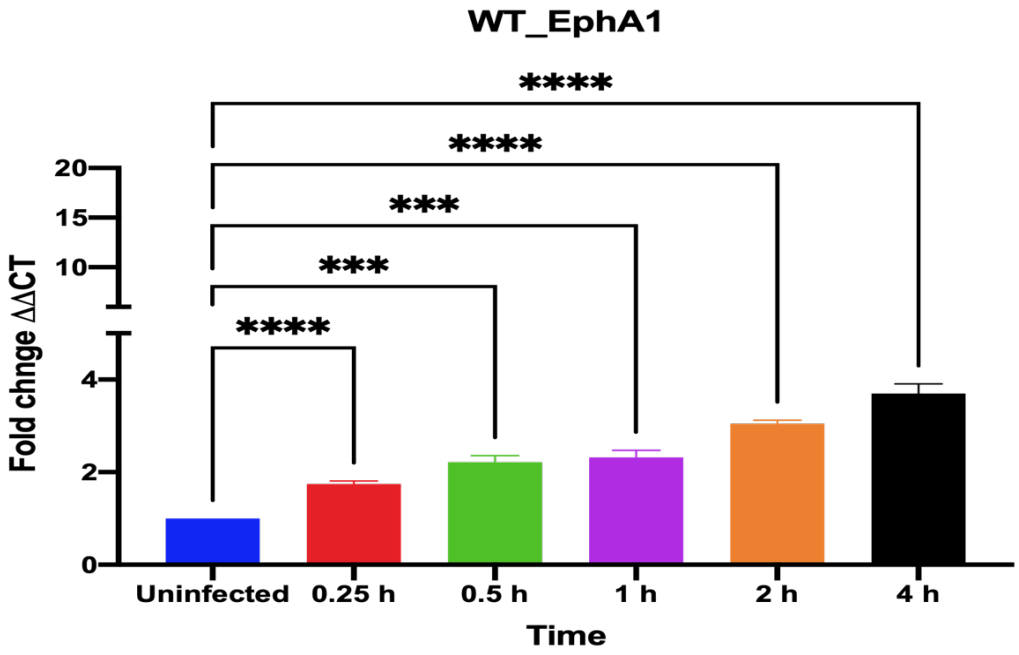

Figure 30. Transcript levels of EphA1 in wild-type THP-1 cells after *Mtb* infection. The EphA1 transcript levels were assessed in different time points (0.25, 0.5, 1, 2, and 4 hrs) after infection by quantitative real-time PCR using total RNA. The transcript levels were calculated relative to GAPDH control housekeeping gene values are expressed to fold change in gene expression for infected cells compared to uninfected controls. Errors bars represent the slandered errors from the means of three independent experiments. *, P < 0.05; **, P < 0.01; ***, P < 0.001; ****, P < 0.0001.

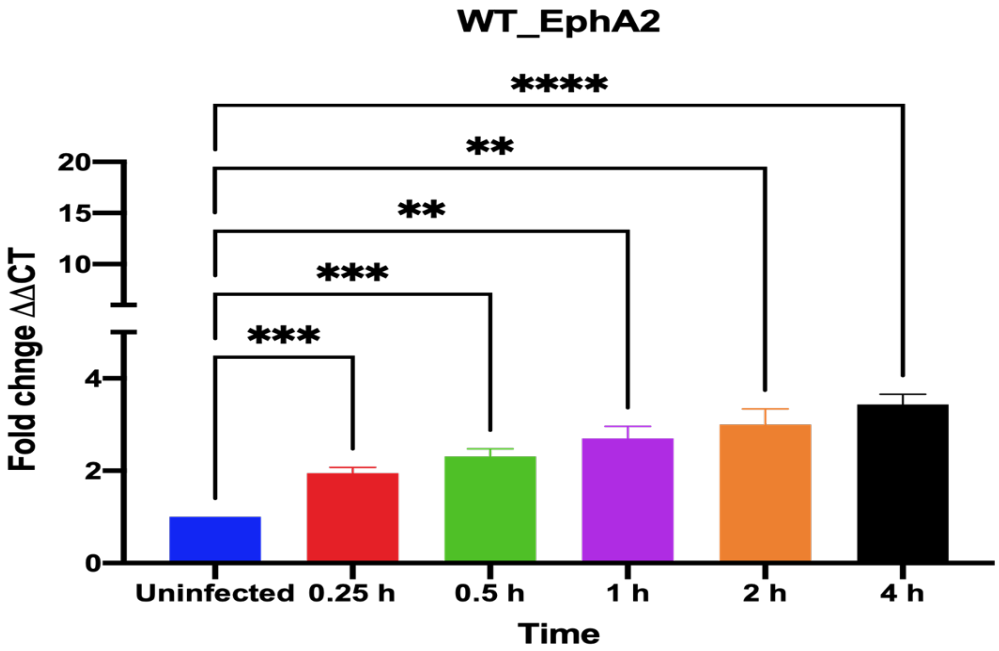

Figure 31. Transcript levels of EphA2 in wild-type THP-1 cells after *Mtb* infection. The EphA2 transcript levels were assessed in different time points (0.25, 0.5, 1, 2, and 4 hrs) after infection by quantitative real-time PCR using total RNA. The transcript levels were calculated relative to GAPDH control housekeeping gene values are expressed to fold change in gene expression for infected cells compared to uninfected controls. Errors bars represent the slandered errors from the means of three independent experiments. *, P < 0.05; **, P < 0.01; ***, P < 0.001; ****, P < 0.0001.

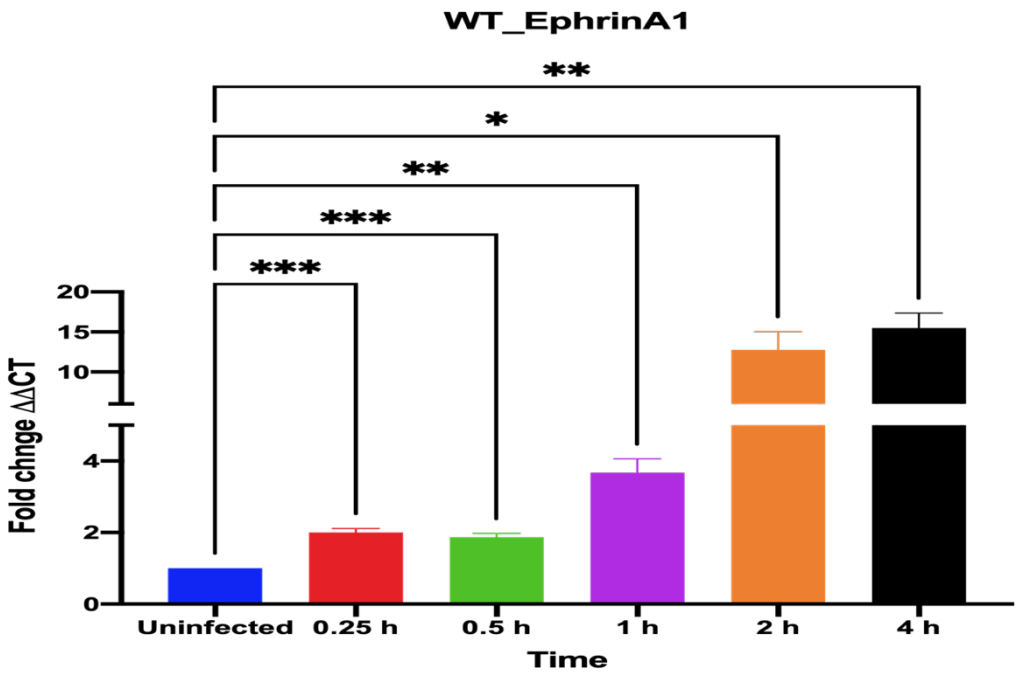

Figure 32. Transcript levels of EphrinA1 in wild-type THP-1 cells after live *Mtb* infection. The EphrinA1 transcript levels were assessed in different time points (0.25, 0.5, 1, 2, and 4 hrs) after infection by quantitative real-time PCR using total RNA. The transcript levels were calculated relative to GAPDH control housekeeping gene values are expressed to fold change in gene expression for infected cells compared to uninfected controls. Errors bars represent the slandered errors from the means of three independent experiments. *, P < 0.05; **, P < 0.01; ***, P < 0.001; ****, P < 0.0001.

RT- PCR, and qPCR to determine the mRNA levels of EphA1, EphA2, and EphrinA1 on wild-type THP-1 cells post-infection by heat-killed Mtb $mc^2$7000

THP-1 cells were differentiated and activated before HK-*Mtb* infection to determine EphA1, EphA2, and EphrinA1 expressions in the mRNA level post-infection. HK-*Mtb*-infected THP-1 revealed that the level of EphA1 gene expression persisted until 2 hours of exposure, then expression increased to a non-significant level after four hours (see Figure 33). EphA2 gene expression fluctuated around a 1-fold change compared to the control at all time points of infection, except at the fourth hour of infection, where gene expression raised more than 2-fold compared to the control group (see Figure 34). At the second hour of HK-*Mtb* infection, there was a significant increase in the expression of the EphrinA1 gene (5-fold), but there were no significant differences in the rest of the time period (see Figure 35).

The comparison between THP-1 infected with live and dead *Mtb* revealed a delay in expressing the EphA1 gene. It was significantly lower in HK-*Mtb*-infected THP-1 than in live-*Mtb*-infected THP-1 after 2 and 4 hours of infection (see Figure 36). The difference in EphA2 gene expression showed a significant reduction at 1 and 2 hours after infection in HK-*Mtb*-infected THP-1 cells below live-*Mtb*-infected THP-1 cells (see Figure 37). Interestingly, EphrinA1 gene expression was significantly low in cells infected with dead *Mtb* compared to live *Mtb* at 2 and 4 hours after infection (see Figure 38).

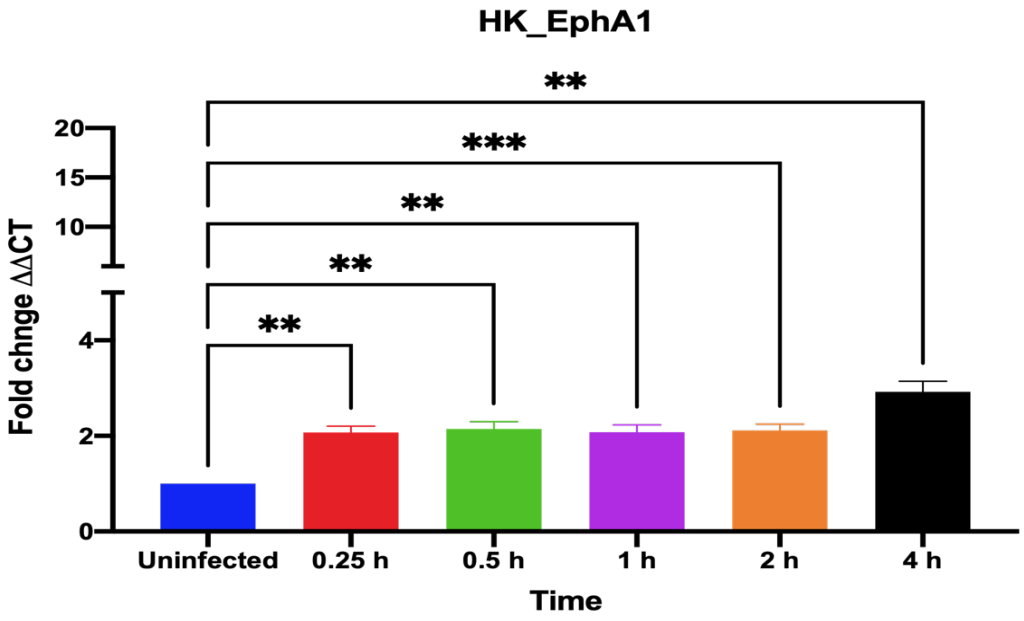

Figure 33. Transcript levels of EphA1 in wild-type THP-1 cells after heat-killed *Mtb* infection. The EphA1 transcript levels were assessed in different time points (0.25, 0.5, 1, 2, and 4 hrs) after infection by quantitative real-time PCR using total RNA. The transcript levels were calculated relative to GAPDH control housekeeping gene values are expressed to fold change in gene expression for infected cells compared to uninfected controls. Errors bars represent the slandered errors from the means of three independent experiments. *, P < 0.05; **, P < 0.01; ***, P < 0.001; ****, P < 0.0001.

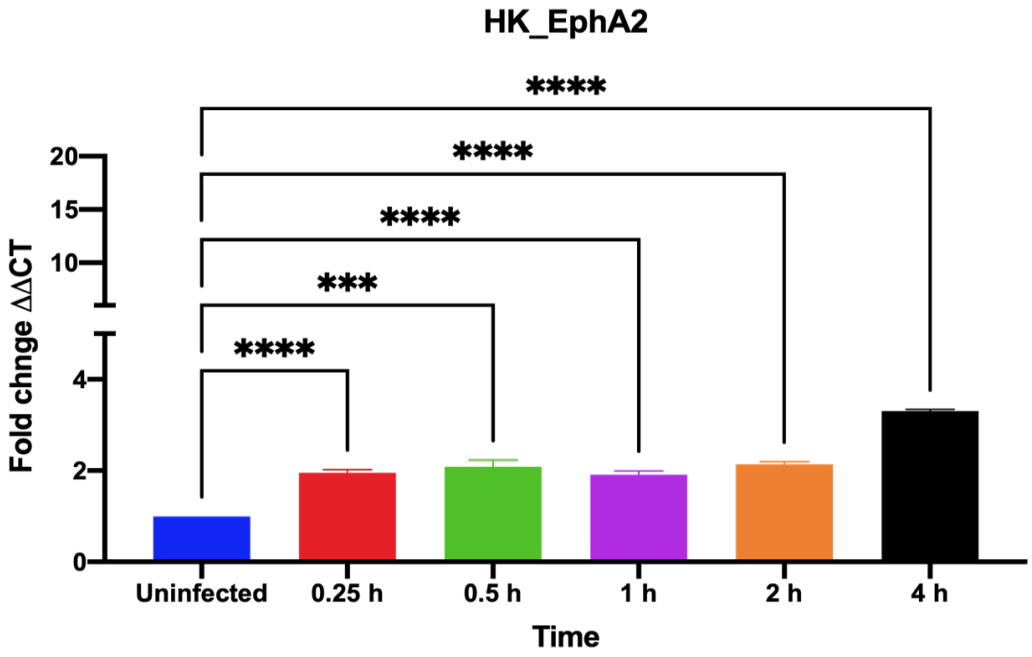

Figure 34. Transcript levels of EphA2 in wild-type THP-1 cells after heat-killed *Mtb* infection. The EphA2 transcript levels were assessed in different time points (0.25, 0.5, 1, 2, and 4 hrs) after infection by quantitative real-time PCR using total RNA. The transcript levels were calculated relative to GAPDH control housekeeping gene values are expressed to fold change in gene expression for infected cells compared to uninfected controls. Errors bars represent the slandered errors from the means of three independent experiments. *, P < 0.05; **, P < 0.01; ***, P < 0.001; ****, P < 0.0001.

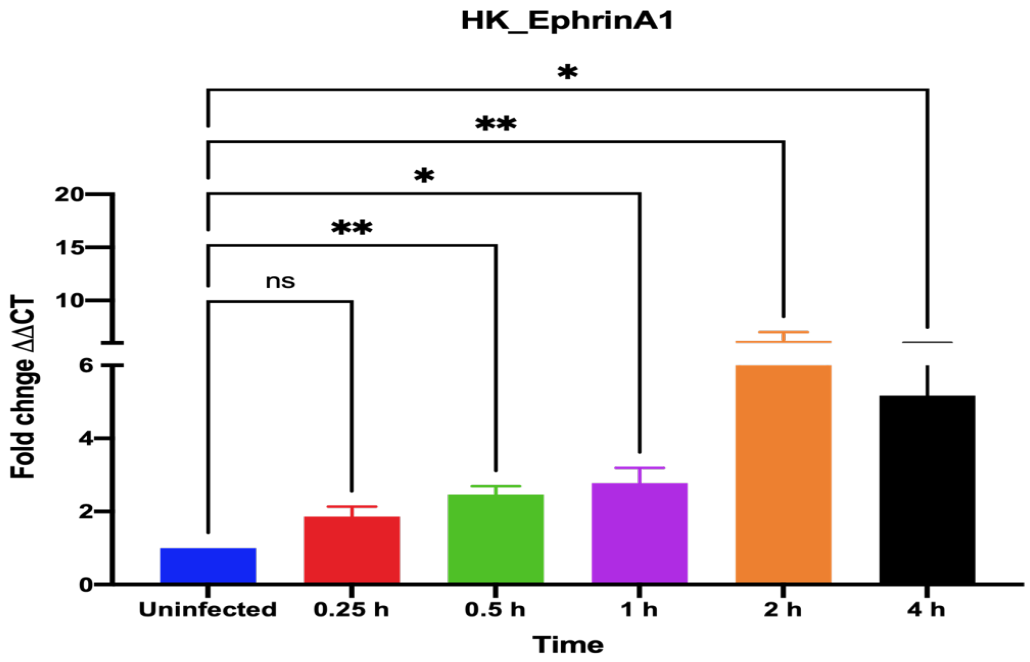

Figure 35. Transcript levels of EphrinA1 in wild-type THP-1 cells after heat-killed *Mtb* infection. The EphrinA1 transcript levels were assessed in different time points (0.25, 0.5, 1, 2, and 4 hrs) after infection by quantitative real-time PCR using total RNA. The transcript levels were calculated relative to GAPDH control housekeeping gene values are expressed to fold change in gene expression for infected cells compared to uninfected controls. Errors bars represent the slandered errors from the means of three independent experiments. *, P < 0.05; **, P < 0.01; ***, P < 0.001; ****, P < 0.0001.

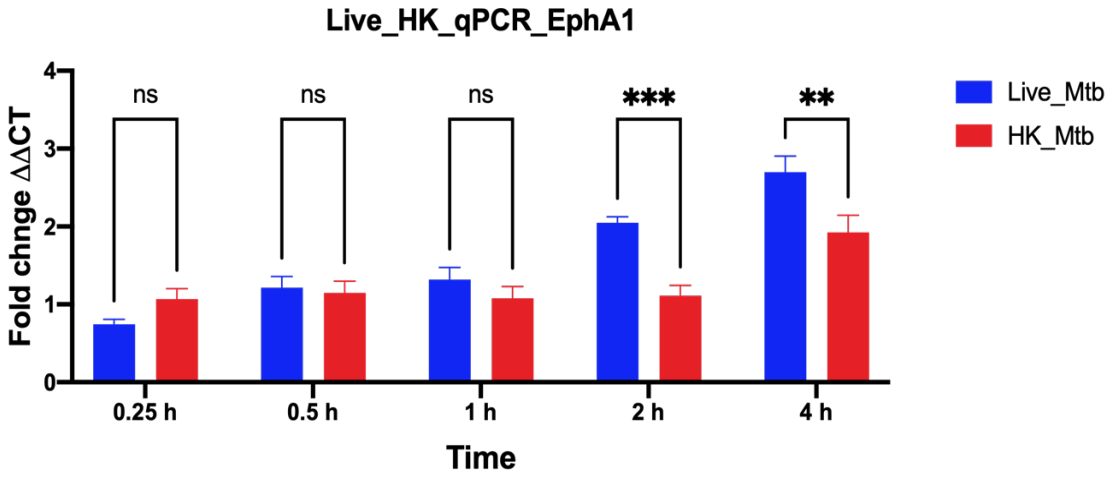

Figure 36. Comparison the transcript levels of EphA1 in wild-type THP-1 cells after live *Mtb* and heat-killed *Mtb* infection. The EphA1 transcript levels were assessed in different time points (0.25, 0.5, 1, 2, and 4 hrs) after infection by quantitative real-time PCR using total RNA. The transcript levels were calculated relative to GAPDH control housekeeping gene values are expressed to fold change in gene expression for infected cells compared to uninfected controls. Errors bars represent the slandered errors from the means of three independent experiments. *, P < 0.05; **, P < 0.01; ***, P < 0.001; ****, P < 0.0001.

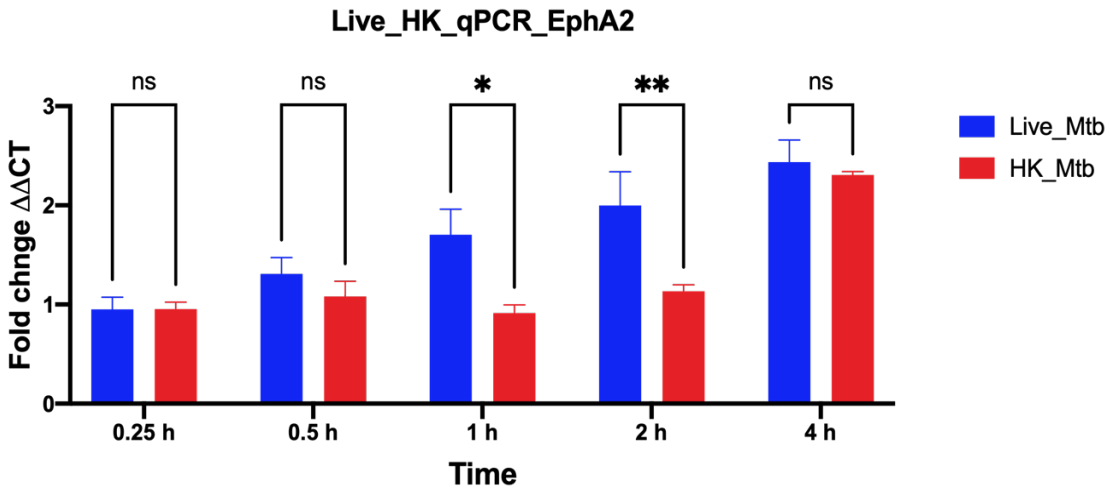

Figure 37. Comparison the transcript levels of EphA2 in wild-type THP-1 cells after live *Mtb* and heat-killed *Mtb* infection. The EphA2 transcript levels were assessed in different time points (0.25, 0.5, 1, 2, and 4 hrs) after infection by quantitative real-time PCR using total RNA. The transcript levels were calculated relative to GAPDH control housekeeping gene values are expressed to fold change in gene expression for infected cells compared to uninfected controls. Errors bars represent the slandered errors from the means of three independent experiments. *, P < 0.05; **, P < 0.01; ***, P < 0.001; ****, P < 0.0001.

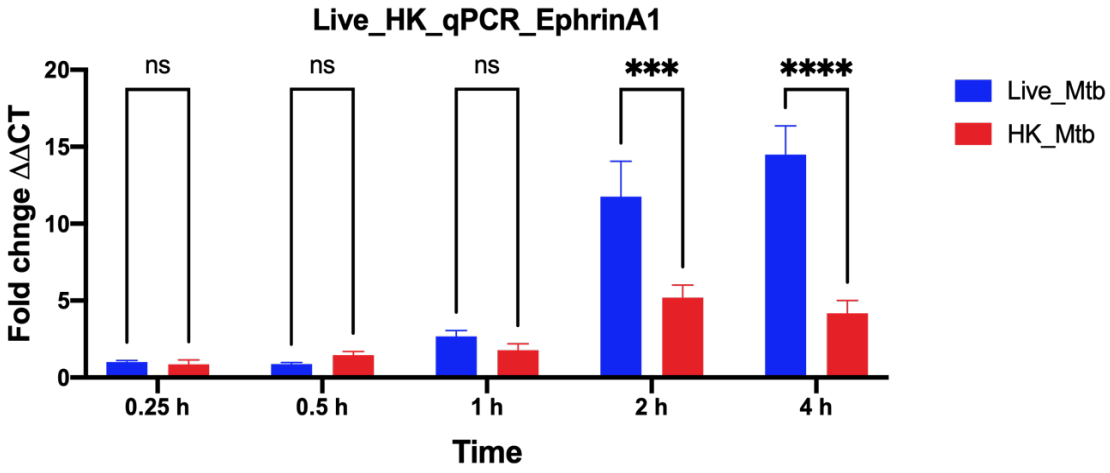

Figure 38. Comparison the transcript levels of EphrinA1 in wild-type THP-1 cells after live *Mtb* and heat-killed *Mtb* infection. The EphrinA1 transcript levels were assessed in different time points (0.25, 0.5, 1, 2, and 4 hrs) after infection by quantitative real-time PCR using total RNA. The transcript levels were calculated relative to GAPDH control housekeeping gene values are expressed to fold change in gene expression for infected cells compared to uninfected controls. Errors bars represent the slandered errors from the means of three independent experiments. *, P < 0.05; **, P < 0.01; ***, P < 0.001; ****, P < 0.0001.

RNA-Seq analysis of the THP-1 cells that infected by live Mtb or heat-killed Mtb

To recognize molecular differences and calculate the expression of the THP-1 genes infected with live-*Mtb* comparable to HK-*Mtb* infected cells, RNA-Seq analysis was conducted using the RNA-Seq analysis. Six samples from each time point (15 m, 30 m, 1 hour, 2 hours, and 4 hrs) were compared to non-infected THP-1 cells following infection with live-*Mtb* or HK-*Mtb* (see Figure 39). 18,182 genes have remained following calculation of levels of expression and the removal of unexpressed genes.

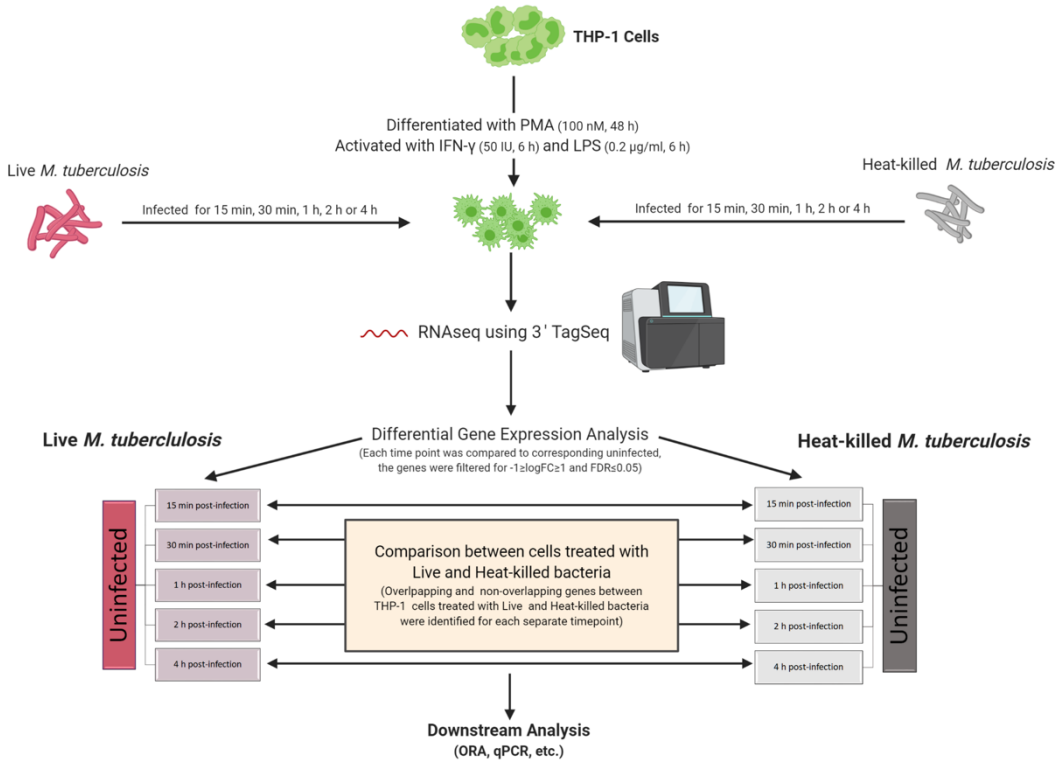

Figure 39. Schematic of RNASeq for the wild type THP-1 cells after live- and dead-*Mtb* infection.

a- Infection of THP-1 cells with live M. tuberculosis induced gene expression

Table 7 displayed upregulated and downregulated genes at different time points in the RNA-Seq analysis of THP-1 infection. Compared to uninfected THP-1 cells, the number of genes expressed has increased from 227 genes at 30 minutes to 904 genes at 4 hours of live-*Mtb* infection.

Table 7. Number of upregulated and downregulated genes in different time point of infection with live-*Mtb* in THP-1 cells

Time point	Upregulated genes	Downregulated genes	Total
15 minutes	0	0	0
30 minutes	15	212	227
1 hour	51	12	63
2 hours	184	61	245
4 hours	569	335	904

The Ingenuity Pathway Analysis (IPA) was classified differentially expressed genes (DEGs) to several annotated molecules at various time points of live-*Mtb*-infected THP-1 cells, as seen in Table 8.

Table 8. Classification of DEGs to canonical pathways at various time points of live-*Mtb*-infected THP-1 cells.

Time point	Top five Canonical Pathways
15 minutes	0
30 minutes	Oxidative Phosphorylation Mitochondrial Dysfunction EIF2 Signaling Clathrin-mediated Endocytosis Signaling Systemic Lupus Erythematosus Signaling
1 hour	HMGB1 Signaling Erythropoietin Signaling Regulation of IL-2 Expression in Activated and Anergic T Lymphocytes Corticotropin Releasing Hormone Signaling Thrombopoietin Signaling
2 hours	Unfolded protein response Inhibition of Angiogenesis by TSP1 NRF2-mediated Oxidative Stress Response Coronavirus Pathogenesis Pathway Endoplasmic Reticulum Stress Pathway
4 hours	Assembly of RNA Polymerase II Complex NRF2-mediated Oxidative Stress Response Senescence Pathway Induction of Apoptosis by HIV1 Pancreatic Adenocarcinoma Signaling

Molecules that engaged in canonical pathways were detected at each time point compared to uninfected cells that were significant based on P-value and Z-score Table 8. After 30 minutes of infection, Coronavirus Pathogenesis Pathway was the most involved pathway. FOS was up-regulated while RPS10, RPS15A, and RPS28 were down-regulated. After 30 minutes of infection, Coronavirus Pathogenesis Pathway was the most involved pathway. FOS was up-regulated while RPS10, RPS15A, and RPS28 were down-regulated. COX6A1, NDUFA11, NDUFA13, NDUFB8, SDHC, and UQCR11 are all genes that are upregulated in the Oxidative phosphorylation pathway that inhibited.

In the following hour after infection, the HMGB1 signaling pathway was the top activated pathway with five up-regulated genes involved in this pathway, FOS, JUN, OSM, RHOB, and TGFB1. By comparison, the inhibited pathway was ERK/MAPK Signaling, based on DUSP1, DUSP2, DUSP4 genes that were down-regulated, and the FOS gene up-regulated.

After two hours of infection, the NRF2-mediated Oxidative Stress Response pathway was the triggered pathway with the highest Z-score. It included DNAJB2, DNAJB9, HERPUD1, JUN, JUND, MAFF, MAFG, and SQSTM1 genes that displayed an upregulation pattern. Simultaneously, the inhibited pathway was p38 MAPK Signaling with two down-regulated genes, DUSP1, DUSP10, and three up-regulated genes, DDIT3, TGFB1, and TIFA.

The upper triggered pathway at the end of the infection was NRF2-mediated Oxidative Stress Response, comprising DNAJB1, DNAJB2, DNAJB4, DNAJB9, EIF2AK3, HERPUD1, HMOX1, JUND, MAFG, MAP2K3, MGST2, PIK3CG, RAP1A, SQSTM1, and TXNRD1 genes that clearly shows upregulation, and KEAP1 genes that demonstrate upregulation. On the other hand, Myc Mediated Apoptosis Signaling was the inhibited pathway of the up-regulated genes ADRB2, CASP8, CASP9, and TNFRSF1A, and the down-regulated genes MDM2, NFKB2, and TRAF2.

b- Infection of THP-1 cells heat-killed M. tuberculosis induced genes expression

Table 9 indicates the sum of up-regulated and down-regulated genes of THP-1 infection at different points in RNA-Seq analysis. The number of deferential genes strongly increased in comparison with uninfected HK-*Mtb*-infected THP-1 cells.

Table 9. Number of upregulated and downregulated genes in different time point of infection with HK-*Mtb* in THP-1 cells

Time point	Upregulated genes	Downregulated genes	Total
15 minutes	0	0	0
30 minutes	100	550	650
1 hour	24	2	26
2 hours	110	43	153
4 hours	406	318	724

DEGs for different annotated molecules are classified at various time points of live-*Mtb*-infected THP-1 cells shown at Ingenuity Pathway Analysis (IPA) as seen in Table 10.

Table 10. Classification of DEGs to canonical pathways at various time points of HK-*Mtb*-infected THP-1 cells.

Time point	Top five Canonical Pathways
15 minutes	0
30 minutes	Oxidative Phosphorylation EIF2 Signaling Mitochondrial Dysfunction Hypusine Biosynthesis Coronavirus Pathogenesis Pathway
1 hour	HMGB1 Signaling CXCR4 Signaling Opioid Signaling Pathway Sumoylation Pathway CDK5 Signaling
2 hours	Unfolded protein response Endoplasmic Reticulum Stress Pathway Circadian Rhythm Signaling p53 Signaling Cell Cycle Regulation by BTG Family Proteins
4 hours	Aldosterone Signaling in Epithelial Cells Sirtuin Signaling Pathway Unfolded protein response NRF2-mediated Oxidative Stress Response EIF2 Signaling

At each time point of infection compared to uninfected cells, molecules involved in canonical pathways were found, which were significant considering P-value and Z score Table 10. Coronavirus Pathogenesis Pathway was shown to be the most activated pathway during HK-*Mtb* infection. FOS was up-regulated while EEF1A1 RPS10, RPS15A, RPS17, RPS9, and RPS28 were down-regulated. ATP5MF, ATP5MGL, ATP5PO, COX17, MT-ND5, COX6A1, NDUFA11, NDUFA13, NDUFB8, SDHC, and UQCR11 are all genes that are upregulated in the Oxidative Phosphorylation pathway. This was the top inhibited pathway during 30 m of infection.

At 1 hour of infection, the HMGB1 signaling pathway was the highest activated pathway with three upregulated genes, FOS, OSM, and RHOB. The sumoylation pathway was inhibited with up-regulated FOS and down-regulated RHOB gene. At 2 hours of infection with HK-*Mtb*, Unfolded protein response was activated with upregulated genes DDIT3, NFE2L2, and PPP1R15A, whereas the inhibited p53 signaling pathway has upregulated genes RRM2B, THBS1, and TP53BP2. At the end of the infection, the topmost activated pathway was Unfolded protein response, comprising DDIT3, DNAJB9, EIF2AK3, HSPA1A/HSPA1B, HSPA5, HSPA6, HSPA8, HSPH1, SEL1L, and TRAF2 genes that showed upregulation. Contrary, EIF2 Signaling was the inhibited pathway with up-regulated genes EIF3E, EIF3K, HNRNPA1, MAP2K2, RPL10A, RPL14, RPL15, RPL27, RPL4, RPL5, and RPL7A, and down-regulated genes DDIT3, EIF2AK3, and HSPA5.

15 min post-infection:

None of the

differentially regulated

genes in had FDR≤0.05

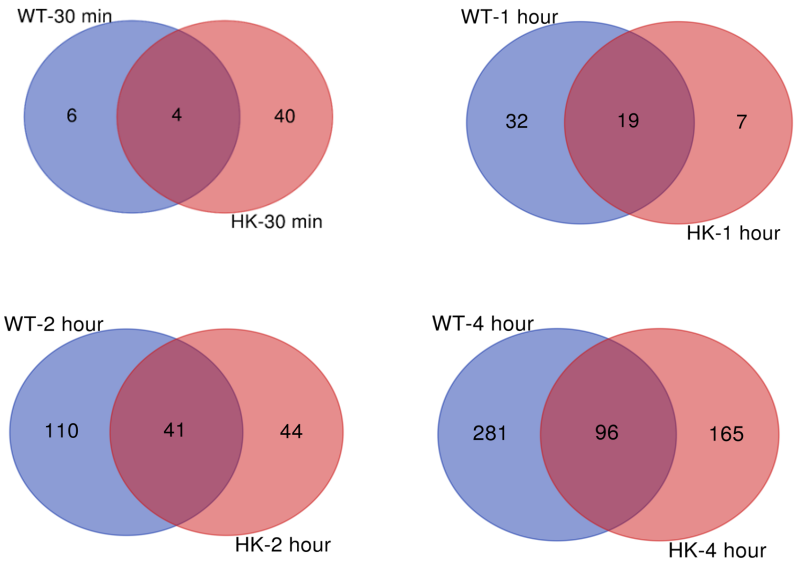

Figure 40. Overlap of differentially expressed upregulated genes between live *Mtb*-infected THP-1 and HK-*Mtb*-infected THP-1 cells.

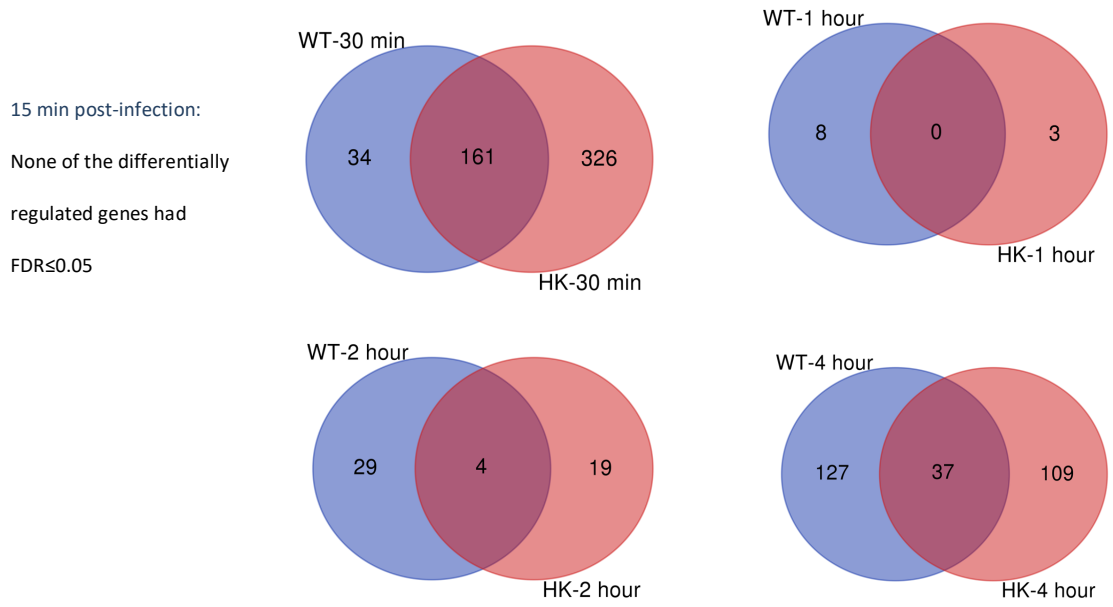

Figure 41. Overlap of differentially expressed downregulated genes between live *Mtb*-infected THP-1 and HK-*Mtb*-infected THP-1 cells.

qRT-PCR analysis of the 12 genes

Twelve genes from DEGs (DUSP1, EGR1, PSAT1, DUSP10, SGK1, CLK1, NFKBIA, RHCG, ANKRD44-IT1, ANKS1A, AMPK, and mTOR) were selected to validate the accuracy of the RNASeq results.

The findings showed that these DEGs in THP-1 cells infected with live-*Mtb* were similar to those observed in the RNASeq study. The DUSP1 gene expression levels were substantially increased by 5-fold and 3-fold at 1 and 2 hours of infection and decreased by 15 m, 30 m, and 4 hours of infection (see Figure 42). The EGR1 gene expression levels displayed a significant rise in the sequence at 30 m and 1 hr as compared to 15 m, 2 and 4 hrs of infected cells (see Figure 44). The PSAT1 gene displayed a small decline in

expression at 2 and 4 hours relative to 30 m. (1.5-fold change) (see Figure 43). The DUSP10 gene expression was less than 2-fold at 15 and 30 m of infection but improved significantly at 1, 2, 4 hrs of infection (Figure 47). Fold change in the gene expression of the SGK1 gene was increased during 1 hour of infection, but decreased during other time points of infection (see Figure 45). CLK1 gene expression increased 4-fold over 1 and 4 hours and was significant compared to 30 m of infection (see Figure 46). NFKBIA gene expression increased significantly at 1 and 2 hrs above 15, 30 m, and 4 hrs (see Figure 49). A significant increase in RHCG gene expression was observed at 2 and 4 hrs (15-fold and 12-fold, respectively), but not at 15 m-1 hr of infection (see Figure 53). ANKRD44-IT1, ANSKS1A, and mTOR gene expressions decreased persistently from 15 m to 4 hours of infection (see Figure 50, Figure 48, and Figure 51). No major changes in the expression of the AMPK gene have been observed at all time points of infection (see Figure 52).

The deferential gene expression of 12 genes were demonstrated in the HK-*Mtb*-infected THP-1 cells. These genes have the following expression patterns. DUSP1 gene expression levels were significantly increased by 10-, 15-, and 13-fold during 0.5, 1, and 4 hrs of infection, while 0.25 and 2 hr of infection were not significantly increased (see Figure 42). There is a significant upregulation of EGR1 gene expressions from 2-folds at 0.25 hr to 3-folds at 0.5 hr peaking to 15-folds at 1 hr and decreased steadily from 2 to 4 hrs of infection (see Figure 44). The PSAT1 gene expression level was significantly increased by 2-fold during 4 hours of infection, whereas the remaining time of infection was not significantly increased (see Figure 43). Fold change in the expression of the SGK1 gene was augmented throughout 1 and 2 hours of infection (4-fold); however, no major

differences were observed at other time points of infection (see Figure 45). After 2 and 4 hours of infection (4-and 3-fold change respectively), the changes in the expression of the gene CLK1 was increased, and there were no significant differences in other infection time points (see Figure 46). Gene expression of DUSP10 was steady at a 2-fold change in the period of 0.25 to 1 hr infection but increased at 2 and 4 hours of infection (4- and 6-fold respectively) (see Figure 47). NFKBIA gene expression was stable at 0.25-1 hour 1-fold change, then increased within 2 and 4 hrs of infection (2.5-folds) (see Figure 49). The expression of the ANKRD44-IT1 gene persistently decreased from 15 m to 4 hrs (see Figure 50). The mTOR gene expression displayed a significant increase from 0.5 to 2 hours, and a marked decline was observed at 4 hrs after infection (see Figure 51). RHCG gene expression was constant at less than 2-folds at the infection duration between 0.25 and 1 hour, then elevated at 2 and 4 hours of the infection (5- and 8-folds, respectively) (see Figure 53). No significant changes were noted in AMPK and ANSKS1A genes' expression at all time points of infection (see Figure 52 and Figure 48).

The comparison between live-*Mtb*-infected THP-1 cells and HK-*Mtb*-infected THP-1 cells in the gene expressions of 12 genes after infection revealed variations and similarities at different times. Significant increases in DUSP1 gene expression were detected in HK-*Mtb*-infected THP-1 compared to the live-*Mtb*-infected THP-1 at 0.5, 1, and 4 hrs of infection (see Figure 42). The increase in EGR1 gene expression continued from 0.25 hr until it reached its peak an hour after infection (15-fold) with HK-*Mtb*, remaining (3-fold) more than the live-*Mtb*-infected cells, followed by a sudden decline without a noticeable increase (see Figure 44). PSAT1 gene expression started to decrease

from 0.25 hr to its lowest level an hour after infection, followed by a sharp increase after 4 hrs (see Figure 43). SGK1, DUSP10, and CLK1 gene expressions decreased significantly in 1 hour of HK-*Mtb*-infected cells, while no significant differences were observed in the remaining time points of infection (see Figure 45, Figure 47, and Figure 46). The NFKBIA gene expression was increased considerably in HK-*Mtb*-infected THP-1 more than in THP-1 infected with live-*Mtb*-infected 2 and 4 hrs after infection (see Figure 49). ANSKS1A gene expressions increased significantly at all time points of the HK-*Mtb*-infected cells, while no significant differences were found at 0.25 hr of infection (see Figure 48). In HK-*Mtb*-infected THP-1, a significant increase in ANKRD44-IT1 gene expression was observed at 0.25 and 4 hrs of infection more than in live-*Mtb*-infected THP-1 (see Figure 50). Expression of the mTOR gene was declined after 0.25 hours, followed by a significant increase at remaining time points of infection in HK-*Mtb*-infected THP-1 comparison to live-*Mtb*-infected THP-1 cells (see Figure 51). Significantly higher expression of the AMPK gene was noted in all HK-*Mtb*-infected THP-1 cells versus live-*Mtb*-infected THP-1 cells in all-time points of infection (see Figure 52). RHCG gene expression was significantly reduced in HK-*Mtb*-infected THP-1 at 2 and 4 hours of infection more than in live-*Mtb*-infected THP-1 at the same time points (see Figure 53).

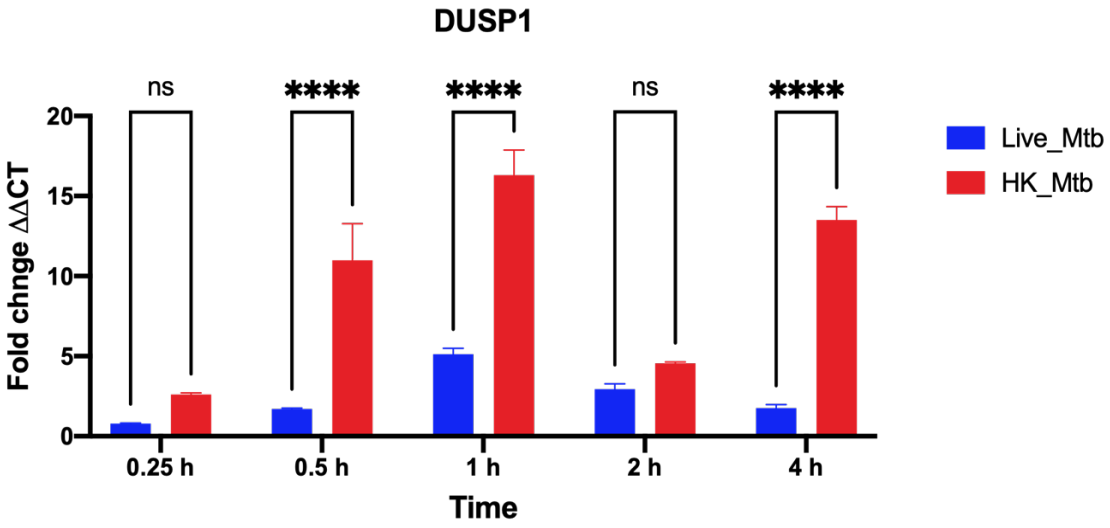

Figure 42. Comparison the transcript levels of DUSP1 in wild-type THP-1 cells after live *Mtb* and heat-killed *Mtb* infection. The DUSP1 transcript levels were assessed in different time points (0.25, 0.5, 1, 2, and 4 hrs) after infection by quantitative real-time PCR using total RNA. The transcript levels were calculated relative to GAPDH control housekeeping gene values are expressed to fold change in gene expression for infected cells compared to uninfected controls. Errors bars represent the slandered errors from the means of three independent experiments. *, P < 0.05; **, P < 0.01; ***, P < 0.001; ****, P < 0.0001.

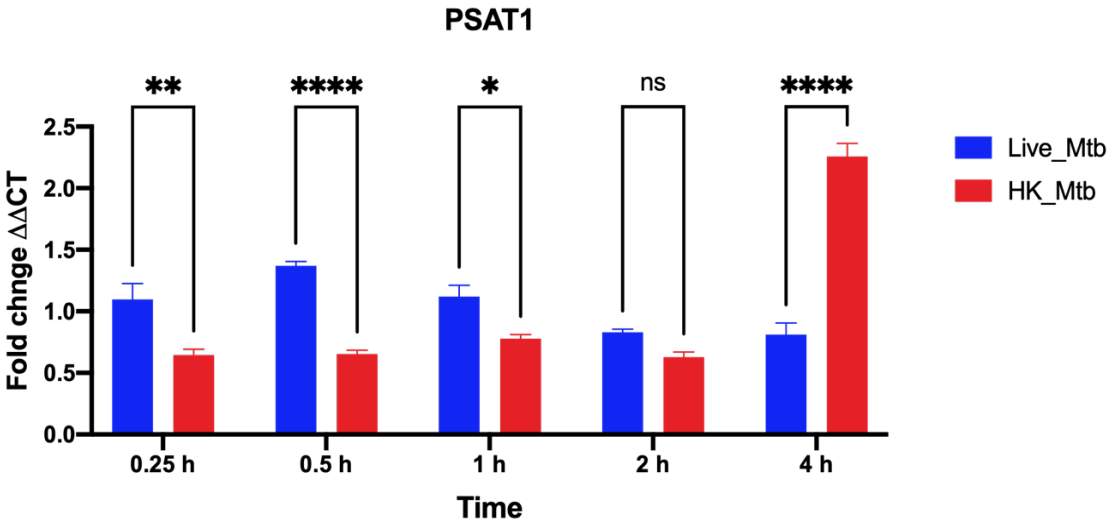

Figure 43. Comparison the transcript levels of PSAT1 in wild-type THP-1 cells after live *Mtb* and heat-killed *Mtb* infection. The PSAT1 transcript levels were assessed in different time points (0.25, 0.5, 1, 2, and 4 hrs) after infection by quantitative real-time PCR using total RNA. The transcript levels were calculated relative to GAPDH control housekeeping gene values are expressed to fold change in gene expression for infected cells compared to uninfected controls. Errors bars represent the slandered errors from the means of three independent experiments. *, P < 0.05; **, P < 0.01; ***, P < 0.001; ****, P < 0.0001.

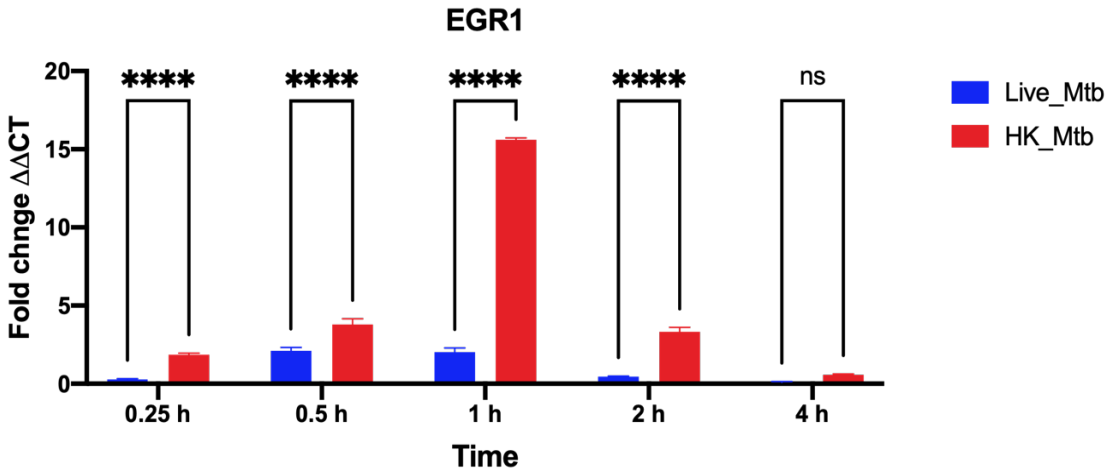

Figure 44. Comparison the transcript levels of EGR1 in wild-type THP-1 cells after live *Mtb* and heat-killed *Mtb* infection. The EGR1 transcript levels were assessed in different time points (0.25, 0.5, 1, 2, and 4 hrs) after infection by quantitative real-time PCR using total RNA. The transcript levels were calculated relative to GAPDH control housekeeping gene values are expressed to fold change in gene expression for infected cells compared to uninfected controls. Errors bars represent the slandered errors from the means of three independent experiments. *, P < 0.05; **, P < 0.01; ***, P < 0.001; ****, P < 0.0001.

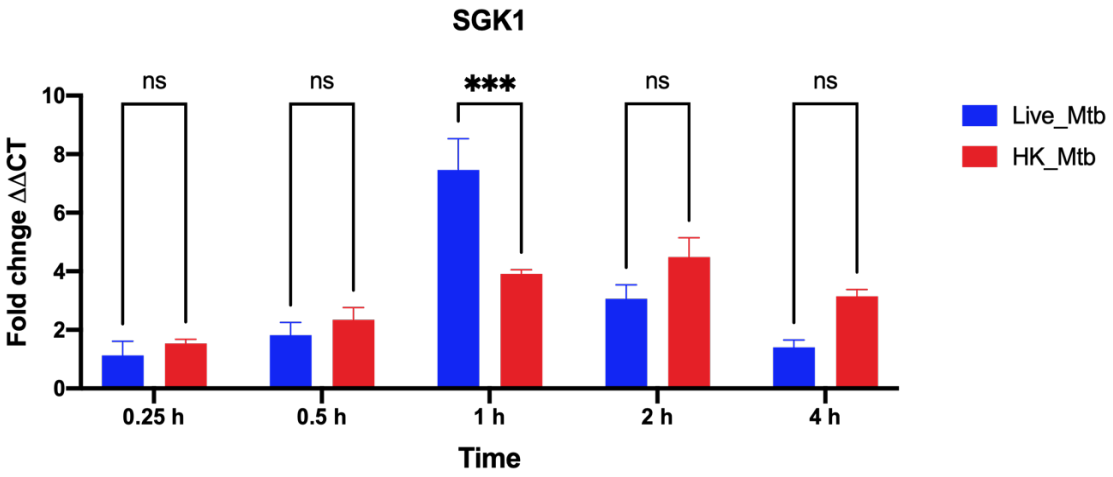

Figure 45. Comparison the transcript levels of SGK1 in wild-type THP-1 cells after live *Mtb* and heat-killed *Mtb* infection. The SGK1 transcript levels were assessed in different time points (0.25, 0.5, 1, 2, and 4 hrs) after infection by quantitative real-time PCR using total RNA. The transcript levels were calculated relative to GAPDH control housekeeping gene values are expressed to fold change in gene expression for infected cells compared to uninfected controls. Errors bars represent the slandered errors from the means of three independent experiments. *, P < 0.05; **, P < 0.01; ***, P < 0.001; ****, P < 0.0001.

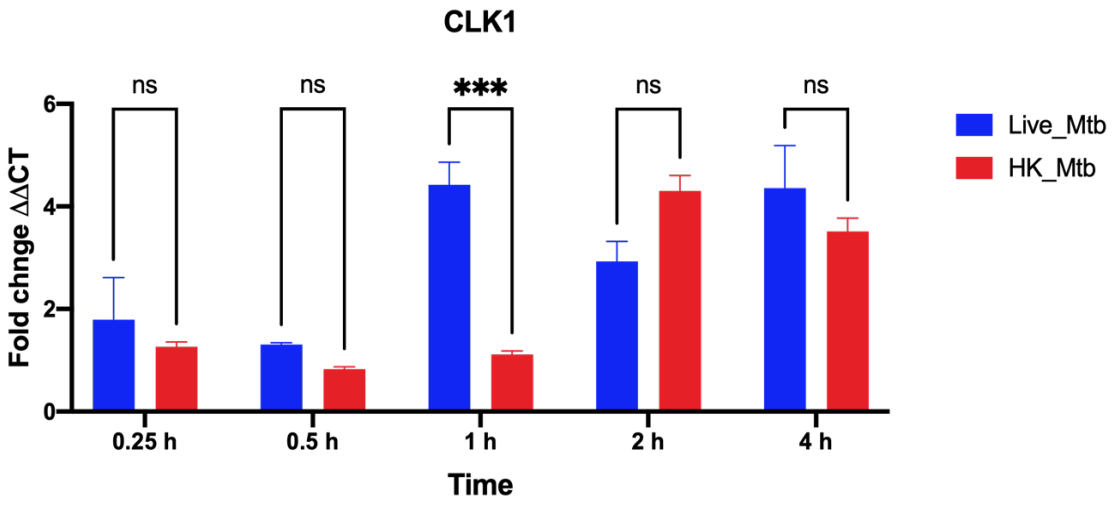

Figure 46. Comparison the transcript levels of CLK1 in wild-type THP-1 cells after live *Mtb* and heat-killed *Mtb* infection. The CLK1 transcript levels were assessed in different time points (0.25, 0.5, 1, 2, and 4 hrs) after infection by quantitative real-time PCR using total RNA. The transcript levels were calculated relative to GAPDH control housekeeping gene values are expressed to fold change in gene expression for infected cells compared to uninfected controls. Errors bars represent the slandered errors from the means of three independent experiments. *, P < 0.05; **, P < 0.01; ***, P < 0.001; ****, P < 0.0001.

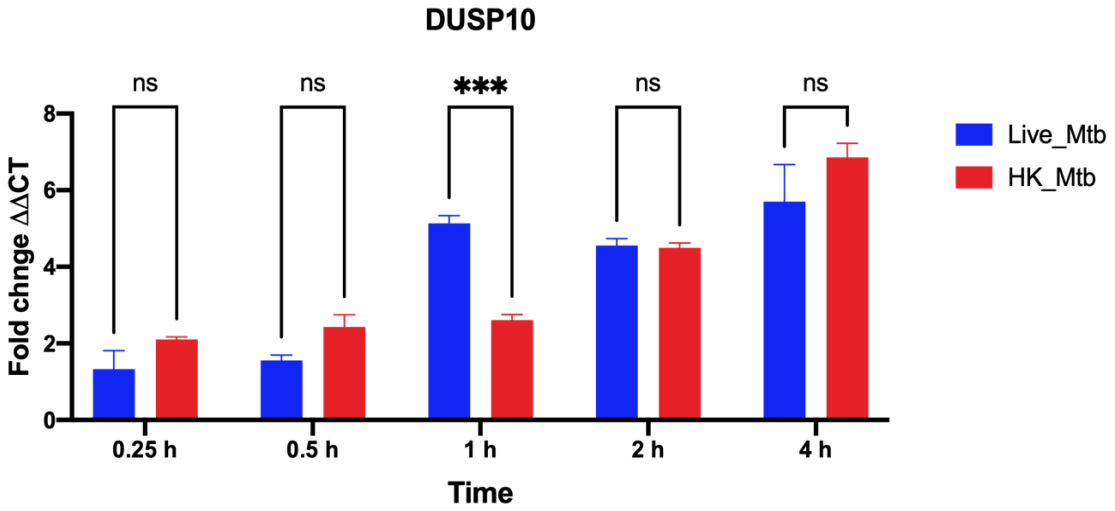

Figure 47. Comparison the transcript levels of DUSP10 in wild-type THP-1 cells after live *Mtb* and heat-killed *Mtb* infection. The DUSP10 transcript levels were assessed in different time points (0.25, 0.5, 1, 2, and 4 hrs) after infection by quantitative real-time PCR using total RNA. The transcript levels were calculated relative to GAPDH control housekeeping gene values are expressed to fold change in gene expression for infected cells compared to uninfected controls. Errors bars represent the slandered errors from the means of three independent experiments. *, P < 0.05; **, P < 0.01; ***, P < 0.001; ****, P < 0.0001.

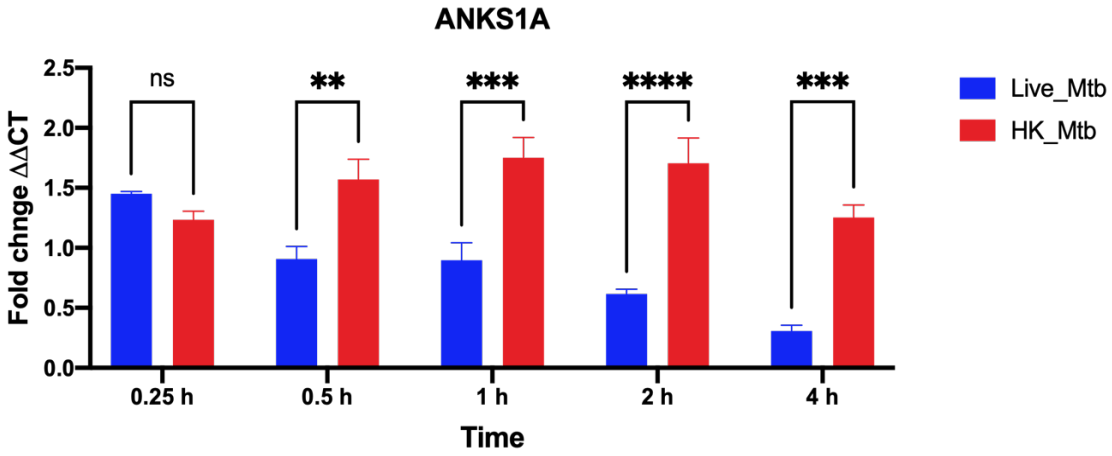

Figure 48. Comparison the transcript levels of ANKS1A in wild-type THP-1 cells after live *Mtb* and heat-killed *Mtb* infection. The ANKS1A transcript levels were assessed in different time points (0.25, 0.5, 1, 2, and 4 hrs) after infection by quantitative real-time PCR using total RNA. The transcript levels were calculated relative to GAPDH control housekeeping gene values are expressed to fold change in gene expression for infected cells compared to uninfected controls. Errors bars represent the slandered errors from the means of three independent experiments. *, P < 0.05; **, P < 0.01; ***, P < 0.001; ****, P < 0.0001.

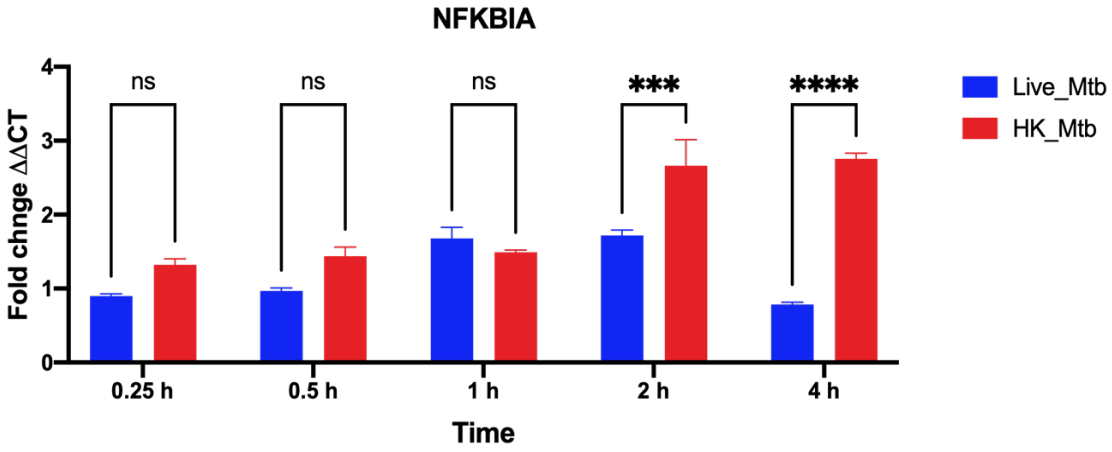

Figure 49. Comparison the transcript levels of NFKBIA in wild-type THP-1 cells after live *Mtb* and heat-killed *Mtb* infection. The NFKBIA transcript levels were assessed in different time points (0.25, 0.5, 1, 2, and 4 hrs) after infection by quantitative real-time PCR using total RNA. The transcript levels were calculated relative to GAPDH control housekeeping gene values are expressed to fold change in gene expression for infected cells compared to uninfected controls. Errors bars represent the slandered errors from the means of three independent experiments. *, P < 0.05; **, P < 0.01; ***, P < 0.001; ****, P < 0.0001.

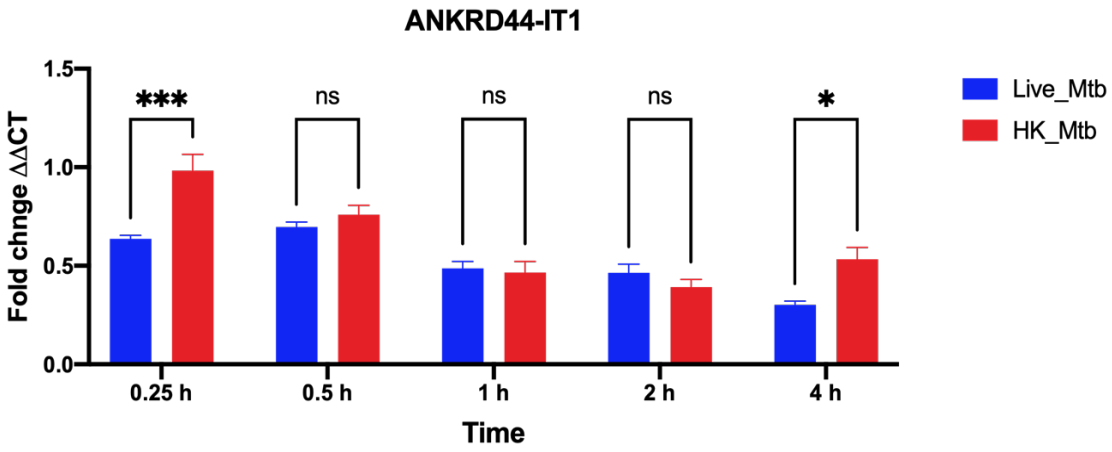

Figure 50. Comparison the transcript levels of ANKRD44-IT1 in wild-type THP-1 cells after live *Mtb* and heat-killed *Mtb* infection. The ANKRD44-IT1 transcript levels were assessed in different time points (0.25, 0.5, 1, 2, and 4 hrs) after infection by quantitative real-time PCR using total RNA. The transcript levels were calculated relative to GAPDH control housekeeping gene values are expressed to fold change in gene expression for infected cells compared to uninfected controls. Errors bars represent the slandered errors from the means of three independent experiments. *, P < 0.05; **, P < 0.01; ***, P < 0.001; ****, P < 0.0001.

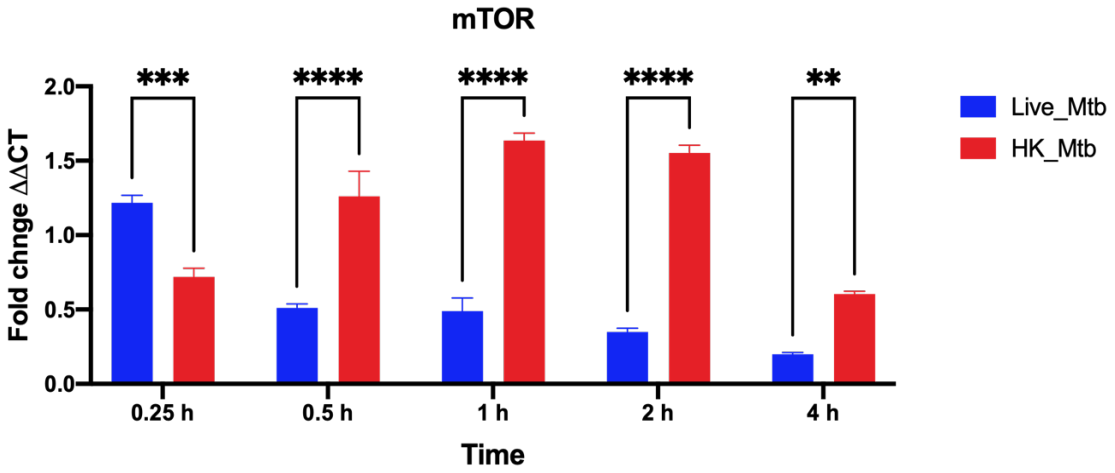

Figure 51. Comparison the transcript levels of mTOR in wild-type THP-1 cells after live *Mtb* and heat-killed *Mtb* infection. The mTOR transcript levels were assessed in different time points (0.25, 0.5, 1, 2, and 4 hrs) after infection by quantitative real-time PCR using total RNA. The transcript levels were calculated relative to GAPDH control housekeeping gene values are expressed to fold change in gene expression for infected cells compared to uninfected controls. Errors bars represent the slandered errors from the means of three independent experiments. *, P < 0.05; **, P < 0.01; ***, P < 0.001; ****, P < 0.0001.

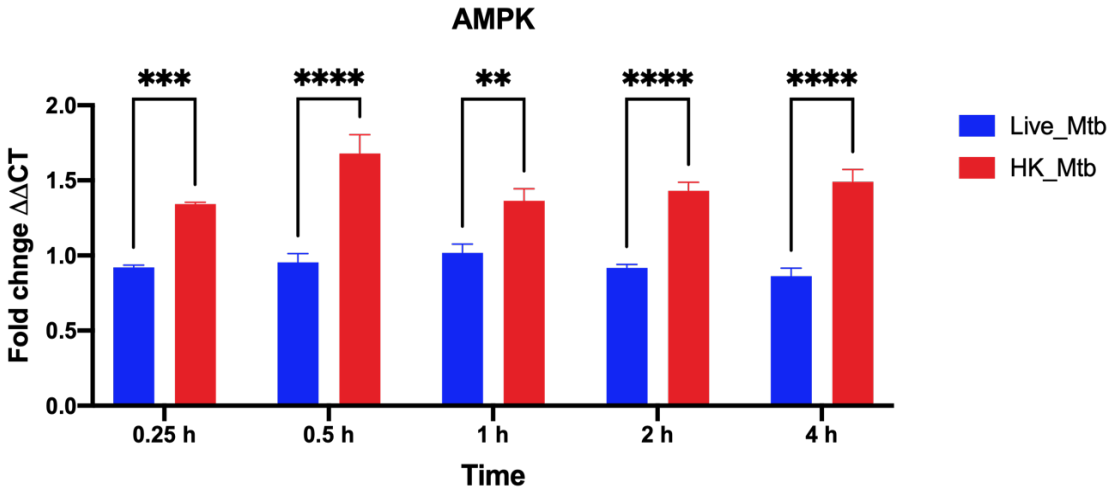

Figure 52. Comparison the transcript levels of AMPK in wild-type THP-1 cells after live *Mtb* and heat-killed *Mtb* infection. The AMPK transcript levels were assessed in different time points (0.25, 0.5, 1, 2, and 4 hrs) after infection by quantitative real-time PCR using total RNA. The transcript levels were calculated relative to GAPDH control housekeeping gene values are expressed to fold change in gene expression for infected cells compared to uninfected controls. Errors bars represent the slandered errors from the means of three independent experiments. *, $P < 0.05$; **, $P < 0.01$; ***, $P < 0.001$; ****, $P < 0.0001$.

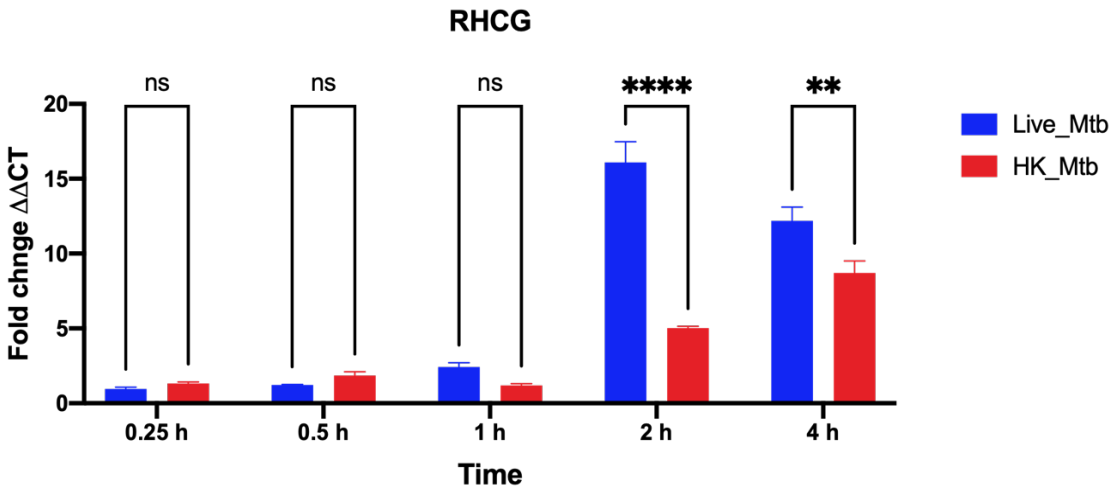

Figure 53. Comparison the transcript levels of RHCG in wild-type THP-1 cells after live *Mtb* and heat-killed *Mtb* infection. The RHCG transcript levels were assessed in different time points (0.25, 0.5, 1, 2, and 4 hrs) after infection by quantitative real-time PCR using total RNA. The transcript levels were calculated relative to GAPDH control housekeeping gene values are expressed to fold change in gene expression for infected cells compared to uninfected controls. Errors bars represent the slandered errors from the means of three independent experiments. *, $P < 0.05$; **, $P < 0.01$; ***, $P < 0.001$; ****, $P < 0.0001$.

Discussion

THP-1 macrophages were utilized to explain the role of Eph receptors in HK-*Mtb* infection. EphA1 was induced by 1-fold at 30 minutes and 3-fold at four hours after *Mtb* exposure to THP-1 cells (compared to the uninfected control). These findings demonstrate the capacity of *Mtb* to induce Ephrin type-A expression in macrophages. EphA2 was induced by the infection of THP-1 cells by *Mtb* at 15 minutes post-infection and peaked at 4 hours later to 2.5-fold (compared to the uninfected control). Induction of EphA2 gene expression was observed in macrophages infected by *Mtb* as EphA1. EphrinA1, a ligand of the EphA1 and EphA2 receptors, was induced at an elevated level in THP-1 cells due to the infection caused by active *Mtb*. This started with a 1-fold increase at 15 m and then increased to over 14-fold at 4 h. According to our experiment results, *Mtb* induces EphrinA1 ligands in THP-1 cells.

These findings show that EphA1 and Epha2 receptors and their ligand EphrinA1 are induced by *Mycobacterium tuberculosis* infection. To fulfill this task, *Mtb* must trigger intracellular molecules and events to activate these cells. Researchers also discovered that active macrophages present "infectious debris" of *Mtb* as antigens for T cells and even contributing to cytokine production such as interleukins-12 (IL-12) and tumor necrosis factor-α (TNF-α) [147-149]. EphA-receptors suppress MAPK by inhibiting signaling [150]. Macrophage cells play a major role in the infection and proliferation of *Mtb*. The best way to decrease microbicidal behavior that in MAPK regulated pathway is to block the MAPK signals. One effect of this blocking is the inhibition of pro-inflammatory cytokines, which are beneficial for removing *Mycobacterium tuberculosis*. Many forms

of immune cells express Eph receptors (e.g., T-cells, dendritic cells, granulocytes), so further studies are needed to establish downstream signaling mechanisms [151]. Research found that EphA1 and EphA2 were induced during *Mtb* infection, and cytokines' expression was increased. The analysis confirmed an increase in nitrous oxide within macrophages of EphA2$^{-/-}$ macrophages after infection with *Mtb*. This illustrates how *Mtb* persists in the EphA2$^{-/-}$ macrophages over those of wild-type macrophage [130].

Effects that were performed on THP-1 cells infected with dead *Mtb* indicated a delay in the expression of the EphA receptor genes. After 2 and 4 hours of infection, the level of EphA1 was lower in HK-*Mtb*-infected THP-1 than in live-*Mtb*-infected THP-1. There was a significant reduction in EphA2 gene expression 1 and 2 hours after infection in HK-*Mtb*-infected THP-1 cells below live-*Mtb*-infected THP-1 cells. Although EphrinA1 gene expression was lower in cells infected with dead *M. tuberculosis* at 2 and 4 hours after infection, it was significantly higher in cells infected with live *Mtb*.

After 30 minutes of live and dead infection, Coronavirus Pathogenesis Pathway was the most involved pathway. Coronavirus pathogenesis pathway genes (RPS10, RPS15A, RPS25, RPS27, RPS28, and RPS3A) are related with encoding ribosomal proteins and involved in protein synthesis [152]. The interactions of these ribosomal proteins with viral RNA for biosynthesis of virus proteins have been shown to be necessary for viral replication in the hosts [153].

RPs genes are also involved in a host of extra-ribosomal functions. Ribosome assembly by individual RNAs and RPs is a closely controlled process in normal situations, with unassembled RPs being rapidly degraded. These free RPs can, in some cases,

participate in a broad range of extra-ribosomal functions, including cell cycle progression control, immune signals, and cellular growth [154]. EEF1A1, a virus target, is known to be triggered in response to inflammation. [153].

Another practical metabolic pathway, Oxidative phosphorylation, was the top inhibited pathway post 30 minutes of live and dead *Mtb* infection. Oxidative phosphorylation is the pathway that cells use to generate adenosine triphosphate (ATP). In the course of cellular respiration, cells oxidize nutrients to create chemical energy. This is found in mitochondria in most eukaryotes. The transcriptional changes identified in the host metabolism indicate the cell is more reliant on glycolysis. Most host immune cells use this glycolysis technique of bioenergetic for rapid ATP development during infection by *Mycobacterium tuberculosis*. May be the short time of infection of *Mtb* is not enough to activate the Oxidative phosphorylation.

High mobility group box Protein1 (HMGB1) was the top pathway that activated post one hour of infection by live and dead *Mtb*. HMGB1 is an endogenous protein produced in the extracellular environment during stress [158-160]. In a concentration-dependent manner, HMGB1 can connect the TLR4 receptor**.** [161, 162]. The CD14 co-receptor on macrophages is primarily responsible for the activity of the HMGB1-dependent TLR4 receptor in vitro. [163]. The HMGB1 protein forms immune-stimulatory complexes with cytokines, endogenous and exogenous ligands (e.g., bacterial lipopolysaccharides (LPS)) that stimulate the innate immune system [164, 165]. HMGB1 is synergistically associated with the activity of several molecules and their ligands, such as LPS (TLR4 ligand), CpG-ODN (TLR9 ligand), or Pam3CSK4 (TLR1: TLR2 ligand)

when applied to human peripheral blood mononuclear cells (PBMC) [165]. *Mycobacterium* infection successfully triggered the release of HMGB1 into both macrophage and monocytic cells. Components of *Mtb*-whole cell lysate include TLR ligands that induce HMGB1 active secretion after 24 hrs of infection [208]. However, in our study, the incubation time (4 hrs) of HK-*Mtb* with THP-1 cells was not enough to induce the HMGB1.

ERK/MAPK Signaling, was the one of pathways that inhibited after one hour of *Mtb* infection in the WT-THP-1 cells. ERK/MAPK kinases possess several targets in the nucleus, which include transcription factors and other kinases such as ERK1, ETS1, ATF2, MITF, MAPKAPK2, amongst others. Production of IFN-γ as a result of *Mtb* infection is related to the ERK/MAPK phosphorylation. Mitogen-activated protein kinases (MAPKs) are responsible for various features of immune responses, involving the start of innate immunity, stimulation of adaptive immunity, and ending of immune responses through cell death and regulatory T cells [163, 164]. MAPKs are essential for macrophage activation as they phosphorylate and activate molecules downstream. *Mycobacterium*-induced proinflammatory cytokines, such as TNF-α and interleukin 1, depend on MAPK activation [165]. There is evidence that the extracellular signal-regulated kinase (ERK) has a role in the antimycobacterial activity of antigen-presenting cells. ERK and MAPKs regulate IFN-γ releasing against *Mtb* by a mechanism that involves cyclic adenosine monophosphate response element-binding protein CREB [166].

After two to four hours of WT-THP-1 and at four of EphA1-KO THP-1 cells infection, the NRF2-mediated Oxidative Stress Response pathway was the activated

pathway. Nuclear respiratory factor 2 (NRF2) is a transcriptional factor that responds to many harmful conditions such as reactive oxygen species [167, 168], and plays an essential function in cellular detoxification and stress responses [169]. Additionally, it is responsible for antioxidation and metabolism [170]. NRF2 was reported to be a prominent player in the inhibition of proinflammatory gene expression [171]. In normal circumstances, NRF2 binds Kelch-like ECH-associated protein 1 (KEAP1) and continues to do so in the cytoplasm [167, 172]. When NRF2 activity occurs due to stress signals, the linkage between KEAP1 protein is detached, releasing NRF2, and then it is present in the nucleus as a transcriptional factor [173].

After two hours of *Mtb* infection WT-THP-1, p38 MAPK Signaling was the top inhibited pathway. The p38 MAP kinases works as a portal for signal transduction and is active in a number of biological processes. Inflammation, cell cycle, cell death, growth, and cell differentiation all support from p38 as a signal transduction mediator [177]. The p38 MAPK plays a major role in organizing the host's immune response by controlling the production of proinflammatory cytokines such as IL-1β or TNF during infection [178]. TNF- stimulates the p38 MAPK pathway [179]. However, stimulation of p38 MAPK in two hours of *Mtb* infection was not enough.

Myc Mediated Apoptosis Signaling was the inhibited pathway after WT-THP-1 infection by *Mtb*. Myc Mediated Apoptosis Signaling, a transcriptional factor associated with apoptosis intracellular environment, showed a reduction of survival factors [174]. Myc is a regulator of cell growth, proliferation, differentiation, metabolism, and apoptosis [175]. Myc expression increases cells' sensitivity to proapoptotic disruption, such as DNA

damage, genotoxic stress, and death receptor signaling [176]. Mitogens is responsible for inducing Myc expression, doing so via downregulation during the differentiation of cells [177]. Myc is associate with many cancer-related mutations that lead to the development of the disease. It is also implicated in many activities of certain enzymes involved in DNA metabolism and many other metabolic pathways. Meanwhile, it suggested that Myc is the regulator of cell cycle machinery [178].

SUMOylation was the inhibited pathway after one hour of HK-*Mtb* infection. SUMOylation is one of the post-translation protein modifications in which lysine (Lys) is conjugated in the target protein with a member of a small ubiquitin-like protein family (SUMO). Change in SUMOylation is a reversible and dynamic mechanism in which sentrin/SUMO-specific proteases can deSUMOylated the proteins [209]. SUMOylation regulates a wide range of biochemical processes, including protein localization, DNA repair, genome arrangement, DNA-protein binding, and transcription regulation [210]. SUMO governs many host proteins involved in adaptive and innate immunity, thus leading to the mechanism of interferon development through infection [211, 212]. The Sumoylation pathway plays a crucial role in plant and mammalian immunity [213, 214]. During *Mtb* infection, TNF-α and IL-6 are expressed by regulating NF-κB singling, which depends on the peroxisome proliferator-activated receptor (PPAR- γ) [215]. PPAR- γ governs the immune response in *Mtb*-infected macrophage. Inhibiting the SUMOylation of PPAR- γ promotes the innate immune response during *Mtb* infection [216].

At 2-4 hours of HK-*Mtb* infection to WT-THP-1 cells, Unfolded protein response (UPR) was the highest activated pathway. UPR is a stress response that happens in the cell

in response to an elevated endoplasmic reticulum (ER) stress [217]. UPR molecule has been determined in most species of mammals. Unfolded protein response in ER stress response reduces a load of unfolded protein to restore ER homeostasis by promoting the secretory pathway [217]. Via several modalities, UPR and inflammatory reaction are related, involving elevated reactive oxygen species (ROS), high calcium release from the ER, initiation of JNK, and stimulation of NF-κB signaling [218]. NF-κB plays a pivotal function in the intracellular inflammatory process [219]. UPR initiates signaling pathways that modulate pro-inflammatory and pro-death signals to increase cell death in the event of extreme and prolonged ER stress [220]. The response to endoplasmic reticulum stress (ERS) is a cellular mechanism caused by mycobacterial infection, which disrupts protein folding in the endoplasmic reticulum (ER). As a result, the unfolded protein response is activated to decrease early protein synthesis and unfolded and misfolded protein aggregation within ER to restore regular cell physiological activity. Prolonged or unregulated ER stress allows the cell to transition into apoptosis through the three signaling pathways (IRE1, PERK, and ATF6) [221].

At 2 hours of infection with HK-*Mtb*, p53 signaling was inhibited pathway. The p53 signaling pathway is responsible for inducing apoptosis or programmed cell death. To decrease mycobacterial viability, apoptosis of *Mtb*-infected macrophages is needed [222]. The mycobacterium inhibits apoptosis of the macrophages by up-regulating IL-10 development, contributing to increase expression of Bcl2 and decrease pro-apoptotic factors such as cleaved caspase-1 and P53 [223].

At four hours after HK-*Mtb* infection, Eukaryotic initiation factor 2 (EIF2) was the inhibited pathway. EIF2 is a fundamental eukaryotic initiation factor implicated in several eukaryotic translation initiation events. EIF2 mediates the ribosome-binding of met-tRNA. EIF2-α kinase phosphorylates EIF2 during the stress response, which controls protein synthesis responses to various stresses [185]. The increased EIF2 activity promotes the proliferation of *Mtb* within macrophages. In TB-associated caseous granulomas in humans, a large increase of the eif2-α kinase was detected. So, HK-*Mtb* may not activate the Eukaryotic initiation factor 2 (EIF2) since it is not a live organism to improve the proliferation of *Mtb***.**

CHAPTER IV

EXPRESSION OF EPHRIN GENES EPHA1, EPHA2 AND EPHRINA1 IN TB-POSITIVE AND NEGATIVE PATIENTS

Introduction

The major family of receptor tyrosine kinases identified in both invertebrates and vertebrates is the erythropoietin-producing hepatoma (Eph) receptors [57, 224]. EphA receptors are part of the Eph family of tyrosine kinase receptors, composed of two main groups (EphA and EphB), characterized by their ligand specificity (Ephrin-A and Ephrin-B, respectively). Axon regulation, vascularization, tissue assembly, cell conformity, and migration are all part of Eph receptors functions [225-227]. Several EphA receptors are expressed in immune cells, including peripheral $CD4^+$ T blood cells, interstitial DC, and Langerhans cells [225, 227-229]. EphA receptors can mediate the migration of T cells following activation by chemokines like stromal cell-derived factor-l α (SDF-l α) and macrophage inflammatory protein-3 β (MIP-3 β) [136, 230]. In *Mtb*-activated human DCs, MIP-3 β is an upregulated ligand for the chemokine receptor CCR7. The ligand MIP-3 β is responsible for interacting with the chemokine CCL21 also [231, 232].

These findings show that EphA receptors play an essential role in chemokine-mediated migration of cells, a process that is able to influence the immune response to *Mtb* infection. Research indicates the upregulation of EphAl and EphA3 genes following *Mtb* infection in the human monocytic/macrophage cell lines THP-1 and U937 [128, 129]. A study revealed how the EphA receptors play a crucial role in the host immune response to Mtb infection [201]. The study showed evidence of expression of the EphA1, EphA2,

and EphrinA1 genes was also seen in macrophages infected with *Mtb* [201]. The study demonstrated increased T cell recruitment in EphA2$^{-/-}$ mice response during Mtb infection. Increased expression of EphA receptors and EphrinA1 led to decreased migration of $CD4^{+}$ and $CD8^{+}$ immune cells and development of proinflammatory cytokines [201]. By regulating gene transcription, biological processes rely on gene expression modification as an essential regulatory change [233]. In blood cells of patients with pulmonary TB or LTBI, notable gene expression regulation has been identified [234]. Immune response-related RNAs in patients with human TB are being used as biomarkers, such as interferon signaling and Toll-like receptors [235, 236]. Another study explained the gradual increase of EphA4 gene expression in peripheral blood of TB patients using RT-qPCR [237]. From this, our hypothesis is that the EphA receptors and EphrinA1 highly decreased in the peripheral blood mononuclear cells, increasing the recruitment of the immune cells to the infection site. We observed differences in gene expressions between positive TB and negative TB patinates of Epha1, EphA2, and EphrinA1 genes.

Materials and Methods

Participants

All eight participants were recruited from February 2015 to February 2018. The number of infected people was four TB-positive people, and similarly, four healthy people. All the infected individuals were females, and their ages were 23, 24, 28, and 29 years old. Three of the healthy individuals were females, and the fourth one was male, and their ages were 20, 23, 49, and 60 years old.

Specimen collection and RNA isolation

Clinical peripheral blood specimens were collected from healthy and TB infected individuals. Peripheral blood mononuclear cells (PBMCs) were isolated using Ficoll tubes approach. The samples were stored at -80 C until RNA extraction.

Total RNA from PBMCs was isolated using Macherey-Nagel NucleoSpin RNA XS kit (Macherey Nagel; 740902.50), following the manufacturer's instructions. The quantity of total RNA was measured by a Nanodrop spectrophotometer (Thermo Scientific; 840-274200).

cDNA synthesis and RT-qPCR relative expression analysis

According to the manufacturer's instructions, total RNA (500 ng) was used for cDNA synthesis using SuperScript IV VILO Mastermix (Thermo Scientific; 11766050).

qPCR was performed by using the primers for EphA1, EphA2, and EphrinA1. The quantity of mRNA for each gene was measured using SYBR Green and a PowerUp Master Mix (A25742; Applied Biosystems). The specific primers for the qRT-PCR were for EphA1, forward EphA1-F 5' - ATC TTT GGG CTG CTG CTT GG-3' and reverse EphA1-R 5' - GCT TGT CCT CTC GAT CCA CAT C-3', for EphA2, forward EphA2-F 5' - GGC AGG AGT TGG CTT CTT TAT-3' and reverse EphA2-R 5' - GGG CTT CAG TTG TTC TGA CTT-3', and for EphrinA1, forward EphA1-F 5' - TCA AAG AAG GAC ACA GCT ACT AC-3' and reverse EphA1-R 5' - CCT GAG GAC TGT GAG TGA TTT-3'. Negative controls for the reaction were total RNA and without temple (NTC). The relative expressions of EphA1, EphA2, and EphrinA1 were normalized to the endogenous control GAPDH gene using the following primers: forward GAPDH-F 5' - CCA GGT

GGT CTC CTC TGA CTT-3' and reverse GAPDH-R 5' - GTT GCT GTA GCC AAA TTC GTT GT-3' using the difference between reference and target Ct values for each sample method [238]. Calculation of fold induction was based on the Ct values to quantify transcript levels. As equation below.

Ratio (reference/target) = $2^{Ct(reference) - Ct(target)}$

Statistical analysis

The experimental data are presented as mean ± SE. The GraphPad Prism9 (GraphPad Software, Inc.) was used to do all statistical analysis. Statistical significance was determined using an ANOVA test. Differences were considered for p-values less than 0.05.

Results

To determine the EphA1, EphA2, and EphrinA1 gene expressions of PBMCs from TB-positive and TB-negative patients, eight cDNA samples were used for RT-qPCR. The results showed ¾ of TB-negative samples were higher than TB-positives patients in EphA1 gene expression (see Figure 54). Similarly, EphA2 gene expressions were higher in ¾ of TB-negative patients than in TB-positives patients (see Figure 55). On the other hand, EphrinA1 gene expression showed no differences between TB-negative and TB-positives patients (see Figure 56).

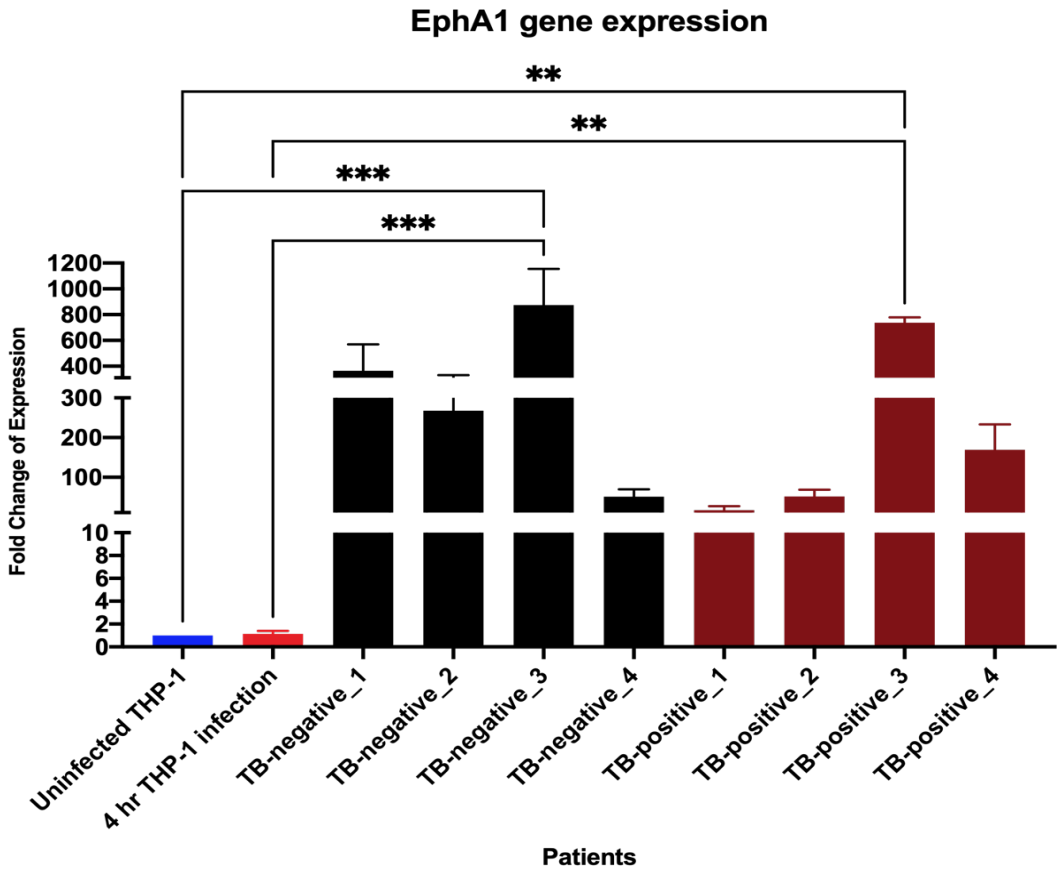

Figure 54. Comparison the transcript levels of EphA1 in PBMCs cells in positive and negative TB patients. The EphA1 transcript levels was assessed in eight people by quantitative real-time PCR using total RNA. The transcript levels were calculated relative to GAPDH control housekeeping gene values are expressed to fold change in gene expression for infected cells compared to uninfected controls. Errors bars represent the slandered errors from the means of three independent experiments. *, P < 0.05; **, P < 0.01; ***, P < 0.001; ****, P < 0.0001.

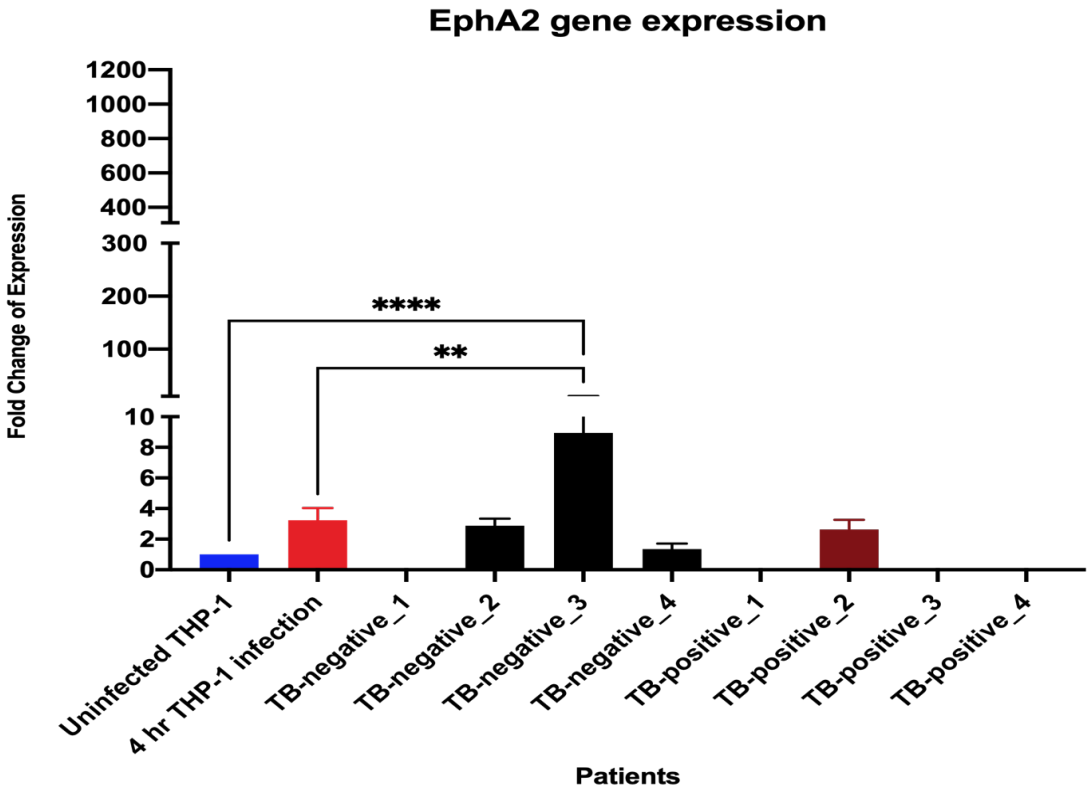

Figure 55. Comparison the transcript levels of EphA2 in PBMCs cells in positive and negative TB patients. The EphA2 transcript levels was assessed in eight people by quantitative real-time PCR using total RNA. The transcript levels were calculated relative to GAPDH control housekeeping gene values are expressed to fold change in gene expression for infected cells compared to uninfected controls. Errors bars represent the slandered errors from the means of three independent experiments. *, $P < 0.05$; **, $P < 0.01$; ***, $P < 0.001$; ****, $P < 0.0001$.

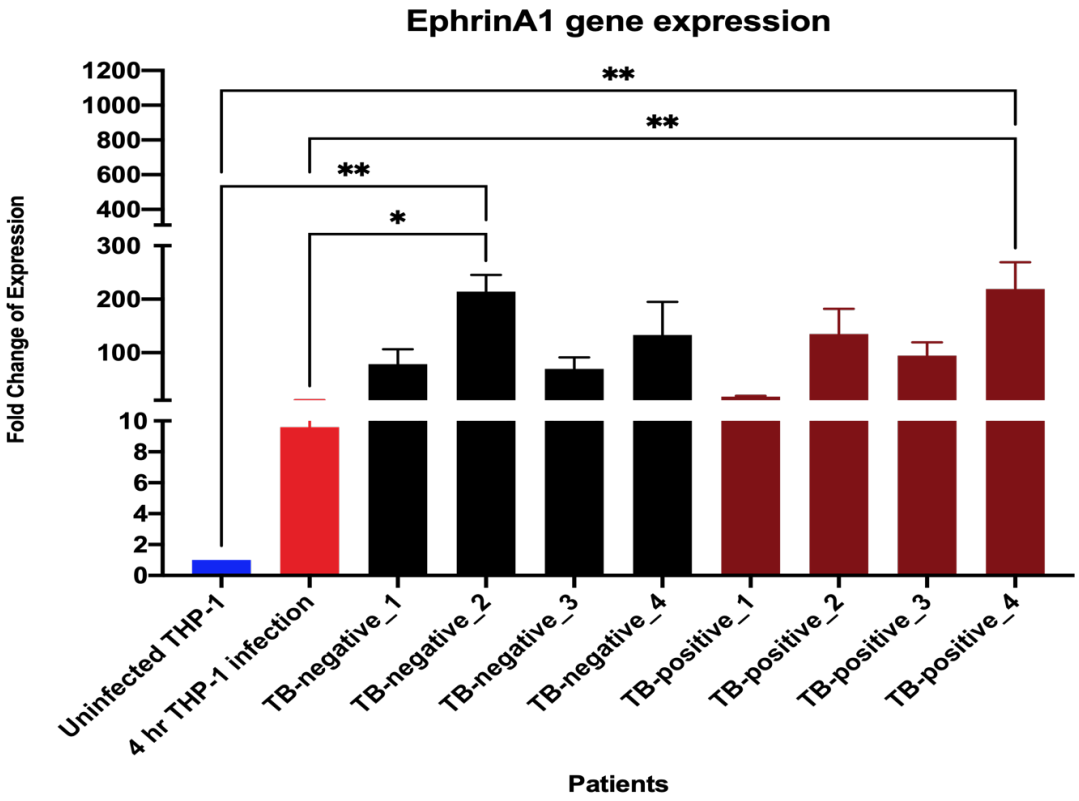

Figure 56. Comparison the transcript levels of EphrinA1 in PBMCs cells in positive and negative TB patients. The EphrinA1 transcript levels was assessed in eight people by quantitative real-time PCR using total RNA. The transcript levels were calculated relative to GAPDH control housekeeping gene values are expressed to fold change in gene expression for infected cells compared to uninfected controls. Errors bars represent the slandered errors from the means of three independent experiments. *, P < 0.05; **, P < 0.01; ***, P < 0.001; ****, P < 0.0001.

Discussion

In our clinical study for Eph receptors' level and their ligand in the positive- and negative patients, peripheral blood mononuclear cells (PBMCs) were collected. Eph receptors and their ligands, Ephrins, are known to play essential roles in several general functions such as cell migration [225, 227, 239]. The report showed Eph receptors' role as mediators in cell adhesion, cell migration, granuloma formation, and immune response in tuberculosis disease [201]. EphA receptors play an essential role in the chemokine-mediated migration of cells. This migration process is able to influence the immune response to *Mtb* infection [128, 129]. EphA receptors play a vital role in the immune response of the host to *Mtb* infection. The expression of the genes EphA1, EphA2, and EphrinA1 was also seen in *Mtb*-infected macrophages.

EphA receptors and their ligands, EphrinA1, have decreased substantially in peripheral blood mononuclear cells of positive-TB patients to improve the recruitment of immune cells to the site of infection. There were variations in gene expression between positive TB and negative TB patinate of the Epha1, Epha2, and EphrinA1 genes.

CHAPTER V

DISCUSSION AND CONCLUSIONS

Humans have suffered from tuberculosis throughout the centuries, and although the causative agent, *Mtb*, has been known for more than hundred years, an effective vaccine is not yet developed for tuberculosis. *Mtb's* magnificent adaptive ability to promote intracellular survival and inadequate host reactions delay the vaccine and drug benefits. In addition, *Mtb* can remain in a latent state for decades, pointing towards pathways that allows bacteria to cause the disease, likely contributing to transmission.

Virulent mycobacteria, similar to many of the pathogens, have developed the ability to evade and inhibiting the host's immune response machinery for survival. Over the years, *Mtb* has transitioned from a simple microbe to a pathogenic bacterium with a wide array of virulence factors, including pathways that can interact with numerous cellular functions, such as cellular signaling, vesicle biogenesis, antimicrobial molecules, inflammatory cytokines, and cell trafficking. The human immune system is one of the most significant challenges for *Mtb* infection and survival. It is difficult to study host-*Mtb* interactions largely due to the complex relationship between *Mtb* and host immunity. For the most part, researchers have identified the immune response members and their role in immune-mediated disease. However, the molecular pathways involved in *Mtb* infection at the cellular level there is much left to study.

To study the molecular pathways involved in *Mtb* infection, THP-1 cells were infected with *Mtb.* Subsequently, their RNAs were sequenced, and analyzed by Ingenuity pathways analysis (IPA). The analysis revealed that *Mtb* infection significantly increased

mRNA levels of genes encoding EphAl, EphA2, and EphrinA1, members of the Eph family of receptor tyrosine kinases. The data presented in this dissertation upheld our hypothesis that upregulation of EphAl, EphA2, and EphrinA1 was induced in live-*Mtb*, but less in heat-killed *Mtb* (HK-*Mtb*) in *Mtb*-infected THP-1 cells. There is some evidence published that support EphAl and EphA2, EphrinA1, and possibly other members of EphA play a role in TB immunity.

The results on THP-1 cells infected with dead-*Mtb* revealed that expression of EphA receptor genes were delayed. EphA1, EphA2, and EphrinA1 levels were all lower in HK-*Mtb* infected THP-1 cells than in live-*Mtb* infected THP-1 cells.

Mtb infection induced expression of EphA1 and EphA2 receptors as well as their ligand, EphrinA1. In order to survive, *Mtb* needs to change and regulate intracellular molecules. As a result, the change of intracellular molecules induces a variety of responses from the host cell including multiple signaling pathways, including mitogen-activated protein kinase MAPK pathways. This occurs after macrophages devour *Mtb* and present it as antigen-presenting cells, resulting in the release of inflammatory cytokines such as interleukin-12 (IL-12) and tumor necrosis factor- α (TNF- α) [147-149]. There is evidence that EphA receptors have an inhibitory role in the regulation of pathways such as MAPK. These pathways depend on the blocking of MAPK signals, thus reducing the activity of microbicides in macrophages. MAPK blockage contributes to the impaired development of inflammatory cytokines that are necessary for the elimination of *Mtb*. Our results show that *Mtb* has higher viability within WT-THP-1 than EphA1$^{-/-}$ THP-1 cells. This

highlighted the EphA1's molecular function in promoting *Mtb* proliferation and survival in macrophages.

Although EphA1 mRNA levels were decreased in the EphA1-KO-THP-1 cells, EphA2 and Ephrina1 mRNA levels increased 3.5-fold and 12-fold, respectively, at 4 hours of infection (see Figure 7 and Figure 8). In the wild-type THP-1 cells, the EphA2 expression increased even more than in the EphA1-KO-THP-1 cells (see Figure 10), which suggested that compensatory expression occurred due to the lack of EphA1 expression as reported earlier [130].

The primary aim of this study was to elucidate the main host factors that facilitate pathogenesis through virulent mycobacteria. To uncover macrophage gene regulation, we developed an approach to reveal global macrophage gene regulation in response to infection with *Mtb*. RNASeq studies investigated the host reaction and molecular events involved in active and dead mycobacterial infections over a period of 15 minutes to four hours during the host-*Mtb* interaction. RNASeq analysis showed that in exposure to *Mtb* caused the genes involved in metabolism, intracellular signaling, and immune response to be differentially regulated compared to uninfected ones. This included genes that had not been identified previously.

Interestingly, we observed coronavirus pathogenesis pathway activated in WT-THP-1 cells that are infected by live- and HK-*Mtb,* while in EphA1-KO-THP-1 cells were inhibited by live-*Mtb*. Pathogenesis genes encoding ribosomal proteins (RPs) are all associated with coronavirus pathogenesis. RPs genes also carry out various extra-ribosomal roles, including cell cycle progression control, immune signals, and cellular growth, indicating cells' propagation during *Mtb* infection. This gives an essential idea about the association of the EphA1 gene in the manifestation of *Mtb* pathogenic effect. The EphA1 gene has an important role in the development and survival of *Mtb* infection in macrophages.

Oxidative phosphorylation was inhibited after 30 minutes post-infection by live- and HK-*Mtb*, which lowered the cells' metabolism rate and energy production. This is found within the mitochondria in most eukaryotes, particularly aerobes. The transcriptional changes of host metabolism observed inhibition in oxidative phosphorylation, which shows that dependency glycolysis pathway. This bioenergetic approach is used by most host immune cells for rapid ATP production during infection. This supports the idea that there is a role for the EphA1 gene in reducing immune cells' response during *Mtb* infection.

Mtb infection in EphA1-KO-THP-1 cells had a milder effect than the WT-THP-1 cells. EIF2 signaling was observed as the most activated pathway within EphA1-KO-THP-1 cells, allowing for a rise in the proliferation of *Mtb* inside macrophages. A significant increase in the eif2-α kinase was discovered in TB-associated caseous granulomas in humans. This explains the increase in the granuloma formation to wall off the *Mtb* seen in

a previous study that used Epha2-KO-mice [201]. This also demonstrates the importance of Eph receptors in *Mtb* infection. However, this pathway was not activated after 4 hrs of HK-*Mtb* particles exposure. This suggests that only live bacilli can induce granuloma formation.

HMGB1 signaling was the most activated pathway after 1 hour of infection in WT-THP-1 cells infected by live- and HK-*Mtb*. The role of CD14 in macrophages as a co-receptor for the HMGB1-dependent TLR4 receptor is an essential factor in the in vitro activation of the receptor. During *Mtb* infection, TLR4 signaling is required to conduct a defensive response. We hypothesize that deactivation of the HMGB1 signaling pathway in EphA1-KO-THP-1 cells improves the EphA1 receptor's role in manipulating the immune response against TB. The activation of this pathway was seen in both HK-*Mtb* and live-*Mtb* infections.

ERK/MAPK signaling was inhibited after 1 hour of live-*Mtb* infection. It is known that activation of MAPKs mediates many features of immune responses. In the nucleus, the ERK/MAPK kinases have many targets, including transcription factors and other kinases such as ERK1, ETS1, ATF2, MITF, and MAPKAPK2. Production of IFN-γ as a result of *Mtb* infection is related to the ERK/MAPK phosphorylation suggesting that live-*Mtb* can delay the immune response, preparing these bacilli to remain and replicate inside the macrophages.

Another highly inhibited pathway was the p38 MAPK Signaling pathway. The p38 MAP kinases work as a portal for signal transduction and are active in a number of biological processes such as inflammation, cell cycle, cell death, growth, and cell

differentiation all support p38 as a signal transduction mediator [177]. p38 MAPK plays a major role in organizing the host's immune response by controlling the production of proinflammatory cytokines such as IL-1β or TNF during infection. It probably that after two hours of live-*Mtb* infection is insufficient to stimulate this pathway.

We observed activation of Hypoxia Signaling in the Cardiovascular System pathway after 2 hours of infection with live-*Mtb* in WT-THP-1 cells. Hypoxia-inducible factor manages the hypoxia signaling pathway (HIF). Many studies suggested that hypoxia and inflammation have a connected relationship [186, 187]. The hypoxia signaling pathway prolongs leukocytes' functions, reduces the bacterial burden, and increases reactive nitrogen species (RNS) by stabilizing HIF during TB infection [191]. Activating this pathway allows macrophages to eliminate the *Mtb* by increasing RNS.

Erythropoietin Signaling was an inhibited pathway in EphA1-KO-THP-1 cells infected by live-*Mtb* at two hours of infection. It was noticed that in untreated chronic bacterial infections such as tuberculosis, erythropoietin is a hormone that suppresses the immune response. Chronic diseases are typically followed by elevated TNF-α and interleukin-6, which boost pathogen development and disease progression. This supports the thought that the EphA1 gene plays a role in repressing immune cell response during *Mtb* infection [201].

Myc Mediated Apoptosis Signaling was another inhibited pathway after WT-THP-1 infection by live-*Mtb*. Myc has the potential to control the following processes: cell formation, replication, differentiation, metabolism, and apoptosis. Myc expression increases cells' sensitivity to proapoptotic disruption, such as DNA damage, genotoxic

stress, and death receptor signaling [182]. This finding is consistent with other studies that *Mtb* has the ability to inhibit macrophage apoptosis [240, 241].

Death Receptor Signaling pathway was inhibited after 4 hours of live-*Mtb* infection to Epha1-KO-THP-1 cells. Death receptor signaling activation plays a vital role in regulating the adaptive immune response [196]. *Mtb* uses cellular necrosis to escape from the immune cells to the outside and recruit the phagocyte cells to uptake the extracellular bacilli leading to more replication and dissemination of *Mtb*. One of the pathways that regulates cellular necrosis is death receptor signaling. It seems here that EphA1-KO-THP-1 cells did not enable *Mtb* to stimulate the death receptor signaling pathway; in contrast, this pathway was inhibited, which suggested the role of the EphA1 gene in curbing the proliferation and spread of *Mtb*. This is explained by the results obtained in this study, such as the lack of bacterial viability in EphA1-KO-THP-1 cells.

NRF2-mediated oxidative stress response was detected in both WT-THP-1 2 and 4 hrs post-infection and in EphA1-KO-THP-1 cells 4 hrs post-infection. A transcriptional factor called nuclear respiratory factor 2 (NRF2) reacts to various adverse factors, such as reactive oxygen species [170, 171], and plays an essential function in cellular detoxification and stress responses [172]. Releasing NRF2 and presents in the nucleus as a transcriptional factor leads to inhibit the proinflammatory gene expression [176] [173]. NRF2-mediated oxidative stress response is required during *Mtb* infection.

SUMOylation pathway was inhibited after one hour of HK-*Mtb* infection to WT-THP-1 cells. SUMO governs many host proteins involved in adaptive and innate immunity, thus leading to the mechanism of interferon development during infection [211,

212]. Peroxisome proliferator-activated receptor (PPAR- γ) governs the immune response in *Mtb*-infected macrophages. Inhibiting the SUMOylation of PPAR- γ promotes the innate immune response during *Mtb* infection [216]. Further studies are required to understand SUMOylation pathway and its role during *Mtb* infection.

Unfolded protein response (UPR) pathway was highly activated pathway at 2-4 hours post-infection of HK-*Mtb* in WT-THP-1 cells. UPR is utilized in cells as a stress response to an increase in endoplasmic reticulum (ER) stress [217]. The response to endoplasmic reticulum stress (ERS) is a cellular mechanism caused by mycobacterial infection, which disrupts protein folding in the endoplasmic reticulum [221]. As a result, the unfolded protein response is stimulated, decreasing early protein synthesis and ER aggregation of unfolded and misfolded proteins, restoring regular cell physiological activity during *Mtb* infection.

Signaling of p53 was also inhibited 2 hours post-infection of HK-*Mtb* in WT-THP-1 cells. The p53 signaling pathway is responsible for inducing apoptosis and programmed cell death. Apoptosis of *Mtb*-infected macrophages reduce mycobacterial viability [222]. This brings the evidence that HK-*Mtb* cannot induce this pathway, and live-*Mtb* can induce it.

The peripheral blood mononuclear cells (PBMCs) from the positive- and negative-TB patients were utilized in our clinical study on Eph receptors' levels and their ligand. Earlier studies show that Eph receptors and their ligands, Ephrins, are involved in many general functions, such as cell migration [225, 227, 239]. The previous studies concluded that Eph receptors play a role in mediating cell adhesion, cell migration, granuloma

development, and tuberculosis's immune response. EphA receptors are essential for the chemokine-mediated migration of cells. The direction of this migration affects the immune response to infection with *Mtb* [128, 129]. EphA receptors characterize the immune response of the host to *Mtb* infection. The *Mtb*-infected macrophages also showed the expression of the genes EphA1, EphA2, and EphrinA1.

Eph receptors and their ligands were not increased in peripheral blood mononuclear cells. The previous study showed increase the Eph receptor in immune cell in the lung of mice, indicating Eph receptors are used to recruit the immune cells from peripheral blood stream to the site of infection. Gene expression differences between positive TB and negative TB subjects were found in Epha1 and Epha2 since EphA1 and EphA2 expression were higher in PBMCs of negative TB subjects (3/4), while lower in positive TB patients.

Finally, we proposed a model that explains the regulation of the immune response during *Mtb* infection where increase of EphA1 gene expression in the WT-THP-1 cells led to highly activated of coronavirus pathogenesis pathway, whereas the EphA1-KO-THP-1 cells showed inhibition of coronavirus pathogenesis pathway (see Figure 57). Consequently, we observed a significant reduction in *Mtb* viability in EphA1-KO-THP-1 cells compared to their WT counterpart, suggesting the role of EphA1 is involved in the clearance of *Mtb* from macrophages.

The other differences in pathways were showed between WT-THP-1 cells and EphA1-KO-THP-1 cells. We observed activation of HMGB1 signaling pathway and inhibition in ERK/MAPK signaling, p38 MAPK signaling, and Myc mediated apoptosis

signaling pathways in the WT-THP-1 cells. On the other side, EphA1-KO-THP-1 cells showed activation of hypoxia signaling pathway and inhibition of erythropoietin signaling and death receptor signaling pathways. Similarly, both WT-THP-1 cells and EphA1-KO-THP-1 cells showed activation of NRF2-mediated oxidative stress response.

These findings explain an earlier study, figure below, which showed similar results in EphA2-/- mice. The EphA2-/- mice showed significant clearance of *Mtb* higher than in the wild-type mice. Herein, the main deference is activated of coronavirus pathogenesis pathway in WT-THP-1 cells and inhibited in EphA1-KO-THP-1 cells. Meanwhile, we consider the differences in the other pathways. To validate these findings, more experiments are required on EphA1 and EphA2, or other Eph receptors *in vivo* and *in vitro* during *Mtb* infection.

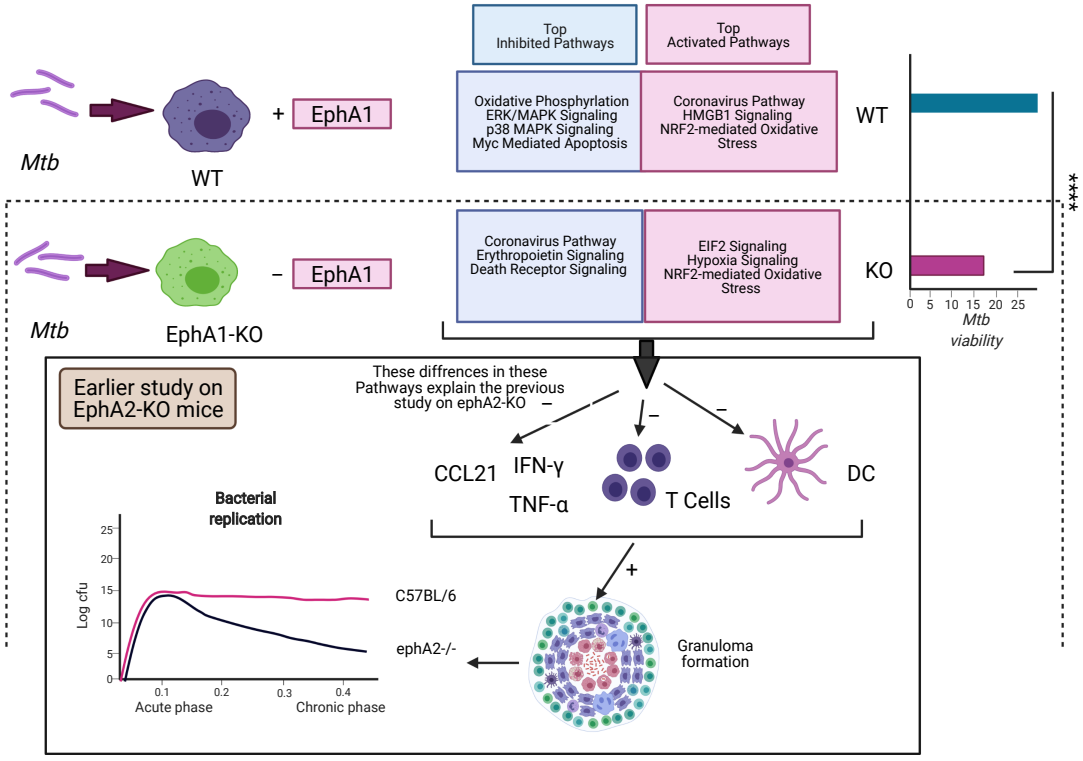

Figure 57. Proposed model that explain the regulation of immune response during *Mtb* infection by EphA1.

In conclusion, *Mycobacterium tuberculosis* induces EphA1, EphA2, and EphrinA1 gene expression during macrophage infection. EphA1$^{-/-}$ display compensatory EphA2 gene expression after *Mycobacterium tuberculosis* infection. Wild-type and EphA1$^{-/-}$ macrophages display a divergent expression of numerous signal transduction and gene regulation pathways after *Mycobacterium tuberculosis* infection.

Heat-killed *Mycobacterium tuberculosis* induces delayed Ephrin gene expressions during infection of macrophages. Live *Mycobacterium tuberculosis* induces EphA1, EphA2, and EphrinA1 gene expression at higher levels than heat-killed bacteria. Several

key signal transduction gene regulatory pathways are differentially induced by live *M. tuberculosis* compared to heat-killed bacilli.

Induction of the EphA1 and EphA2 was higher in negative TB patients (3/4), while EphrinA1 is similar in TB negative and positive PBMCs. This result needs to be further confirmed in a higher volume of samples from TB patients. Data suggest that TB induces Ephrin genes in the lungs and suppresses expression in peripheral blood, increasing migration of immune cells from peripheral organs and reducing migration out from the infection site, possibly reducing antigen presentation and increasing access to cells for bacterial replication. To evaluate this hypothesis, further examination of alveolar lavage cells for expression of Eph receptors genes in the future or macrophages in sputum may also use to study these genes in TB patients.

REFERENCES

1. Bynum, H., *Spitting Blood: The history of tuberculosis*. 2012: Oxford University Press.

2. Madkour, M.M., K.E. Al-Otaibi, and R. Al Swailem, *Historical Aspects of Tuberculosis*, in *Tuberculosis*. 2004, Springer. p. 15-30.

3. Zink, A.R., et al., *Characterization of Mycobacterium tuberculosis complex DNAs from Egyptian mummies by spoligotyping.* Journal of clinical microbiology, 2003. **41**(1): p. 359-367.

4. Lawn, S. and A. Zumla, *Seminar tuberculosis.* Lancet, 2011. **378**(9785): p. 57-72.

5. Balasubramanian, V., et al., *Pathogenesis of tuberculosis: pathway to apical localization.* Tubercle and Lung Disease, 1994. **75**(3): p. 168-178.

6. Mcdonough, K.A., Y. Kress, and B. Bloom, *Pathogenesis of tuberculosis: interaction of Mycobacterium tuberculosis with macrophages.* Infection and immunity, 1993. **61**(7): p. 2763-2773.

7. McCune, R.M., F.M. Feldmann, and W. McDermott, *Microbial persistence: II. Characteristics of the sterile state of tubercle bacilli.* The Journal of experimental medicine, 1966. **123**(3): p. 469-486.

8. Aly, S., et al., *Oxygen status of lung granulomas in Mycobacterium tuberculosis-infected mice.* The Journal of Pathology: A Journal of the Pathological Society of Great Britain and Ireland, 2006. **210**(3): p. 298-305.

9. Via, L.E., et al., *Tuberculous granulomas are hypoxic in guinea pigs, rabbits, and nonhuman primates.* Infection and immunity, 2008. **76**(6): p. 2333-2340.

10. Lenaerts, A.J., et al., *Location of persisting mycobacteria in a Guinea pig model of tuberculosis revealed by r207910.* Antimicrobial agents and chemotherapy, 2007. **51**(9): p. 3338-3345.

11. Boshoff, H.I. and C.E. Barry, *Tuberculosis—metabolism and respiration in the absence of growth.* Nature Reviews Microbiology, 2005. **3**(1): p. 70-80.

12. Park, M.K., R.A. Myers, and L. Marzella, *Oxygen tensions and infections: modulation of microbial growth, activity of antimicrobial agents, and immunologic responses.* Clinical infectious diseases, 1992. **14**(3): p. 720-740.

13. Comstock, G.W., *Epidemiology of tuberculosis.* American Review of Respiratory Disease, 1982. **125**(3P2): p. 8-15.

14. Ernst, J.D., *The immunological life cycle of tuberculosis.* Nature Reviews Immunology, 2012. **12**(8): p. 581-591.

15. Kwan, C.K. and J.D. Ernst, *HIV and tuberculosis: a deadly human syndemic.* Clinical microbiology reviews, 2011. **24**(2): p. 351-376.

16. De Backer, A., et al., *Tuberculosis: epidemiology, manifestations, and the value of medical imaging in diagnosis.* JBR BTR, 2006. **89**(5): p. 243.

17. Hernandez-Pando, R., et al., *Persistence of DNA from Mycobacterium tuberculosis in superficially normal lung tissue during latent infection.* The Lancet, 2000. **356**(9248): p. 2133-2138.

18. Neyrolles, O., et al., *Is adipose tissue a place for Mycobacterium tuberculosis persistence?* PloS one, 2006. **1**(1): p. e43.

19. Hunter, R.L., C. Jagannath, and J.K. Actor, *Pathology of postprimary tuberculosis in humans and mice: contradiction of long-held beliefs.* Tuberculosis, 2007. **87**(4): p. 267-278.

20. Canetti, G., *Exogenous reinfection and pulmonary tuberculosis a study of the pathology.* Tubercle, 1950. **31**(10): p. 224-248.

21. Ozaki, T., et al., *Differential cell analysis in bronchoalveolar lavage fluid from pulmonary lesions of patients with tuberculosis.* Chest, 1992. **102**(1): p. 54-59.

22. Cohn, D.L., et al., *Targeted tuberculin testing and treatment of latent tuberculosis infection.* MMWR Morb Mortal Wkly Rep, 2000. **49**(6): p. 1-54.

23. Castro, K.G., et al., *Updated guidelines for using interferon gamma release assays to detect Mycobacterium tuberculosis infection--United States, 2010.* 2010.

24. Pai, M., et al., *Gamma interferon release assays for detection of Mycobacterium tuberculosis infection.* Clinical microbiology reviews, 2014. **27**(1): p. 3-20.

25. Molicotti, P., A. Bua, and S. Zanetti, *Cost-effectiveness in the diagnosis of tuberculosis: choices in developing countries.* The Journal of Infection in Developing Countries, 2014. **8**(01): p. 024-038.

26. Colebunders, R. and I. Bastian, *A review of the diagnosis and treatment of smear-negative pulmonary tuberculosis.* The international journal of tuberculosis and lung disease, 2000. **4**(2): p. 97-107.

27. Steingart, K.R., et al., *Fluorescence versus conventional sputum smear microscopy for tuberculosis: a systematic review.* The Lancet infectious diseases, 2006. **6**(9): p. 570-581.

28. Lawn, S.D., et al., *Advances in tuberculosis diagnostics: the Xpert MTB/RIF assay and future prospects for a point-of-care test.* The Lancet infectious diseases, 2013. **13**(4): p. 349-361.

29. Sia, I.G. and M.L. Wieland. *Current concepts in the management of tuberculosis*. in *Mayo Clinic Proceedings*. 2011. Elsevier.

30. Selwyn, P.A., et al., *A prospective study of the risk of tuberculosis among intravenous drug users with human immunodeficiency virus infection.* New England journal of medicine, 1989. **320**(9): p. 545-550.

31. Markowitz, N., et al., *Incidence of tuberculosis in the United States among HIV-infected persons.* Annals of Internal Medicine, 1997. **126**(2): p. 123-132.

32. Barnes, P.F., L.S. Chan, and S.F. Wong, *The course of fever during treatment of pulmonary tuberculosis.* Tubercle, 1987. **68**(4): p. 255-260.

33. Kiblawi, S.S., et al., *Fever response of patients on therapy for pulmonary tuberculosis.* American Review of Respiratory Disease, 1981. **123**(1): p. 20-24.

34. Society, A.T., C.f.D. Control, and Prevention, *Diagnostic standards and classification of tuberculosis in adults and children.* Am. J. Respir. Crit. Care Med., 2000. **161**: p. 1376-1395.

35. Organization, W.H. and S.T. Initiative, *Treatment of tuberculosis: guidelines*. 2010: World Health Organization.

36. Günther, G.J.C.m., *Multidrug-resistant and extensively drug-resistant tuberculosis: a review of current concepts and future challenges.* 2014. **14**(3): p. 279.

37. Society, J.T.C.o.t.B.T., *Chemotherapy and management of tuberculosis in the United Kingdom: recommendations 1998.* Thorax, 1998. **53**(7): p. 536-548.

38. Jindani, A., et al., *The early bactericidal activity of drugs in patients with pulmonary tuberculosis.* American Review of Respiratory Disease, 1980. **121**(6): p. 939-949.

39. Rouillon, A., S. Perdrizet, and R. Parrot, *Transmission of tubercle bacilli: the effects of chemotherapy.* Tubercle, 1976. **57**(4): p. 275-299.

40. Zumla, A.I., et al., *New antituberculosis drugs, regimens, and adjunct therapies: needs, advances, and future prospects.* 2014. **14**(4): p. 327-340.

41. Khademi, F., et al., *Potential of polymeric particles as future vaccine delivery systems/adjuvants for parenteral and non-parenteral immunization against tuberculosis: A systematic review.* Iranian journal of basic medical sciences, 2018. **21**(2): p. 116.

42. Frick, M., *2015 report on tuberculosis research funding trends, 2005–2014: a decade of data*. 2015, Treatment Action Group, New York.

43. Ly, L.H. and D.N. McMurray, *Tuberculosis: vaccines in the pipeline.* Expert Review of Vaccines, 2008. **7**(5): p. 635-650.

44. Rangaka, M.X., et al., *Controlling the seedbeds of tuberculosis: diagnosis and treatment of tuberculosis infection.* The Lancet, 2015. **386**(10010): p. 2344-2353.

45. Organization, W.H., *Global tuberculosis report 2013*. 2013: World Health Organization.

46. Detels, R. and C.C. Tan, *Oxford textbook of global public health*. Vol. 2. 2015: Oxford University Press, USA.

47. Barry, C.E., et al., *The spectrum of latent tuberculosis: rethinking the biology and intervention strategies.* Nature Reviews Microbiology, 2009. **7**(12): p. 845-855.

48. Organization, W.H., *Global tuberculosis report 2018. 2018.* Geneva: World Health Organization, 2019.

49. Cole, S.T., et al., *Tuberculosis and the tubercle bacillus*. 2005: ASM press.

50. Sneath, P., *Bergey's Manual of Systematic Bacteriology, t. II*. 1986, Baltimore.

51. Ziehl, F., *Zur Färbung des tuberkelbacillus.* DMW-Deutsche Medizinische Wochenschrift, 1882. **8**(33): p. 451-451.

52. Neelsen, F., *Ein casuistischer Beitrag zur Lehre von der Tuberkulose.* Centralblatt für die medizinischen Wissenschaften, 1883. **28**: p. 497-501.

53. Hagemann, P., *Fluoreszenzfärbung von tuberkelbakterien mit auramin.* Munich Med Wschr, 1938. **85**: p. 1066-1068.

54. Cole, S., et al., *Deciphering the biology of Mycobacterium tuberculosis from the complete genome sequence.* Nature, 1998. **393**(6685): p. 537-544.

55. Naya, H., et al., *Aerobiosis increases the genomic guanine plus cytosine content (GC%) in prokaryotes.* Journal of molecular evolution, 2002. **55**(3): p. 260-264.

56. Poulet, S. and S.T. Cole, *Repeated DNA sequences in mycobacteria.* Archives of microbiology, 1995. **163**(2): p. 79-86.

57. Hirai, H., et al., *A novel putative tyrosine kinase receptor encoded by the eph gene.* Science, 1987. **238**(4834): p. 1717-1720.

58. Committee, E.N., *Unified nomenclature for Eph family receptors and their ligands, the ephrins.* Cell, 1997. **90**(3): p. 403-404.

59. Bowden, T.A., et al., *Structural plasticity of eph receptor A4 facilitates cross-class ephrin signaling.* Structure, 2009. **17**(10): p. 1386-1397.

60. Gale, N.W., et al., *Eph receptors and ligands comprise two major specificity subclasses and are reciprocally compartmentalized during embryogenesis.* 1996. **17**(1): p. 9-19.

61. Klein, R.J.D., *Eph/ephrin signalling during development.* 2012. **139**(22): p. 4105-4109.

62. Pitulescu, M.E., R.H.J.G. Adams, and development, *Eph/ephrin molecules—a hub for signaling and endocytosis.* 2010. **24**(22): p. 2480-2492.

63. Cheng, N., et al., *The ephrins and Eph receptors in angiogenesis.* 2002. **13**(1): p. 75-85.

64. Egea, J. and R.J.T.i.c.b. Klein, *Bidirectional Eph–ephrin signaling during axon guidance.* 2007. **17**(5): p. 230-238.

65. Klein, R.J.N.n., *Bidirectional modulation of synaptic functions by Eph/ephrin signaling.* 2009. **12**(1): p. 15.

66. Genander, M. and J.J.C.o.i.c.b. Frisén, *Ephrins and Eph receptors in stem cells and cancer.* 2010. **22**(5): p. 611-616.

67. Pasquale, E.B.J.N.R.C., *Eph receptors and ephrins in cancer: bidirectional signalling and beyond.* 2010. **10**(3): p. 165-180.

68. Pasquale, E.B.J.C., *Eph-ephrin bidirectional signaling in physiology and disease.* 2008. **133**(1): p. 38-52.

69. Himanen, J.-P. and D.B.J.T.i.n. Nikolov, *Eph signaling: a structural view.* 2003. **26**(1): p. 46-51.

70. Qin, H., et al., *Structural characterization of the EphA4-Ephrin-B2 complex reveals new features enabling Eph-ephrin binding promiscuity.* 2010. **285**(1): p. 644-654.

71. Hubbard, S.R.J.N.R.M.C.B., *Juxtamembrane autoinhibition in receptor tyrosine kinases.* 2004. **5**(6): p. 464-471.

72. Johnson, L.N., M.E. Noble, and D.J.J.C. Owen, *Active and inactive protein kinases: structural basis for regulation.* 1996. **85**(2): p. 149-158.

73. Hubbard, S.R.J.F.B., *Autoinhibitory mechanisms in receptor tyrosine kinases.* 2002. **7**(d330-340): p. d330-40.

74. Wybenga-Groot, L.E., et al., *Structural basis for autoinhibition of the Ephb2 receptor tyrosine kinase by the unphosphorylated juxtamembrane region.* 2001. **106**(6): p. 745-757.

75. Himanen, J.-P., N. Saha, and D.B.J.C.o.i.c.b. Nikolov, *Cell–cell signaling via Eph receptors and ephrins.* 2007. **19**(5): p. 534-542.

76. Seiradake, E., et al., *An extracellular steric seeding mechanism for Eph-ephrin signaling platform assembly.* 2010. **17**(4): p. 398.

77. Falivelli, G., et al., *Attenuation of eph receptor kinase activation in cancer cells by coexpressed ephrin ligands.* 2013. **8**(11).

78. Singh, D.R., et al., *Unliganded EphA3 dimerization promoted by the SAM domain.* 2015. **471**(1): p. 101-109.

79. Boyd, A.W., P.F. Bartlett, and M. Lackmann, *Therapeutic targeting of EPH receptors and their ligands.* Nature reviews Drug discovery, 2014. **13**(1): p. 39.

80. Serra-Pagès, C., et al., *The LAR transmembrane protein tyrosine phosphatase and a coiled-coil LAR-interacting protein co-localize at focal adhesions.* The EMBO Journal, 1995. **14**(12): p. 2827-2838.

81. Stein, E., et al., *Eph receptors discriminate specific ligand oligomers to determine alternative signaling complexes, attachment, and assembly responses.* Genes & development, 1998. **12**(5): p. 667-678.

82. Lim, Y.-S., et al., *p75NTR mediates ephrin-A reverse signaling required for axon repulsion and mapping.* Neuron, 2008. **59**(5): p. 746-758.

83. Bonanomi, D., et al., *Ret is a multifunctional coreceptor that integrates diffusible-and contact-axon guidance signals.* Cell, 2012. **148**(3): p. 568-582.

84. Daar, I.O. *Non-SH2/PDZ reverse signaling by ephrins*. in *Seminars in cell & developmental biology*. 2012. Elsevier.

85. Palmer, A., et al., *EphrinB phosphorylation and reverse signaling: regulation by Src kinases and PTP-BL phosphatase.* Molecular cell, 2002. **9**(4): p. 725-737.

86. Kullander, K. and R. Klein, *Mechanisms and functions of Eph and ephrin signalling.* Nature reviews Molecular cell biology, 2002. **3**(7): p. 475-486.

87. Himanen, J.-P. and D.B. Nikolov, *Eph signaling: a structural view.* Trends in neurosciences, 2003. **26**(1): p. 46-51.

88. Himanen, J.-P., et al., *Crystal structure of an Eph receptor–ephrin complex.* Nature, 2001. **414**(6866): p. 933-938.

89. Wimmer-Kleikamp, S.H., et al., *Recruitment of Eph receptors into signaling clusters does not require ephrin contact.* The Journal of cell biology, 2004. **164**(5): p. 661-666.

90. Himanen, J.P. *Ectodomain structures of Eph receptors*. in *Seminars in cell & developmental biology*. 2012. Elsevier.

91. Himanen, J.P., et al., *Architecture of Eph receptor clusters.* Proceedings of the National Academy of Sciences, 2010. **107**(24): p. 10860-10865.

92. Marquardt, T., et al., *Coexpressed EphA receptors and ephrin-A ligands mediate opposing actions on growth cone navigation from distinct membrane domains.* Cell, 2005. **121**(1): p. 127-139.

93. Pitulescu, M.E. and R.H. Adams, *Eph/ephrin molecules—a hub for signaling and endocytosis.* Genes & development, 2010. **24**(22): p. 2480-2492.

94. Miao, H., et al., *Activation of EphA2 kinase suppresses integrin function and causes focal-adhesion-kinase dephosphorylation.* Nature cell biology, 2000. **2**(2): p. 62-69.

95. Arvanitis, D.N. and A. Davy, *Regulation and misregulation of Eph/ephrin expression.* Cell adhesion & migration, 2012. **6**(2): p. 131-137.

96. Shintani, T., et al., *Eph receptors are negatively controlled by protein tyrosine phosphatase receptor type O.* Nature neuroscience, 2006. **9**(6): p. 761-769.

97. Georgakopoulos, A., et al., *Metalloproteinase/Presenilin1 processing of ephrinB regulates EphB-induced Src phosphorylation and signaling.* The EMBO journal, 2006. **25**(6): p. 1242-1252.

98. Emrich, S.J., et al., *Gene discovery and annotation using LCM-454 transcriptome sequencing.* Genome research, 2007. **17**(1): p. 69-73.

99. Lister, R., et al., *Highly integrated single-base resolution maps of the epigenome in Arabidopsis.* Cell, 2008. **133**(3): p. 523-536.

100. Wang, Z., M. Gerstein, and M. Snyder, *RNA-Seq: a revolutionary tool for transcriptomics.* Nature reviews genetics, 2009. **10**(1): p. 57-63.

101. Zhao, S., et al., *Comparison of RNA-Seq and microarray in transcriptome profiling of activated T cells.* PloS one, 2014. **9**(1): p. e78644.

102. Marioni, J.C., et al., *RNA-seq: an assessment of technical reproducibility and comparison with gene expression arrays.* Genome research, 2008. **18**(9): p. 1509-1517.

103. Cloonan, N., et al., *Stem cell transcriptome profiling via massive-scale mRNA sequencing.* Nature methods, 2008. **5**(7): p. 613-619.

104. Rouet, P., F. Smih, and M. Jasin, *Introduction of double-strand breaks into the genome of mouse cells by expression of a rare-cutting endonuclease.* Molecular and cellular biology, 1994. **14**(12): p. 8096-8106.

105. Porteus, M., *Genome editing: a new approach to human therapeutics.* Annual review of pharmacology and toxicology, 2016. **56**: p. 163-190.

106. Charpentier, E. and J.A. Doudna, *Biotechnology: Rewriting a genome.* Nature, 2013. **495**(7439): p. 50-51.

107. Charpentier, E. and L.A. Marraffini, *Harnessing CRISPR-Cas9 immunity for genetic engineering.* Current opinion in microbiology, 2014. **19**: p. 114-119.

108. Doudna, J.A. and E. Charpentier, *The new frontier of genome engineering with CRISPR-Cas9.* Science, 2014. **346**(6213).

109. Amitai, G. and R. Sorek, *CRISPR–Cas adaptation: insights into the mechanism of action.* Nature Reviews Microbiology, 2016. **14**(2): p. 67.

110. Cong, L., et al., *Multiplex genome engineering using CRISPR/Cas systems.* Science, 2013. **339**(6121): p. 819-823.

111. Dominguez, A.A., W.A. Lim, and L.S. Qi, *Beyond editing: repurposing CRISPR–Cas9 for precision genome regulation and interrogation.* Nature reviews Molecular cell biology, 2016. **17**(1): p. 5.

112. Shalem, O., N.E. Sanjana, and F. Zhang, *High-throughput functional genomics using CRISPR–Cas9.* Nature Reviews Genetics, 2015. **16**(5): p. 299-311.

113. Barrangou, R. and J.A. Doudna, *Applications of CRISPR technologies in research and beyond.* Nature biotechnology, 2016. **34**(9): p. 933-941.

114. Heidenreich, M. and F. Zhang, *Applications of CRISPR–Cas systems in neuroscience.* Nature Reviews Neuroscience, 2016. **17**(1): p. 36.

115. Xiong, X., et al., *CRISPR/Cas9 for human genome engineering and disease research.* Annual review of genomics and human genetics, 2016. **17**: p. 131-154.

116. Cox, D.B.T., R.J. Platt, and F. Zhang, *Therapeutic genome editing: prospects and challenges.* Nature medicine, 2015. **21**(2): p. 121-131.

117. Sander, J.D. and J.K. Joung, *CRISPR-Cas systems for editing, regulating and targeting genomes.* Nature biotechnology, 2014. **32**(4): p. 347-355.

118. Tsai, S.Q. and J.K. Joung, *Defining and improving the genome-wide specificities of CRISPR–Cas9 nucleases.* Nature Reviews Genetics, 2016. **17**(5): p. 300-312.

119. Wang, H., M. La Russa, and L.S. Qi, *CRISPR/Cas9 in genome editing and beyond.* Annual review of biochemistry, 2016. **85**: p. 227-264.

120. Jinek, M., et al., *A programmable dual-RNA–guided DNA endonuclease in adaptive bacterial immunity.* science, 2012. **337**(6096): p. 816-821.

121. Shalem, O., et al., *Genome-scale CRISPR-Cas9 knockout screening in human cells.* Science, 2014. **343**(6166): p. 84-87.

122. Koike-Yusa, H., et al., *Genome-wide recessive genetic screening in mammalian cells with a lentiviral CRISPR-guide RNA library.* Nature biotechnology, 2014. **32**(3): p. 267-273.

123. Shen, B., et al., *Generation of gene-modified mice via Cas9/RNA-mediated gene targeting.* Cell research, 2013. **23**(5): p. 720-723.

124. Ma, Y., et al., *Generating rats with conditional alleles using CRISPR/Cas9.* Cell research, 2014. **24**(1): p. 122-125.

125. Wang, H., et al., *One-step generation of mice carrying mutations in multiple genes by CRISPR/Cas-mediated genome engineering.* Cell, 2013. **153**(4): p. 910-918.

126. Yang, H., et al., *One-step generation of mice carrying reporter and conditional alleles by CRISPR/Cas-mediated genome engineering.* Cell, 2013. **154**(6): p. 1370-1379.

127. Plant, L., et al., *Epithelial cell responses induced upon adherence of pathogenic Neisseria.* Cellular microbiology, 2004. **6**(7): p. 663-670.

128. Ragno, S., et al., *Changes in gene expression in macrophages infected with Mycobacterium tuberculosis: a combined transcriptomic and proteomic approach.* Immunology, 2001. **104**(1): p. 99-108.

129. McGarvey, J., D. Wagner, and L. Bermudez, *Differential gene expression in mononuclear phagocytes infected with pathogenic and non-pathogenic mycobacteria.* Clinical & Experimental Immunology, 2004. **136**(3): p. 490-500.

130. Khounlotham, M., *Host-mycobacterial interactions: Dissecting the role of EphA receptor tyrosine kinases in modulating the host response to Mycobacterium tuberculosis infection*. 2008, The Texas A&M University System Health Science Center.

131. Taylor, H., J. Campbell, and C.D. Nobes, *Ephs and ephrins.* Current Biology, 2017. **27**(3): p. R90-R95.

132. Janes, P.W., E. Nievergall, and M. Lackmann. *Concepts and consequences of Eph receptor clustering*. in *Seminars in cell & developmental biology*. 2012. Elsevier.

133. Munthe, E., E.F. Finne, and H.-C. Aasheim, *Expression and functional effects of Eph receptor tyrosine kinase A family members on Langerhans like dendritic cells.* BMC immunology, 2004. **5**(1): p. 9.

134. Aasheim, H.-C., et al., *A splice variant of human ephrin-A4 encodes a soluble molecule that is secreted by activated human B lymphocytes.* Blood, The Journal of the American Society of Hematology, 2000. **95**(1): p. 221-230.

135. Luo, H., et al., *EphB6 crosslinking results in costimulation of T cells.* The Journal of clinical investigation, 2002. **110**(8): p. 1141-1150.

136. Aasheim, H.-C., J. Delabie, and E.F. Finne, *Ephrin-A1 binding to CD4+ T lymphocytes stimulates migration and induces tyrosine phosphorylation of PYK2.* Blood, 2005. **105**(7): p. 2869-2876.

137. Hjorthaug, H.S. and H.C. Aasheim, *Ephrin-A1 stimulates migration of CD8+ CCR7+ T lymphocytes.* European journal of immunology, 2007. **37**(8): p. 2326-2336.

138. Russell, D.G., *Who puts the tubercle in tuberculosis?* Nature Reviews Microbiology, 2007. **5**(1): p. 39-47.

139. Cohen, S.B., et al., *Alveolar macrophages provide an early Mycobacterium tuberculosis niche and initiate dissemination.* Cell host & microbe, 2018. **24**(3): p. 439-446. e4.

140. Antonelli, L.R., et al., *Intranasal Poly-IC treatment exacerbates tuberculosis in mice through the pulmonary recruitment of a pathogen-permissive monocyte/macrophage population.* The Journal of clinical investigation, 2010. **120**(5): p. 1674-1682.

141. ROHDE, K.H. and D.G. RUSSELL, *The Minimal Unit of Infection: Mycobacterium tuberculosis in the Macrophage.* 2016.

142. Lerner, T.R., et al., *Mycobacterium tuberculosis replicates within necrotic human macrophages.* Journal of Cell Biology, 2017. **216**(3): p. 583-594.

143. Genin, M., et al., *M1 and M2 macrophages derived from THP-1 cells differentially modulate the response of cancer cells to etoposide.* BMC cancer, 2015. **15**(1): p. 1-14.

144. Bartzatt, R., et al., *Aromatic Hydrazide Compounds That Inhibit the Growth of Mycobacterium tuberculosis.* Journal of Advances in Medical and Pharmaceutical Sciences, 2019: p. 1-11.

145. Vilchèze, C., et al., *Novel inhibitors of InhA efficiently kill Mycobacterium tuberculosis under aerobic and anaerobic conditions.* Antimicrobial agents and chemotherapy, 2011. **55**(8): p. 3889-3898.

146. Subbian, S., et al., *A Mycobacterium marinum mel2 mutant is defective for growth in macrophages that produce reactive oxygen and reactive nitrogen species.* Infection and immunity, 2007. **75**(1): p. 127-134.

147. Fratti, R.A., J. Chua, and V. Deretic, *Induction of p38 mitogen-activated protein kinase reduces early endosome autoantigen 1 (EEA1) recruitment to phagosomal membranes.* Journal of Biological Chemistry, 2003. **278**(47): p. 46961-46967.

148. Jo, E.K., et al., *Intracellular signalling cascades regulating innate immune responses to Mycobacteria: branching out from Toll-like receptors.* Cellular microbiology, 2007. **9**(5): p. 1087-1098.

149. Roach, S.K. and J.S. Schorey, *Differential regulation of the mitogen-activated protein kinases by pathogenic and nonpathogenic mycobacteria.* Infection and immunity, 2002. **70**(6): p. 3040-3052.

150. Miao, H., et al., *Activation of EphA receptor tyrosine kinase inhibits the Ras/MAPK pathway.* Nature cell biology, 2001. **3**(5): p. 527-530.

151. Ivanov, A.I. and A.A. Romanovsky, *Putative dual role of ephrin-Eph receptor interactions in inflammation.* IUBMB life, 2006. **58**(7): p. 389-394.

152. Dong, H.-J., et al., *Selective regulation in ribosome biogenesis and protein production for efficient viral translation.* Archives of Microbiology, 2020: p. 1-12.

153. Maruyama, T., et al., *Txk, a member of the non-receptor tyrosine kinase of the Tec family, forms a complex with poly (ADP-ribose) polymerase 1 and elongation factor 1α and regulates interferon-γ gene transcription in Th1 cells.* Clinical & Experimental Immunology, 2007. **147**(1): p. 164-175.

154. Dolezal, J.M., A.P. Dash, and E.V. Prochownik, *Diagnostic and prognostic implications of ribosomal protein transcript expression patterns in human cancers.* BMC cancer, 2018. **18**(1): p. 1-14.

155. Schmidt-Rohr, K., *Oxygen Is the High-Energy Molecule Powering Complex Multicellular Life: Fundamental Corrections to Traditional Bioenergetics.* ACS omega, 2020. **5**(5): p. 2221-2233.

156. Shi, L., et al., *Infection with Mycobacterium tuberculosis induces the Warburg effect in mouse lungs.* Scientific reports, 2015. **5**: p. 18176.

157. Mehrotra, P., et al., *Pathogenicity of Mycobacterium tuberculosis is expressed by regulating metabolic thresholds of the host macrophage.* PLoS Pathog, 2014. **10**(7): p. e1004265.

158. Andersson, U., et al., *High mobility group 1 protein (HMG-1) stimulates proinflammatory cytokine synthesis in human monocytes.* Journal of Experimental Medicine, 2000. **192**(4): p. 565-570.

159. Scaffidi, P., T. Misteli, and M.E. Bianchi, *Release of chromatin protein HMGB1 by necrotic cells triggers inflammation.* Nature, 2002. **418**(6894): p. 191-195.

160. Yang, H., et al., *The many faces of HMGB1: molecular structure-functional activity in inflammation, apoptosis, and chemotaxis.* Journal of leukocyte biology, 2013. **93**(6): p. 865-873.

161. Yang, H., et al., *A critical cysteine is required for HMGB1 binding to Toll-like receptor 4 and activation of macrophage cytokine release.* Proceedings of the National Academy of Sciences, 2010. **107**(26): p. 11942-11947.

162. Yang, H., et al., *MD-2 is required for disulfide HMGB1–dependent TLR4 signaling.* Journal of Experimental Medicine, 2015. **212**(1): p. 5-14.

163. Kim, S., et al., *Signaling of high mobility group box 1 (HMGB1) through toll-like receptor 4 in macrophages requires CD14.* Molecular Medicine, 2013. **19**(1): p. 88-98.

164. Wähämaa, H., et al., *High mobility group box protein 1 in complex with lipopolysaccharide or IL-1 promotes an increased inflammatory phenotype in synovial fibroblasts.* Arthritis research & therapy, 2011. **13**(4): p. R136.

165. Hreggvidsdottir, H.S., et al., *The alarmin HMGB1 acts in synergy with endogenous and exogenous danger signals to promote inflammation.* Journal of leukocyte biology, 2009. **86**(3): p. 655-662.

166. Dong, C., R.J. Davis, and R.A. Flavell, *MAP kinases in the immune response.* Annual review of immunology, 2002. **20**(1): p. 55-72.

167. Adler, H.S., et al., *Activation of MAP kinase p38 is critical for the cell-cycle–controlled suppressor function of regulatory T cells.* Blood, 2007. **109**(10): p. 4351-4359.

168. Blumenthal, A., et al., *Control of mycobacterial replication in human macrophages: roles of extracellular signal-regulated kinases 1 and 2 and p38 mitogen-activated protein kinase pathways.* Infection and immunity, 2002. **70**(9): p. 4961-4967.

169. Pasquinelli, V., et al., *Phosphorylation of mitogen-activated protein kinases contributes to interferon γ production in response to mycobacterium tuberculosis.* The Journal of infectious diseases, 2013. **207**(2): p. 340-350.

170. Osburn, W.O. and T.W. Kensler, *Nrf2 signaling: an adaptive response pathway for protection against environmental toxic insults.* Mutation Research/Reviews in Mutation Research, 2008. **659**(1-2): p. 31-39.

171. Liu, Q., et al., *The NRF2-mediated oxidative stress response pathway is associated with tumor cell resistance to arsenic trioxide across the NCI-60 panel.* BMC medical genomics, 2010. **3**(1): p. 37.

172. Itoh, K., et al., *An Nrf2/small Maf heterodimer mediates the induction of phase II detoxifying enzyme genes through antioxidant response elements.* Biochemical and biophysical research communications, 1997. **236**(2): p. 313-322.

173. Walsh, J., et al., *Identification and quantification of the basal and inducible Nrf2-dependent proteomes in mouse liver: biochemical, pharmacological and toxicological implications.* Journal of proteomics, 2014. **108**: p. 171-187.

174. Kobayashi, E.H., et al., *Nrf2 suppresses macrophage inflammatory response by blocking proinflammatory cytokine transcription.* Nature communications, 2016. **7**(1): p. 1-14.

175. Tong, K.I., et al., *Keap1 recruits Neh2 through binding to ETGE and DLG motifs: characterization of the two-site molecular recognition model.* Molecular and cellular biology, 2006. **26**(8): p. 2887-2900.

176. Zhang, D.D. and M. Hannink, *Distinct cysteine residues in Keap1 are required for Keap1-dependent ubiquitination of Nrf2 and for stabilization of Nrf2 by chemopreventive agents and oxidative stress.* Molecular and cellular biology, 2003. **23**(22): p. 8137-8151.

177. Zarubin, T. and H. Jiahuai, *Activation and signaling of the p38 MAP kinase pathway.* Cell research, 2005. **15**(1): p. 11-18.

178. Arthur, J.S.C. and S.C. Ley, *Mitogen-activated protein kinases in innate immunity.* Nature Reviews Immunology, 2013. **13**(9): p. 679-692.

179. Nick, J.A., et al., *Role of p38 mitogen-activated protein kinase in a murine model of pulmonary inflammation.* The Journal of Immunology, 2000. **164**(4): p. 2151-2159.

180. Amati, B., et al., *The c-Myc protein induces cell cycle progression and apoptosis through dimerization with Max.* The EMBO journal, 1993. **12**(13): p. 5083-5087.

181. Xu, J., Y. Chen, and O.I. Olopade, *MYC and breast cancer.* Genes & cancer, 2010. **1**(6): p. 629-640.

182. Juin, P., et al., *c-Myc-induced sensitization to apoptosis is mediated through cytochrome c release.* Genes & development, 1999. **13**(11): p. 1367-1381.

183. Nesbit, C.E., J.M. Tersak, and E.V. Prochownik, *MYC oncogenes and human neoplastic disease.* Oncogene, 1999. **18**(19): p. 3004-3016.

184. Dang, C.V., *c-Myc target genes involved in cell growth, apoptosis, and metabolism.* Molecular and cellular biology, 1999. **19**(1): p. 1-11.

185. Baird, T.D. and R.C. Wek, *Eukaryotic initiation factor 2 phosphorylation and translational control in metabolism.* Advances in nutrition, 2012. **3**(3): p. 307-321.

186. Eltzschig, H.K. and P. Carmeliet, *Hypoxia and inflammation.* New England Journal of Medicine, 2011. **364**(7): p. 656-665.

187. Bartels, K., A. Grenz, and H.K. Eltzschig, *Hypoxia and inflammation are two sides of the same coin.* Proceedings of the National Academy of Sciences, 2013. **110**(46): p. 18351-18352.

188. Bowser, J.L., et al., *The hypoxia-adenosine link during inflammation.* Journal of Applied Physiology, 2017. **123**(5): p. 1303-1320.

189. Riegel, A.-K., et al., *Selective induction of endothelial P2Y6 nucleotide receptor promotes vascular inflammation.* Blood, The Journal of the American Society of Hematology, 2011. **117**(8): p. 2548-2555.

190. Yuan, X., et al., *Targeting hypoxia signaling for perioperative organ injury.* Anesthesia and analgesia, 2018. **126**(1): p. 308.

191. Elks, P.M., et al., *Hypoxia inducible factor signaling modulates susceptibility to mycobacterial infection via a nitric oxide dependent mechanism.* PLoS Pathog, 2013. **9**(12): p. e1003789.

192. Youssoufian, H., et al., *Structure, function, and activation of the erythropoietin receptor.* 1993.

193. Livnah, O., et al., *Crystallographic evidence for preformed dimers of erythropoietin receptor before ligand activation.* Science, 1999. **283**(5404): p. 987-990.

194. James, C., et al., *naceur-Griscelli A, Villeval JL, Constantinescu SN, Casadevall N, Vainchenker W. A unique clonal JAK2 mutation leading to constitutive signalling causes polycythaemia vera.* Nature, 2005. **434**(7037): p. 1144-1148.

195. Nairz, M., et al., *The pleiotropic effects of erythropoietin in infection and inflammation.* Microbes and infection, 2012. **14**(3): p. 238-246.

196. Fas, S.C., et al., *Death receptor signaling and its function in the immune system*, in *Apoptosis and Its Relevance to Autoimmunity*. 2006, Karger Publishers. p. 1-17.

197. Vanlangenakker, N., T.V. Berghe, and P. Vandenabeele, *Many stimuli pull the necrotic trigger, an overview.* Cell Death & Differentiation, 2012. **19**(1): p. 75-86.

198. Sridharan, H. and J.W. Upton, *Programmed necrosis in microbial pathogenesis.* Trends in microbiology, 2014. **22**(4): p. 199-207.

199. Pasquale, E.B., *Eph-ephrin bidirectional signaling in physiology and disease.* Cell, 2008. **133**(1): p. 38-52.

200. Singh, P.P. and A. Goyal, *Interleukin-6: a potent biomarker of mycobacterial infection.* Springerplus, 2013. **2**(1): p. 686.

201. Khounlotham, M., et al., *Mycobacterium tuberculosis interferes with the response to infection by inducing the host EphA2 receptor.* The Journal of infectious diseases, 2009. **199**(12): p. 1797-1806.

202. Bolger, A.M., M. Lohse, and B. Usadel, *Trimmomatic: a flexible trimmer for Illumina sequence data.* Bioinformatics, 2014. **30**(15): p. 2114-2120.

203. Dobin, A. and T.R. Gingeras, *Mapping RNA-seq reads with STAR.* Current protocols in bioinformatics, 2015. **51**(1): p. 11.14. 1-11.14. 19.

204. Dobin, A. and T.R. Gingeras, *Optimizing RNA-Seq mapping with STAR*, in *Data Mining Techniques for the Life Sciences*. 2016, Springer. p. 245-262.

205. Anders, S., P.T. Pyl, and W. Huber, *HTSeq—a Python framework to work with high-throughput sequencing data.* Bioinformatics, 2015. **31**(2): p. 166-169.

206. Robinson, M.D., D.J. McCarthy, and G.K. Smyth, *edgeR: a Bioconductor package for differential expression analysis of digital gene expression data.* Bioinformatics, 2010. **26**(1): p. 139-140.

207. Nygaard, V., E.A. Rødland, and E. Hovig, *Methods that remove batch effects while retaining group differences may lead to exaggerated confidence in downstream analyses.* Biostatistics, 2016. **17**(1): p. 29-39.

208. Grover, A., et al., *Mycobacterial infection induces the secretion of high-mobility group box 1 protein.* Cellular microbiology, 2008. **10**(6): p. 1390-1404.

209. Guo, C. and J.M. Henley, *Wrestling with stress: roles of protein SUMOylation and deSUMOylation in cell stress response.* IUBMB life, 2014. **66**(2): p. 71-77.

210. Hickey, C.M., N.R. Wilson, and M. Hochstrasser, *Function and regulation of SUMO proteases.* Nature reviews Molecular cell biology, 2012. **13**(12): p. 755-766.

211. Hannoun, Z., G. Maarifi, and M.K. Chelbi-Alix, *The implication of SUMO in intrinsic and innate immunity.* Cytokine & growth factor reviews, 2016. **29**: p. 3-16.

212. Liu, J., C. Qian, and X. Cao, *Post-translational modification control of innate immunity.* Immunity, 2016. **45**(1): p. 15-30.

213. Miura, K., J.B. Jin, and P.M. Hasegawa, *Sumoylation, a post-translational regulatory process in plants.* Current opinion in plant biology, 2007. **10**(5): p. 495-502.

214. Stulemeijer, I.J. and M.H. Joosten, *Post-translational modification of host proteins in pathogen-triggered defence signalling in plants.* Molecular Plant Pathology, 2008. **9**(4): p. 545-560.

215. Rajaram, M.V., et al., *Mycobacterium tuberculosis activates human macrophage peroxisome proliferator-activated receptor γ linking mannose receptor recognition to regulation of immune responses.* The Journal of Immunology, 2010. **185**(2): p. 929-942.

216. Hu, S., et al., *Vitamin B1 helps to limit Mycobacterium tuberculosis growth via regulating innate immunity in a peroxisome proliferator-activated receptor-γ-dependent manner.* Frontiers in immunology, 2018. **9**: p. 1778.

217. Hetz, C. and F.R. Papa, *The unfolded protein response and cell fate control.* Molecular cell, 2018. **69**(2): p. 169-181.

218. Zhang, K. and R.J. Kaufman, *From endoplasmic-reticulum stress to the inflammatory response.* Nature, 2008. **454**(7203): p. 455-462.

219. Rius, J., et al., *NF-κB links innate immunity to the hypoxic response through transcriptional regulation of HIF-1α.* Nature, 2008. **453**(7196): p. 807-811.

220. Chakrabarti, A., A.W. Chen, and J.D. Varner, *A review of the mammalian unfolded protein response.* Biotechnology and bioengineering, 2011. **108**(12): p. 2777-2793.

221. Cui, Y., et al., *The endoplasmic reticulum stress response: a link with tuberculosis?* Tuberculosis, 2016. **97**: p. 52-56.

222. Lee, J., M. Hartman, and H. Kornfeld, *Macrophage apoptosis in tuberculosis.* Yonsei medical journal, 2009. **50**(1): p. 1.

223. Balcewicz-Sablinska, M.K., H. Gan, and H. Remold, *Interleukin 10 produced by macrophages inoculated with Mycobacterium avium attenuates mycobacteria-induced apoptosis by reduction of TNF-α activity.* The Journal of infectious diseases, 1999. **180**(4): p. 1230-1237.

224. Nakamoto, M., *Eph receptors and ephrins.* The international journal of biochemistry & cell biology, 2000. **32**(1): p. 7-12.

225. Brantley-Sieders, D.M., et al., *EphA2 receptor tyrosine kinase regulates endothelial cell migration and vascular assembly through phosphoinositide 3-kinase-mediated Rac1 GTPase activation.* Journal of cell science, 2004. **117**(10): p. 2037-2049.

226. Cheng, N., et al., *Blockade of EphA Receptor Tyrosine Kinase Activation Inhibits Vascular Endothelial Cell Growth Factor-Induced Angiogenesis11 NIH Grants HD36400 and DK47078; JDF grant I-2001-519; DOD grant BC010265; American Heart Association Grant 97300889N; ACS Institutional Research Grant IN-25-38 (to J. Chen); Vascular Biology Training Grant T32-HL-07751-06 and American Heart Association Fellowship 0120147B (to D. Brantley); Cancer training Grant T-32 CA09592 (to N. Cheng); and a core facilities Grant 2P30CA68485 to the Vanderbilt-Ingram Cancer Center.* Molecular Cancer Research, 2002. **1**(1): p. 2-11.

227. Coulthard, M.G., et al., *Characterization of the Epha1 receptor tyrosine kinase: expression in epithelial tissues.* Growth Factors, 2001. **18**(4): p. 303-317.

228. Aasheim, H.-C., et al., *Characterization of a novel Eph receptor tyrosine kinase, EphA10, expressed in testis.* Biochimica Et Biophysica Acta (BBA)-General Subjects, 2005. **1723**(1-3): p. 1-7.

229. Ivanov, A.I., et al., *Expression of Eph receptors and their ligands, ephrins, during lipopolysaccharide fever in rats.* Physiological genomics, 2005. **21**(2): p. 152-160.

230. Sharfe, N., et al., *Ephrin stimulation modulates T cell chemotaxis.* European journal of immunology, 2002. **32**(12): p. 3745-3755.

231. Lande, R., et al., *IFN-αβ released by Mycobacterium tuberculosis-infected human dendritic cells induces the expression of CXCL10: selective recruitment of NK and activated T cells.* The Journal of Immunology, 2003. **170**(3): p. 1174-1182.

232. Marsland, B.J., et al., *CCL19 and CCL21 induce a potent proinflammatory differentiation program in licensed dendritic cells.* Immunity, 2005. **22**(4): p. 493-505.

233. Riedmaier, I. and M.W. Pfaffl, *Transcriptional biomarkers–high throughput screening, quantitative verification, and bioinformatical validation methods.* Methods, 2013. **59**(1): p. 3-9.

234. Berry, M.P., et al., *An interferon-inducible neutrophil-driven blood transcriptional signature in human tuberculosis.* Nature, 2010. **466**(7309): p. 973-977.

235. Blankley, S., et al., *The application of transcriptional blood signatures to enhance our understanding of the host response to infection: the example of tuberculosis.* Philosophical Transactions of the Royal Society B: Biological Sciences, 2014. **369**(1645): p. 20130427.

236. Deffur, A., R.J. Wilkinson, and A.K. Coussens, *Tricks to translating TB transcriptomics.* Annals of translational medicine, 2015. **3**(Suppl 1).

237. de Araujo, L.S., et al., *transcriptomic biomarkers for tuberculosis: evaluation of DOCK9. EPHA4, and NPC2 mRNA expression in peripheral blood.* Frontiers in microbiology, 2016. **7**: p. 1586.

238. Bio-Rad, L., *Real-Time PCR Applications Guide. Bio-Rad Laboratories*. 2006, Inc.

239. Zhang, J. and S. Hughes, *Role of the ephrin and Eph receptor tyrosine kinase families in angiogenesis and development of the cardiovascular system.* The Journal of Pathology:

A Journal of the Pathological Society of Great Britain and Ireland, 2006. **208**(4): p. 453-461.

240. Abebe, M., et al., *Modulation of cell death by M. tuberculosis as a strategy for pathogen survival.* Clinical and Developmental Immunology, 2011. **2011**.

241. Briken, V. and J.L. Miller, *Living on the edge: inhibition of host cell apoptosis by Mycobacterium tuberculosis.* 2008.